AD-A071 664 COLUMBIA RADIATION LAB NEW YORK F/G 5/1
RESEARCH INVESTIGATION DIRECTED TOWARD EXTENDING THE USEFUL RAN--ETC(U)
MAR 79 G W FLYNN DAAG29-77-C-0019
UNCLASSIFIED NL

1 OF 2
AD A071664

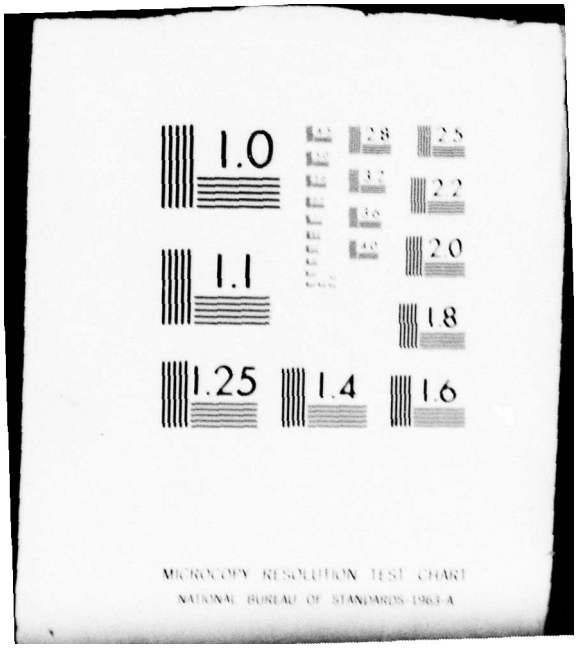
1.0
1.1
1.25
1.4
1.6
2.8
2.5
2.2
2.0
1.8
MICROCOPY RESOLUTION TEST CHART
NATIONAL BUREAU OF STANDARDS 1963-A

COLUMBIA RADIATION LABORATORY

RESEARCH INVESTIGATION DIRECTED TOWARD
EXTENDING THE USEFUL RANGE OF THE
ELECTROMAGNETIC SPECTRUM

Progress Report No. 29

April 1, 1978 through March 31, 1979

Contract DAAG29-77-C-0019

Object of the research:

Basic research in the fields of quantum electronics, electromagnetic propagation detection and sensing, and solid state electronics.

The research reported in this document was made possible through support extended the Columbia Radiation Laboratory, Columbia University, by the Joint Services Electronics Program (U.S. Army Electronics Command and U.S. Army Research Office, Office of Naval Research, and the Air Force Office of Scientific Research) under Contract DAAG29-77-C-0019.

Submitted by: G. W. Flynn, Director

Coordinated by: P. A. Pohlman, Administrative Assistant

COLUMBIA UNIVERSITY

Division of Government-Aided Research

New York, New York 10027

March 31, 1979

Approved for public release; distribution unlimited.

The research reported in this document was made possible through support extended the Columbia Radiation Laboratory, Columbia University, by the Joint Services Electronics Program (U.S. Army Electronics Command and U.S. Army Research Office, Office of Naval Research, and the Air Force Office of Scientific Research) under Contract DAAG29-77-C-0019.

Portions of this work were also supported by:

Air Force Office of Scientific Research

Grant AFOSR-74-2685

Army Research Office

Grant DAAG29-77-G-0015

National Aeronautics and Space Administration

Grant NSG-5163 Scope L

National Science Foundation

Grant NSF-ENG 75-09325

Grant NSF-ENG 76-16424

Grant NSF-ENG 76-15063

Grant NSF-DMR 77-05995

Grant NSF-CHE 77-24343

Office of Naval Research

Contract NC0014-78-C-0517

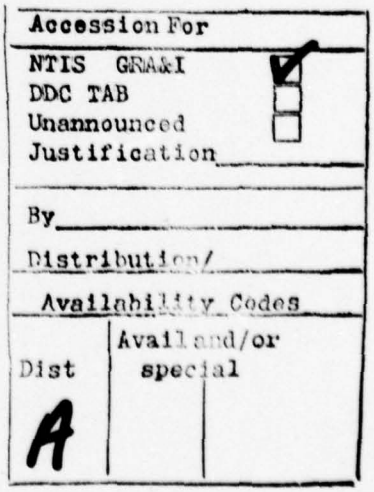

The support of these agencies is acknowledged in footnotes in the text.

Unclassified

SECURITY CLASSIFICATION OF THIS PAGE (When Data Entered)

REPORT DOCUMENTATION PAGE

READ INSTRUCTIONS BEFORE COMPLETING FORM

1. REPORT NUMBER: Progress Report No. 29	2. GOVT ACCESSION NO.
3. RECIPIENT'S CATALOG NUMBER	
4. TITLE (and Subtitle): RESEARCH INVESTIGATION DIRECTED TOWARD EXTENDING THE USEFUL RANGE OF THE ELECTROMAGNETIC SPECTRUM,	5. TYPE OF REPORT & PERIOD COVERED: Progress rept. no. 29, 1 April 78-31 March 79
	6. PERFORMING ORG. REPORT NUMBER: 29
7. AUTHOR(s): George W. Flynn	8. CONTRACT OR GRANT NUMBER(s): DAAG29-77-C-0019
9. PERFORMING ORGANIZATION NAME AND ADDRESS: Columbia Radiation Laboratory, Columbia University, New York, New York 10027	10. PROGRAM ELEMENT, PROJECT, TASK AREA & WORK UNIT NUMBERS: 1L161102BH57-03
11. CONTROLLING OFFICE NAME AND ADDRESS: Department of the Army, U.S. Army Research Office, Research Triangle Park, NC 27709	12. REPORT DATE: 31 March 1979
	13. NUMBER OF PAGES: 126
14. MONITORING AGENCY NAME & ADDRESS(if different from Controlling Office): (12) 145 p.	15. SECURITY CLASS. (of this report): Unclassified
	15a. DECLASSIFICATION/DOWNGRADING SCHEDULE

16. DISTRIBUTION STATEMENT (of this Report)

Approved for public release; Distribution unlimited

17. DISTRIBUTION STATEMENT (of the abstract entered in Block 20, if different from Report)

18. SUPPLEMENTARY NOTES

Portions of this work were also supported by the Air Force Office of Scientific Research, the Army Research Office, the National Science Foundation, the Office of Naval Research, and the National Aeronautics and Space Administration.

19. KEY WORDS (Continue on reverse side if necessary and identify by block number)

Fluorescence lifetimes
N_2 laser
Time resolved spectroscopy
Alkali dimer absorption spectrum

continued on page v

20. ABSTRACT (Continue on reverse side if necessary and identify by block number)

We have completed the design of an experimental system for time-resolved studies of alkali-noble-gas excimer molecules. The aim of this work is to determine the dominant formation and destruction mechanisms of the higher excited states of these interesting and potentially useful molecules.

A new region of infrared absorption has been found for saturated alkali vapors. The absorption shows the analog of the ultraviolet emission continuum

DD FORM 1 JAN 73 1473 EDITION OF 1 NOV 65 IS OBSOLETE

Unclassified 089 600

SECURITY CLASSIFICATION OF THIS PAGE (When Data Entered)

Block 20 continued - Abstract

of the H_2 molecule. In addition evidence is found for alkali trimers absorbing in the infrared.

Preliminary studies of the spin relaxation rates of sodium in xenon gas have been completed. The aim of these studies is to develop an efficient way to polarize the nucleus of Xe^{129}, a very slowly relaxing species which would be of great interest as a component of nuclear magnetic resonance gyroscopes.

We have discovered a novel spatially propagating wavefront which is generated by laser pumping of an optically thick medium to a state of complete transparency. The wavefront velocity v is related to the number of photons n absorbed per atom by $v = I_o(N_n)-1$, where I_o is the photon flux and N is the atomic number density.

The design of an experiment to measure the magnetic circular dichroism of saturated alkali vapors has been completed. The results of this experiment will be used to assign quantum numbers to several prominent but poorly understood absorption bands in the visible and near ultraviolet region of the spectrum.

We have completed the preliminary design of an experiment to measure the hyperfine structure of the unusually long-lived 5D state of the cesium atom. Because of the very narrow natural width of this state, exceptionally high resolution is possible. We hope to use the results of these measurements to make the first precise determination of the nuclear quadrupole moment of the cesium nucleus.

Optical pumping of Cs vapor using second resonance-D_1 light at 4593 Å, has been achieved. The percent spin-polarization appears to saturate with dye laser power at levels much lower than 100% and to decrease with Cs temperature. This saturation of polarization is somewhat reduced by the addition of N_2 gas, but persists even at a N_2 pressure of 200 torr for which no radiation trapping is possible. It appears that spin-exchange between Cs atoms is the mechanism limiting spin polarization at high ($>10^{13}$ cm^{-3}) Cs densities. Theoretical calculations of the spin polarization, taking into account spin-exchange, were carried out and are in qualitative agreement with the experiment.

Intermode energy transfer processes have been investigated in COF_2, OCS CH_3COF and $SO_2/^{18}O_2$. Rates and cross sections for individual kinetic steps due to collisions have been obtained.

Preliminary measurements of vibrational temperatures have been made in COF_2 which indicate that ν_1 and ν_2 modes can be made very hot. Multiphoton dissociation of COF_2 using a CO_2 laser has been observed to produce F atoms.

We have continued our investigation of coherent transient effects in gases. We have made the unprecedented finding that an echo can be generated from the information stored in a single atomic state. This enables echoes to be used to study the effect of collisions on atoms in one state. An echo detection technique which utilizes the relative polarizations of the excitation pulses and the echo has been developed which makes echo effects much easier

Block 20 continued - Abstract

to observe. Finally the tri-level echo technique (which we recently developed) has been used to perform the first comprehensive study of collisionally-induced relaxation of high Rydberg S and D states in an alkali atom.

Two newly developed nitrogen pumped dye lasers are used to generate photon echoes in $LaF_3:Pr^{3+}$ at pulse separations as large as 8.0 μsec. Data analysis yields excited state nuclear quadrupole splittings of 0.73 MHz and 1.12 MHz. Inhomogeneous broadenings associated with these splittings are found to lead to echo modulation damping. We have also observed an unusual dependence of homogeneous relaxation on detuning in the inhomogeneous profile as well as long-lived stimulated photon echoes.

A heterodyne correlation radiometer for the sensitive detection of radiating species whose Doppler shift is known, but whose presence we wish to affirm has been considered. Such radiation (which may be actively induced) can arise, for example, from remote molecular emitters, impurities and pollutants, trace minerals, chemical agents, or a general multiline source. A radiating sample of the species to be detected is physically made a part of the laboratory receiver, and serves as a kind of frequency-domain template with which the remote radiation is correlated, after heterodyne detection. The system is expected to be especially useful for the detection of sources whose radiated energy is distributed over a large number of lines, with frequencies that are not necessarily known. We have also considered the performance of a conventional optical heterodyne system in estimating the mean intensity of a Gaussian random signal, and shown that it depends on the degeneracy parameter of the signal radiation.

A single-threshold processor has been derived for a wide class of classical binary decision problems involving the likelihood-ratio detection of a signal embedded in noise. The class of problems we considered encompasses the case of multiple independent (but not necessarily identically distributed) observations of a nonnegative (nonpositive) signal, embedded in additive, independent, and noninterfering noise, where the range of the signal and noise is discrete. We have shown that a comparison of the sum of the observations with a unique threshold comprises optimum processing, if a weak condition on the noise is satisfied, independent of the signal. Examples of noise densities that satisfy and violate our condition were tabulated. The results were applied to a generalized photocounting optical communication system, and it was shown that most components of the system could be incorporated into our model. We also obtained exact photocounting distributions for a pulse of light whose intensity is exponentially decaying in time, when the underlying photon statistics are Poisson. It was assumed that the starting time for the sampling interval (which is of arbitrary duration) is uniformly distributed. The probability of registering n counts in the fixed time T was shown to be given in terms of the incomplete gamma function for $n \geq 1$ and in terms of the exponential integral for $n = 0$. Simple results are of interest in certain studies involving spontaneous emission, radiation

Block 20 continued - Abstract

damage in solids, and nuclear counting.

Stable, thermally re-cyclable Niobium point-contact Josephson junctions have been fabricated which are suitable for operation in heterodyne detectors (mixers) at millimeter wavelengths. A Josephson mixer at 115 GHz (2.5 mm-λ) has demonstrated an efficiency more than an order of magnitude greater than the best room temperature detectors. A complete receiver is now being constructed.

Efforts to understand the noise properties of a Josephson mixer have led to a digital computer simulation which agrees well with measurements at 115 GHz.

A fundamental asymmetry between the tunneling probabilities for electrons and holes has been observed in ultrathin SiO_2 layers (20-30 Å) which is explained in terms of the E-K dispersion relation in the energy gap of the SiO_2. These probabilities have been measured on the same MOS samples using a new experimental technique combining dark characteristics with measurements of photocurrent suppression by the SiO_2 layer.

A general theory is presented to describe the carrier transport across heterojunction interfaces. In matching the boundary conditions at the interface, the conservation of total energy and perpendicular momentum is assumed and the difference of effective masses on two sides of the junction is taken into account. The quantum mechanical transmission coefficient is calculated by a combined numerical and WKB method. Application of the present model to an $Al_xGa_{1-x}AsGaAs$ N-n heterojunction is performed and it gives rise to rectifying characteristics together with non-saturated reverse current. Comparison with the classical thermionic emission model is made to show the significance of tunneling and the effect of quantum mechanical reflection.

An experimental study has been made of the electronic properties of rectifying metal-Ge (n-type) contacts for a range of metals (Au, Cu, Ag, Pb and Ni) and their optoelectronic characteristics under monochromatic illumination for λ = 0.6328 μm. For each metal, very nearly ideal I-V characteristics were obtained with n values from the exponential forward bias region of 1.02 to 1.08 and excellent reverse saturation at 300°K. The dependence of photoresponse on thickness of various metal electrodes (from 50 Å to more than 1000 Å) was observed. ϕ_B's found from I-V and C-V measurements are in close agreement within ± 0.03 eV. The dependence of quantum efficiency (Q.E.) upon metal thickness was measured for all metals and these results exhibit the expected decline in Q.E. with $d \geq$ 100 Å. For $d \leq$ 100 Å, Q.E. can go as high as 75% at λ = 6328 Å.

Block 19 continued - Key Words

Alkali vapors
Heat pipe
Activation energy
Absorption coefficient
Electronic potential surface
Loosely bound trimers
Optical pumping wavefronts
Optically thick media
Propagation velocity
Photon absorption rate
Spin exchange
Spin relaxation
Magnetic circular dichroism
Coupling schemes
Radiofrequency spectroscopy
Optical pumping
Cs
Second resonance
Polarization saturation
N_2 quenching
Bottleneck
COF_2
OCS
SO_2
$^{18}O_2$
Multiphoton
Energy transfer
Relaxation
Collisions
Infrared
Laser
Rydberg states
Two-photon echo
Raman echo
Tri-level echo
Stimulated photon echo
Collisional relaxation
Velocity-Changing collisions
Total elastic scattering cross section atom-atom
Echo modulation damping
Secondorder hyperfine interaction
Heterodyne correlation radiometry
Optical radar
Optical heterodyne detection
Infrared radar
Photon counting
Optical communications
Likelihood-ratio detection
Spontaneous emission
Josephson-junctions

Block 19 continued - Key Words

Millimeter-wave
Detectors
Superconducting
Tunneling
MOS devices
Ultrathin SiO_2 layers
Semiconductor interfaces
Heterojunctions
Transport properties
Thermionic emission
Diffusion
Optoelectronics
Schottky barriers
Germanium
Quantum detectors

TABLE OF CONTENTS

PUBLICATIONS AND REPORTS ix

FACTUAL DATA, CONCLUSIONS, AND PROGRAMS FOR THE NEXT INTERVAL

I. RELAXATION AND ENERGY TRANSFER IN ALKALI METALS 1

A. Time-Resolved Spectroscopy of Alkali-Noble Gas Excimers. . 1

B. Cross Fluorescence of Alkali Dimers and Alkali-Noble Gas Excimers 4

C. Spin Exchange and Relaxation in Na Noble Gas Mixtures . . 13

D. Propagating Optical Pumping Wavefronts 18

E. Magnetic Circular Dichroism (MCD) of Alkali Vapors . . . 24

F. Infrared Absorption of Alkali Molecules 33

G. Optical Pumping of Alkali Vapors with Second Resonance Light and the Spin-Exchange Bottleneck 38

H. Spectroscopy of the 5D State of Cs^{133} 49

II. RELAXATION AND ENERGY TRANSFER IN SMALL POLYATOMIC MOLECULES . . 52

A. Relaxation, Infrared Multiphoton Photodissociation, and Vibrational Temperatures in Laser Pumped COF_2 52

B. Energy Transfer in $SO_2/^{18}O_2$ Mixtures 55

C. Energy Transfer Map for OCS 60

D. Infrared Laser Induced Fluorescence in CH_3COF 65

III. GENERATION AND CONTROL OF RADIATION 67

A. Relaxation and Excitation Transfer of Optically Excited States in Solids 67

B. Spontaneous and Induced Coherent Radiation Generation and Control in Atomic Vapors. 76

IV. QUANTUM DETECTION AND SENSING OF RADIATION 85

A. Nonlinear Heterodyne Detection and Sensing in the Infrared and Optical 85

B. Photon Counting Detection for Communications, Radar, and Imaging 88

C. Millimeter- and Submillimeter-Wave Mixers Using Josephson Junctions. 92

V. PHYSICAL PROPERTIES AND EFFECTS OF ELECTRONIC MATERIALS. . . . 94

A. Tunneling in Ultrathin SiO_2 Layers on Silicon. 94

B. Carrier Transport Across Heterojunction Interfaces . . . 99

C. Metal-Germanium Schottky Barrier Quantum Detectors . . . 106

PERSONNEL 117

JSEP REPORTS DISTRIBUTION LIST 119

PUBLICATIONS AND REPORTS

Publications

E. Y. Chan and H. C. Card, "Optoelectronic Properties of Metal-Germanium Schottky Barrier Quantum Detectors," IEEE-IEDM, Digest of Tech. papers, 653 (1978).

H. C. Card, "Electrically Erasable FAMOS Memory Structure Using Avalanche-Injection from Floating Gate," Electron. Lett. 14, 674 (1978).

P. Panayotatos and H. C. Card, "Experimental Critique of the Simple Schottky Theory of Metal-Silicon Solar Cells," Proc. 13th IEEE Phot. Spec. Conf., 634 (1978).

J. M. Presses, E. Weitz, and G. W. Flynn, "Laser Fluorescence Study of Vibrational Energy Equilibration in $CH_3F:O_2$ Mixtures: "Impurity" Molecules as Probes of Mode to Mode Energy Flow Pathways," J. Chem. Phys. 69, 2782 (1978).

Irwin Shamah and G. W. Flynn, "Translational and Vibrational Energy Distributions in Metastable Laser Pumped Polyatomic Molecules: A Quasi-thermodynamic Description," J. Chem. Phys. 69, 2474 (1978).

K. H. Liao and R. Gupta, "I_2 Vapor Cell as Narrow Band Optical Filter," Rev. Sci. Instrum. 49, 867 (1978).

B. B. Bulos, A. J. Glassman, R. Gupta, and G. W. Moe, "Measurement of the Lifetimes of the $Z^2F_{5/2}$, $Z^2D_{3/2}$, $Z^4G_{5/2}$, and $y^2D_{3/2}$ States of Lanthanum," J. Opt. Soc. Am. 68, 842 (1978).

W. Nagourney, W. Happer, and A. Lurio, "Level-crossing Study of the Hyperfine Structure of Lithium," Phys. Rev. A 17, 1394 (1978).

A. C. Tam, T. Yabuzaki, S. M. Curry, M. Hou, and W. Happer, "Inelastic Cross Sections in $Cs(n^2D_J) + Cs(6^2S_{1/2})$ Collisions," Phys. Rev. A 17, 1862 (1978).

A. C. Tam, T. Yabuzaki, S. M. Curry, and W. Happer, "Visible Excimer Bands of the K-noble-gas and Na-noble-gas Molecules: Comparison of Experiment with Theory," Phys. Rev. A 18, 196 (1978).

T. Yabuzaki, A. C. Tam, S. M. Curry, and W. Happer, "Visible Emission Bands of KXe_n Polyatomic Exciplexes," Phys. Rev. Lett. 41, 543 (1978).

W. Happer and R. Gupta, "Perturbed Fluorescence Spectroscopy," Progress in Atomic Spectroscopy, PT. A. Edited by W. Hanle and H. Kleinpoppen, Plenum Publishing Corporation, 1978.

T. Mossberg, A. Flusberg, and S. R. Hartmann, "Optical Second-Harmonic Generation Atomic Thallium Vapor," Opt. Comm. 25, 121 (1978).

A. Flusberg, T. Mossberg, R. Kachru, and S. R. Hartmann, "Observation and Relaxation of the Two-Photon Echo in Na Vapor," Phys. Rev. Lett. 41, 305 (1978).

Y. C. Chen, K. P. Chiang, and S. R. Hartmann, "Photon Echo "decay" in $LaF_3:Pr^{3+}$ as a Modulation Process," Opt. Comm. 26, 269 (1978).

A. Flusberg, T. Mossberg, and S. R. Hartmann, "The Multiphoton Coherent Hanle Effect," Coherence and Quantum Optics IV, 695 (1978).

Y. Taur and A. R. Kerr, "Low-Noise Josephson Mixers at 115 GHz Using Recyclable Point Contacts," Applied Phys. Lett. 32, 775 (1978).

Y. Taur and A. R. Kerr, "Progress on Multimeter-Wave Josephson Junctions," AIP Conference Proceedings, No. 44, On Future Trends in Superconductive Electronics, P. 254 (1978).

I. Shamah, "Vibrational Steady States Produced by the Vibrational Relaxation of Laser Pumped Polyatomic Molecules," Ph.D. Thesis, Dept. of Chem., Columbia University, 1978.

Y. Taur, "Noise Down-Conversion in a Pumped Josephson Junction," Journal de Physique 39, C6-575 (1978).

G. Vannucci and M. C. Teich, "Effects of Rate Variation on the Counting Statistics of Dead-Time-Modified Poisson Processes," Opt. Comm. 25, 267 (1978).

M. C. Teich and G. Vannucci, "Observation of Dead-Time-Modified Photocounting Distributions for Modulated Laser Radiation," J. Opt. Soc. Am. 68, 1338 (1978).

P. R. Prucnal and M. C. Teich, "Single-Threshold Detection of a Random Signal in Noise with Multiple Independent Observations: 1. Discrete Case with Application to Optical Communication," Applied Optics 17, 3576 (1978).

M. Elbaum and M. C. Teich, "Heterodyne Detection of Random Gaussian Signals in the Optical and Infrared: Optimization of Pulse Duration," Opt. Comm. 27, 257 (1978).

M. C. Teich and B. I. Cantor, "Information, Error, and Imaging in Deadtime-Perturbed Doubly-Stochastic Poisson Counting Systems," IEEE J. Quantum Electron. QE-14, 993 (1978).

L. Matin, M. C. Teich, M. E. Breton, G. Vannucci, P. R. Prucnal, and W. J. McGill, "Quantum Requirement at the Absolute Threshold with Non-Poisson Visual Stimuli," Assoc. Res. Vis. Ophthal. (ARVO) Abstr. 1, 132 (1978).

M. C. Teich, "Photon Counting," in Proc. NSF Grantee-User Meeting, edited by M. Gottlieb, C. Tsai, G. Brandt, and J. Blanchard (Carnegie-Mellon University, Pittsburgh, 1978), Optical Communication Systems, pp. 68-69 (1978).

M. C. Teich, "Atmospherically Disturbed Photon Counting Optical Communications," URSI Optical Communications Abstracts OS3, 36 (1978).

P. R. Prucnal and M. C. Teich, "Optimum Detection in Optical Communications with a Simple Counting Processor," J. Opt. Soc. Am. 68, 1384 (1978).

G. Vannucci and M. C. Teich, "Dead-Time-Modified Photon Statistics and Their Relationship to the Optical Power Spectrum," J. Opt. Soc. Am. 68, 1421 (1978).

P. R. Prucnal and M. C. Teich, "Statistical Properties of Counting Distributions for Intensity-Modulated Radiation," J. Opt. Soc. Am. 68, 1421 (1978).

M. Elbaum and M. C. Teich, "Optimal Condition for Pulsed Heterodyne Detection of Random Signals," J. Opt. Soc. Am. 68, 1421 (1978).

M. C. Teich, P. R. Prucnal, G. Vannucci, M. E. Breton, and W. J. McGill, "Non-Poisson Nature of the Effective Noise in the Visual System Near Threshold," J. Opt. Soc. Am. 68, 1454 (1978).

Chii-Ming Wu and E. S. Yang, "Physical Mechanisms of Carrier Leakage in DH Injection Lasers," J. Appl. Phys. 49, 3114 (1978).

N. D. Bhaskar, E. Zouboulis, T. McClelland, and W. Happer, "New Infrared Absorption Bands of Alkali Vapors," Phys. Rev. Lett. 42, 641 (1979).

N. D. Bhaskar, E. Zouboulis, R. Novak, and W. Happer, "Laser-excited Cross Fluorescent Emission from Cesium Molecules," Chem. Phys. Lett. (1979).

P. R. Prucnal, "Chain Rule for Finite Differences," Proceedings of IEEE 67, 445 (1979).

A. C. Tam, "Optical Pumping of a Dense Na + He + Ne_2 System: Application as an rf Spectrum Analyzer," (1979).

Y. Taur, "Characteristics of a Josephson Junction Harmonic Mixer with External Pumping," IEEE Transactions on Magnetics, January, 1979.

P. R. Prucnal and M. C. Teich, "Single-Threshold Detection of a Random Signal in Noise with Multiple Independent Observations: 2. Continuous Case," IEEE Trans. Inform. Theory IT-25, 213 (1979).

H. C. Card and R. W. Ulmer, "On the Temperature Dependence of Subthreshold Currents in MOS Electron Inversion Layers," Solid St. Electron., in press.

H. C. Card, "MOS Circuit Applications: Nonvolatile Memories," Chap. 10 of Digital Integrated Circuits: Technology, Device Structures, and Applications, Eds. M. I. Elmasry and R. W. Dutton, Wiley, New York, in press.

H. C. Card, "Electrostatic Effects of Interface States on Carrier Transport in Semiconductor Heterojunctions," J. Appl. Phys., in press.

E. Y. Chan, H. C. Card, E. S. Yang, A. R. Kerr, and R. J. Mattauch, "Transport of Majority and Minority Carriers in 2 μm Diameter Pt-GaAs Schottky Barriers," IEEE Trans. on Electron Devices, in press.

Irwin Shamah and G. W. Flynn, "Laser Catalyzed Translational to Vibrational Energy Conversion in CH_3F-O_2 Mixtures," J. Chem. Phys., in press.

Y. C. Chen, K. Chiang, and S. R. Hartmann, "Photon Echo Relaxation in LaF_3: Pr^{3+}," Phys. Rev. A, in press.

A. Flusberg, R. Kachru, T. Mossberg, and S. R. Hartmann, "Foreign-Gas-Induced Relaxation of Rydberg S and D States in Atomic Sodium," Phys. Rev., in press.

A. Flusberg, T. Mossberg, R. Kachru, and S. R. Hartmann, "Multilevel Echo Relaxation Studies in Gaseous Media," Opt. Soc. Am., in press.

C. M. Wu and E. S. Yang, "Carrier Transport Across Heterojunction Interfaces," Solid St. Electron., in press.

Papers by CRL Staff Members Presented at Scientific Meetings

H. C. Card, "The Theory of MIS Solar Cells", Gordon Research Conference on Metal-Insulator-Semiconductor Contacts", Kimball Union Academy, Meriden, New Hampshire, August 21-25, 1978.

E. Y. Chan and H. C. Card, "Optoelectronic Properties of Metal-Ge Schottky Barrier Quantum Detectors", The International Electronic Device Meeting, Washington, D.C., December 4-6, 1978.

E. Y. Chan, "Infrared Optoelectronic Properties of Metal-Ge Schottky Barriers", Western Electric Research Center, Princeton, New Jersey, March 13, 1979.

M. Elbaum and M. C. Teich, "Optimal Condition for Pulsed Heterodyne Detection of Random Signals", Annual Meeting of the Optical Society of America, San Francisco, California, November, 1978.

A. Flusberg, T. Mossberg, R. Kachru, and S. R. Hartmann, "Multilevel Echo Relaxation Studies in Gaseous Media", Tenth International Quantum Electronics Conference, Atlanta, Georgia, February 1, 1978.

G. W. Flynn, "Intermode Energy Transfer in Small Molecules", Distinguished Speaker Series, University of Utah, Salt Lake City, Utah, April 6, 1978; Gordon Conference on Radiation Chemistry, Holderness School, Plymouth, New Hampshire, July 17, 1978.

R. Kachru, A. Flusberg, T. Mossberg, and S. R. Hartmann, "Foreign-gas-Induced Relaxation of the Rydberg S and D States of the Alkalis", APS Meeting, New York, New York, January 29, 1979.

M. I. Lester, "Vibrational Energy Equilibration in $SO_2/^{18}O_2$ Mixtures", APS Meeting, New York, New York, January 31, 1979.

T. Mossberg, A. Flusberg, R. Kachru, and S. R. Hartmann, "Study of the Velocity-Changing Collisions Between Na Atoms and either He or CO", APS Meeting, New York, New York, January 29, 1979.

P. Panayotatos and H. C. Card, "Separation of the Basic Mechanisms in Optically-Illuminated Metal-Semiconductor Contacts", 36th Annual Device Research Conference, University of California at Santa Barbara, June 26-27, 1978.

P. Prucnal and M. C. Teich, "Optimum Detection in Optical Communications With a Simple Counting Processor", Annual Meeting of the Optical Society of America, San Francisco, California, November, 1978.

P. Prucnal and M. C. Teich, "Statistical Properties of Counting Distributions for Intensity-Modulated Radiation", Annual Meeting of the Optical Society of America, San Francisco, California, November, 1978.

R. Sheorey, "Intermode Energy Flow in Laser Pumped CH_3F", APS Meeting, New York, New York, January 31, 1979.

M. C. Teich, L. Matin, M. E. Breton, G. Vannucci, P. Prucnal, and W. J. McGill, "Quantum Requirements at the Absolute Threshold with Non-Poisson Visual Stimuli", Annual Meeting of the Association for Research in Vision and Ophthamology (ARVO), Sarasota, Florida, May, 1978.

M. C. Teich, "Photon Counting", NSF Grantee-User Group in Optical Communication Systems", Pittsburgh, Pennsylvania, June, 1978.

M. C. Teich, "Atmospherically Disturbed Photon Counting Optical Communications", International Symposium on Optical Communication and URSI General Assembly, Helsinki, Finland, August, 1978.

M. C. Teich, P. R. Prucnal, G. Vannucci, M. E. Breton and W. J. McGill, "Non-Poisson Nature of the Effective Noise in the Visual System Near Threshold", Annual Meeting of the Optical Society of America, San Francisco, California, November, 1978.

G. Vannucci and M. C. Teich, "Dead-Time-Modified Photon Statistics and Their Relationship to the Optical Power Spectrum", Annual Meeting of the Optical Society of America, San Francisco, California, November, 1978.

C. M. Wu, E. S. Yang, and H. C. Card, "Current Conduction Across Heterojunction Interfaces", Semiconductor Interfaces Specialists Conference, Miami, Florida, November 30-December 2, 1978.

Lectures

H. C. Card, "Solar Cells, Basic Principles, and Some Recent Research", Departments of Physics, Electrical Engineering, and Energy Research Center, Lehigh University, November 15, 1978.

G. W. Flynn, "Collision Induced Mode to Mode Energy Transfer and Metastability in Laser Pumped Molecules", University of Nevada, Reno, Nevada, April 5, 1978; University of Colorado, Boulder, Colorado, April 10, 1978; Colorado State University, Fort Collins, Colorado, April 11, 1978; University of Chicago, Chicago, Illinois, June 6, 1978; University of North Carolina, Chapel Hill, North Carolina, October 17, 1978; University of California, Berkeley, California, October 24, 1978; California Institute of Technology, Pasadena, California, October 25, 1978; University of Nebraska, Lincoln, Nebraska, March 2, 1979.

W. Happer, "Attraction and Repulsion of Laser Beams", Department of Physics, University of Illinois, October 12, 1978; Department of Physics, Princeton University, November 9, 1978.

W. Happer, "Laser Snow", Department of Physics, Texas A & M University, October 19, 1978; Department of Physics, University of Texas at Dallas, February 1, 1979; JILA Colloquium, University of Colorado, March 8, 1979.

W. Happer, "Laser Photochemistry of Alkali Vapor Hydrogen System", Seminar, Exxon Research Laboratories, December 21, 1978.

J. Liran, "Two Photon Near Resonance Scattering From Sodium Vapor", Resonance Seminar, Columbia University, New York, New York, December 15, 1978.

P. Prucnal, "A New Statistical Discussion Theory Model for Processing in the Visual System", Seminar, Columbia University, New York, New York, February 14, 1979; Bell Laboratories, Holmdel, New Jersey, February 21, 1979; Texas Tech University, Lubbock, Texas, March 5, 1979; Penn State University, State College, Pennsylvania, March 23, 1979.

P. Prucnal, "Optical Communications and Visual Psychophysics", Seminar, Riverside Research Institute, New York, New York, January, 1979.

M. C. Teich, "Dead-Time Effects in the Maintained Discharge of the Cat's Retinal Ganglion Cell", Biomedical Engineering Seminar, Carnegie-Mellon University, Pittsburgh, Pennsylvania, June, 1978.

M. C. Teich, "The Role of Quantum Optics in Optical Communications", Laboratory of Optics Colloquium, Palacký University, Olomouc, Czechoslovakia, August, 1978.

Resonance Seminars

Meetings are held periodically at Columbia University, New York, New York, during the academic year and are open to all members of the New York scientific community. Guest speakers are invited to discuss work in the general area of the research in the Columbia Radiation Laboratory.

Nat Bhaskar, Columbia University, "Electron Scattering from Laser Excited Atom- A New and Novel Approach," April 7, 1978.

Lester Eastman, Cornell University, "Compound Semiconductor Device Research and the National Sub-Micron Facility at Cornell," April 10, 1978.

William Happer, Columbia University, "Laser Production and Destruction of Alkali Hydride Crystals," April 28, 1978.

Andrew Kaldor, Exxon, "Laser Chemistry at Exxon," May 5, 1978.

Jean Delpech, University of Paris at Orsay, "Conditions Between Rydberg Level of Helium Induced by Electron and Neutral Collisions," September 22, 1978.

F. Laloe, Ecole Normale Superieure, Paris France, "Velocity Selective Optical Pumping," September 28, 1978.

C. A. Nicolaides, Theoretical Chemistry Institute, "Many Body Approaches to the Complex Coordinate Rotation Method for Resonances and to the Photo-Absorption Problem in Atoms and Molecules," October 13, 1978.

W. Faust, Naval Research Laboratory, "Short Pulse Photolysis Experiments," November 3, 1978.

R. Sternheimer, Brookhaven National Laboratory, "K-Ordering of Atomic and Ionic Energy Levels," November 10, 1978.

William Reinhardt, Univeristy of Colorado, "Instabilities in Classical Mechanics and Intramolecular Energy Transfer," November 17, 1978.

J. Yardley, Allied Chemical Research Laboratory, "Laser Induced Nonlinear Photochemistry in Homogeneous and Heterogeneous Systems," December 1, 1978.

J. Liran, Nuclear Research Center, Negev, Israel and Columbia University, "Two-Photon Near Resonance Light Scattering from Sodium Vapor," December 8, 1978.

Thomas Marshall, Columbia University, "High Power Free Electron Laser Based on Stimulated Raman Backscatter," December 15, 1978.

J. Hall, Joint Institute for Laboratory Astrophysics, "High Resolution Optical Spectroscopy with the Ramsey Effect," January 31, 1979.

Andrew Tam, Bell Laboratories, "Spectroscopy of Liquids by Optoacoustics," February 16, 1979.

H. Mahr, Cornell University, "Charge Exchange Experiments Towards Soft X-Ray Lasing," February 23, 1979.

Stephen R. Leone, Joint Institute for Laboratory Astrophysics, "State Selected Laser Kinetics," March 22, 1979.

David Stoler, Perkin-Elmer Corp., "Photon Anti-Bunching," March 30, 1979.

I. RELAXATION AND ENERGY TRANSFER IN ALKALI METALS

A. TIME-RESOLVED SPECTROSCOPY OF ALKALI-NOBLE GAS EXCIMERS*

(W. Happer, N. D. Bhaskar, A. Vasilakis)

The lifetimes of the alkali-noble gas molecules are of great interest. These excimer molecules are potential laser candidates.[1][2] Lifetime measurements would also be a check on existing potential curves for the alkali-noble gas pairs.[3] In our first attempts to measure these lifetimes we encountered various difficulties which required us to modify our system. We began a series of improvements on our system, which we hoped would improve our accuracy and quicken data accumulation.

The apparatus consists of a tunable dye laser pumped by a nitrogen laser. The laser pulses are passed through a filter and focused on a heated cell containing an alkali and a noble gas. Fluorescence is then focused into a 3/4 meter SPEX monochromator after passing through a filter and is detected by a suitable photomultiplier having a fast risetime (1.2 ns RCA C31024A). The signal is then put into a sampling oscilloscope which is triggered by part of the dye laser pulse going to a photodiode (risetime < .5 ns). Finally, the oscilloscope is connected to a PDP8/E minicomputer operating as a signal averager. The data for the laser pulse and for the fluorescent decay are then put into a computer which deconvolutes the lifetime from the instrumental time response.

Modifications were done to our nitrogen laser to improve its peak power and stability. We found that the spark gap triggering for the nitrogen laser was a major problem. It fired eratically and did not produce regular and identical pulse shapes. Besides this problem, the spark gap needed frequent spark plug changes, due to rapid destruction of the electrode. This led us to

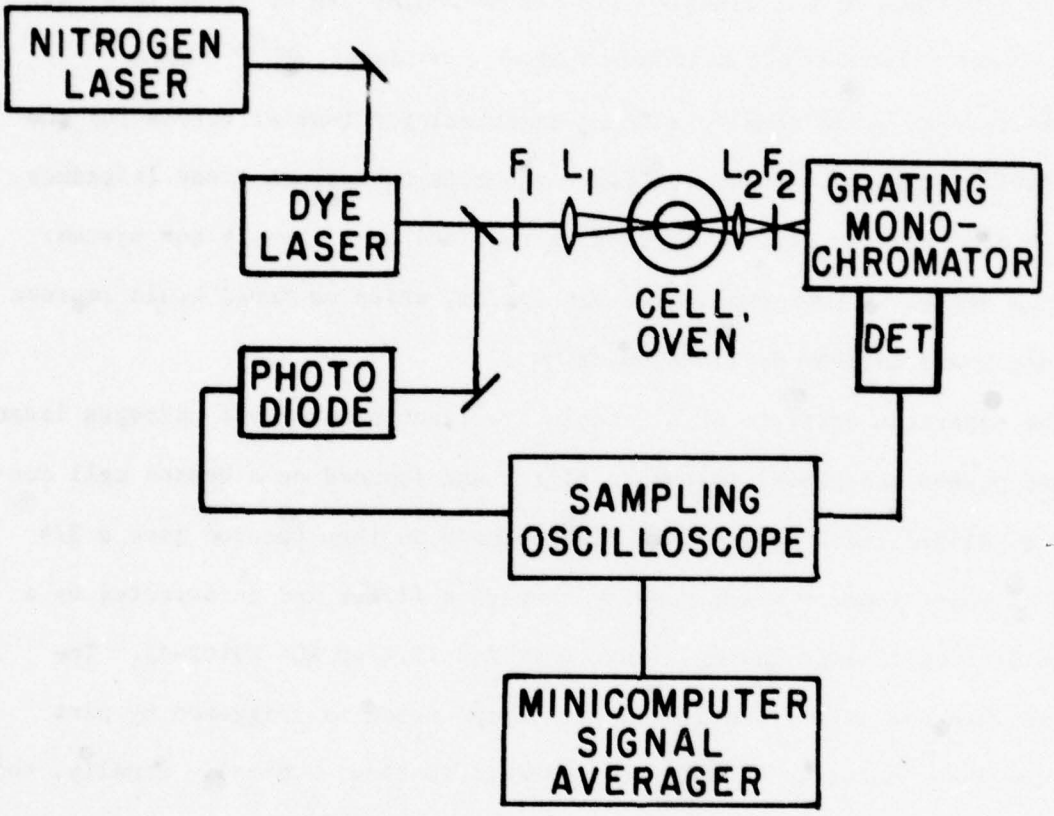

Figure 1: Schematic of experimental apparatus for time-resolved spectroscopy.

replace the spark gap with a thyratron (EG & G model HY-1102) which is more reliable and would allow us to pulse the laser faster (0 to 40 pps). The wiring information for the thyratron can be obtained from EG & G and information on the Marx circuit can be found in reference 4.

Since the thyratron would cause us to lose peak power, we replaced the mirror in the nitrogen laser with a dielectric mirror for the UV, which has better reflecting qualities. Installing a stirring motor under the dye cruet ensures that a new volume of dye is pumped after every pulse. Because of the higher pulse rates, we will be using this to maintain high peak power from the dye laser. In addition, to help maintain peak power from the nitrogen laser, the flow of nitrogen through the laser cavity was increased. This helps to remove the remaining unrelaxed nitrogen from the laser.

At present the problem which is hampering our progress on the experiment is RF noise generated by the triggering of the nitrogen laser. We are confident that we can remove the RF noise by using some electronics and by adding more rf shielding on the nitrogen laser.

*This work also supported by the Army Research Office (Durham) under Grant DAAG29-77-G-0015.

(1) A. V. Phelps, JILA Report No. 110, September 15, 1972.

(2) George York and Alan Gallagher, JILA Report No. 114, October 15, 1974.

(3) J. Pascale and J. Vandeplanque, Service de Physique Atomique Centre d' Etudes Nucleaires de Saclay France, March 1974

(4) S. I. Parker and C. A. Rey, Nucl. Instr. and Methods 43, 361 (1966).

B. CROSS FLUORESCENCE OF ALKALI DIMERS AND ALKALI-NOBLE GAS EXCIMERS*

(N. D. Bhaskar, E. Zouboulis, R. Novak, W. Happer)

Preceding progress reports have discussed emission and absorption bands in alkali dimers and alkali-noble gas excimers.[1] The bands studied indicated transitions between the ground state and an excited state. These transitions occurred in the visible and near infrared region of the spectrum, a region detected by photomultiplier tubes. During the past year, laser induced transitions between two excited states have been studied. Such transitions occur at wavelengths beyond 1.0 μ; molecular transitions in this region have not been studied extensively since it is beyond the range of photomultiplier tubes.

A commercial dewar-type lead sulfide detector was used in the apparatus shown in Fig. 1. Considerable work was done to optimize the signal to noise ratio of this detector. For the spectral region between 1.0 μ and 2.0 μ, best results were obtained with a load resistor which had approximately the same resistance as the dry ice cooled lead sulfide detector. The signal was taken across the load resistor in series with the lead sulfide crystal; the chopping frequency was 75 Hertz.

The first studies were made on Cs_2 molecules. An evacuated cell containing cesium was placed in a glass oven and heated to temperatures between 250°C and 350°C. In this range, the saturated cesium vapor has a number density of .75 ~ 8.5 x $10^{16}/cm^3$; of this, Cs_2 is approximately 1% of the total vapor pressure. Several lines of the argon-ion laser fall within the C-band of the absorption spectra of Cs_2. Using these lines, an emission band was found between 1.50 μ and 1.63 μ. The shape of the emission band depends on the wavelength of the exciting laser line; the spectra in Fig. 2a were produced using the 4880 Å and 5145 Å lines. The energy levels appear in Fig. 2b; the

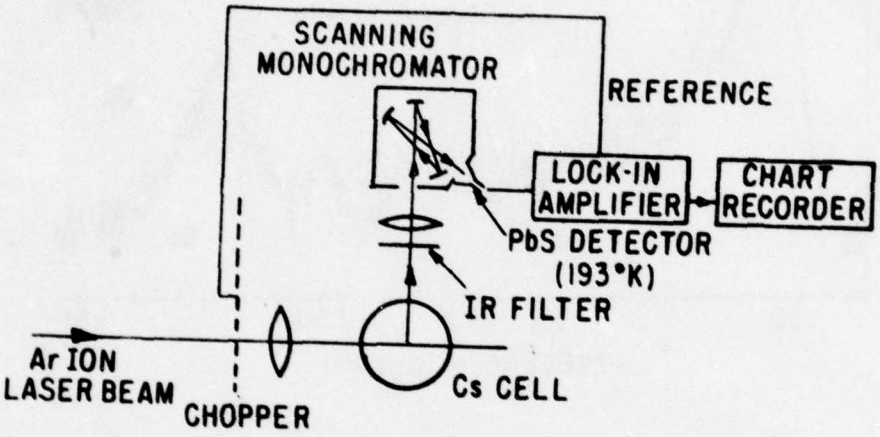

Figure 1: Apparatus used to detect bands between 1.0 μ and 2.0 μ.

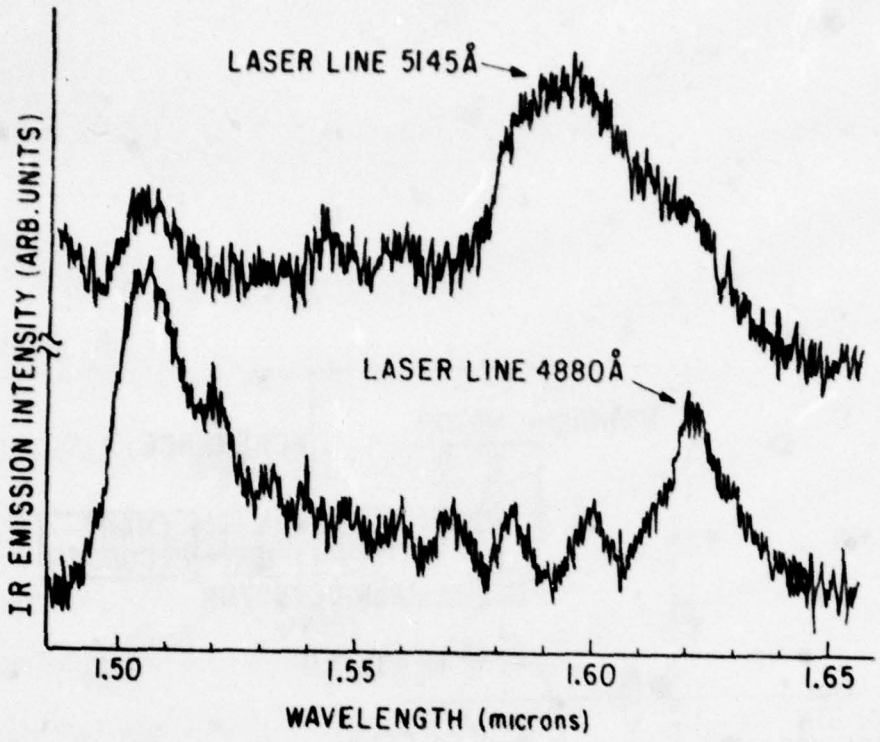

Figure 2a: Infrared spectra of Cs_2 when excited with two laser lines in the C absorption band.

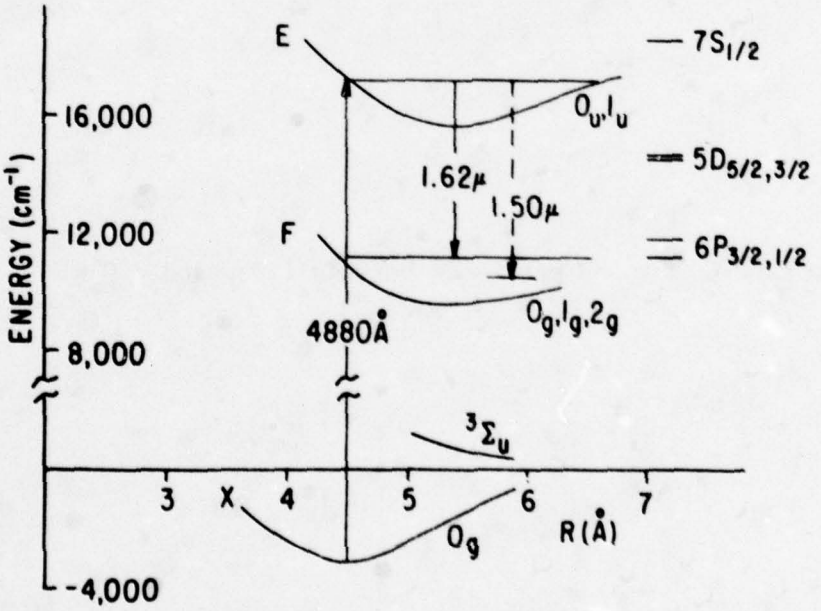

Figure 2b: Energy level diagram of Cs_2 indicating the absorption of the laser line and the cross fluorescence observed.

laser line might populate several closely spaced excited states; a single state E has been used to signify these states. The transition detected is believed to be from this E state to a final state or states F. The symmetry of the ground state is 0_g; of state E, 0_u or 1_u; of state F, 0_g, 1_g, or 2_g. These results will be published shortly.[2]

Cells with cesium and several atmospheres of an inert gas were also studied. The 4579 Å line of the argon ion laser lies between the two second resonance lines of cesium. Through pressure broadening, the cesium atom may be excited to the 7P state and forms an excimer with a noble gas atom. Decays of the excimer to the ground state have been extensively studied in recent years.[3] The excimer transitions between the 7S and 6P excited states were studied using cells with approximately three amagats of noble gas. As shown in Fig. 3, in the excited state, there is an attractive potential between a cesium atom and a noble gas atom. From the potential energy diagram of the 7S and 6P states, an excimer transition ($7S_{1/2,1/2} \rightarrow 6P_{1/2,1/2}$) is expected on the red side of the $7S_{1/2} \rightarrow 6P_{1/2}$ atomic line; two excimer transitions ($7S_{1/2,1/2} \rightarrow 6P_{3/2,3/2}$ and $7S_{1/2,1/2} \rightarrow 6P_{3/2,1/2}$) are expected on the red side of the $7S_{1/2} \rightarrow 6P_{3/2}$ atomic line. These transitions have been found in cesium cells containing Ne, Ar, Kr, and Xe (Fig. 4). No excimer peaks have been seen in the cesium helium cell above the noise level. Cesium-helium excimer absorption has recently been found by Sayer[4]; the corresponding transition studied here would be too small to detect above the noise level.

Table I contains the position of the peaks. The $7S_{1/2,1/2}$ potentials have been plotted experimentally by Sayer,[5] the 6P potentials by Hedges.[6] Both sets of potentials have errors of approximately 100 cm^{-1}. The differences between the minima of the potential wells in these papers agree fairly well

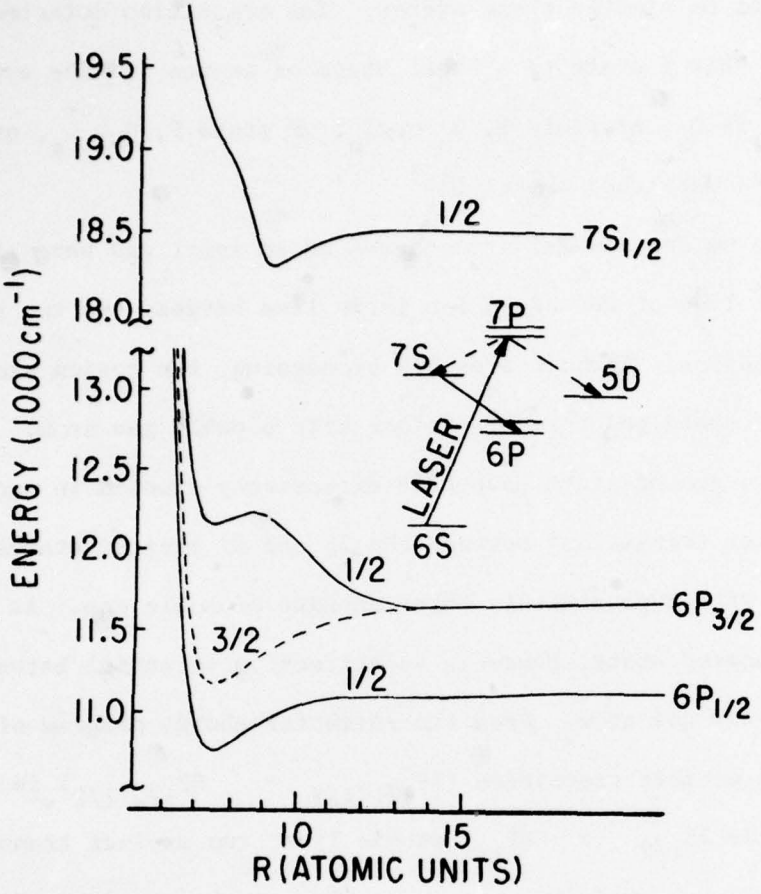

Figure 3: Qualitative potential energy curves of the 7S and 6P states of cesium noble gas molecules taken from the curves of Pascale.[7]

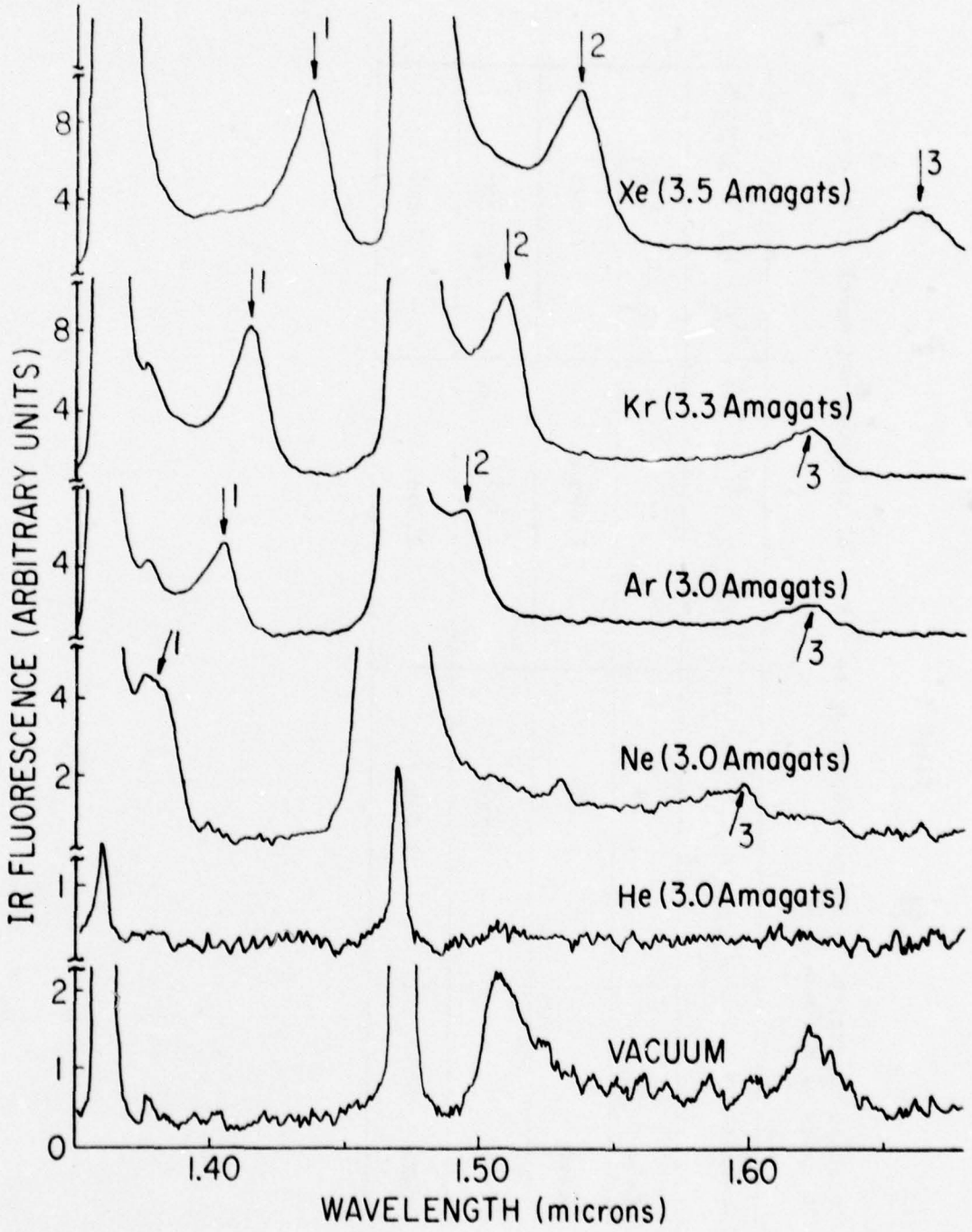

Figure 4: Infrared spectra of cesium noble gas excimers when excited by 4880 Å line (1 watt) of an argon ion laser. The cells were heated to a temperature of 380°.

TABLE I

Location of excimer peaks corresponding to $7S \rightarrow 6P$ transitions; wavelengths are in units of microns

Transitions	$7S_{1/2,1/2} \rightarrow 6P_{1/2,1/2}$	$7S_{1/2,1/2} \rightarrow 6P_{3/2,3/2}$	$7S_{1/2,1/2} \rightarrow 6P_{3/2,1/2}$
CsNe	1.379	-	1.595
CsAr	1.405	1.495	1.623
CsKr	1.415	1.505	1.622
CsXe	1.439	1.538	1.665

with our measurements for the $7S_{1/2,1/2} \rightarrow 6P_{1/2,1/2}$ and $7S_{1/2,1/2} \rightarrow 6P_{3/2,3/2}$ transitions. A discussion of these bands appears in a paper to be published shortly.

Preliminary work has been done on potassium and rubidium noble gas excimers to find similar emission bands. Cells containing potassium and xenon were excited to the second resonance state by the 4067 Å line of a krypton ion laser; rubidium cells with krypton or xenon were excited using the 5145 Å and 5017 Å lines of an argon ion laser. Their spectra appear in Fig. 5. Work is planned to identify the rubidium, potassium, and also sodium-noble gas infrared bands. The ultraviolet lines of the krypton-ion laser fall close to the second resonance lines of sodium. Temperature and pressure profiles of these bands should help to clarify the potential energy curves for these states.

*This research was also supported by the Army Research Office (Durham) under Grant DAAG29-77-G-0015.

(1) Progress Report, June 30, 1976 p.38; March 31, 1977 p.57; March 31, 1978 p.144, p.155.

(2) N. D. Bhaskar, E. Zouboulis, R. Novak, and W. Happer, "Laser-Excited Cross Fluorescent Emission from Cesium Molecules," to be publihsed in Chemical Physics Letters.

(3) A. C. Tam, T. Yabuzaki, S. M. Curry, and W. Happer, Phys. Rev. A 18, 196 (1978).

(4) B. Sayer, M. Ferray, J. P. Visitcot, and J. Lozingot, J. Chem. Phys. 68, 3618 (1978).

(5) B. Sayer, J. P. Visitcot, and J. Pascole, J. De Physique, 39, 361 (1978).

(6) R. E. M. Hedges, D. L. Drummond, and A. Gallagher, Phys. Rev. A. 6, 1519 (1972).

(7) J. Pascale and J. Vandoplanque, J. Chem. Phys. 60, 2279 (1974).

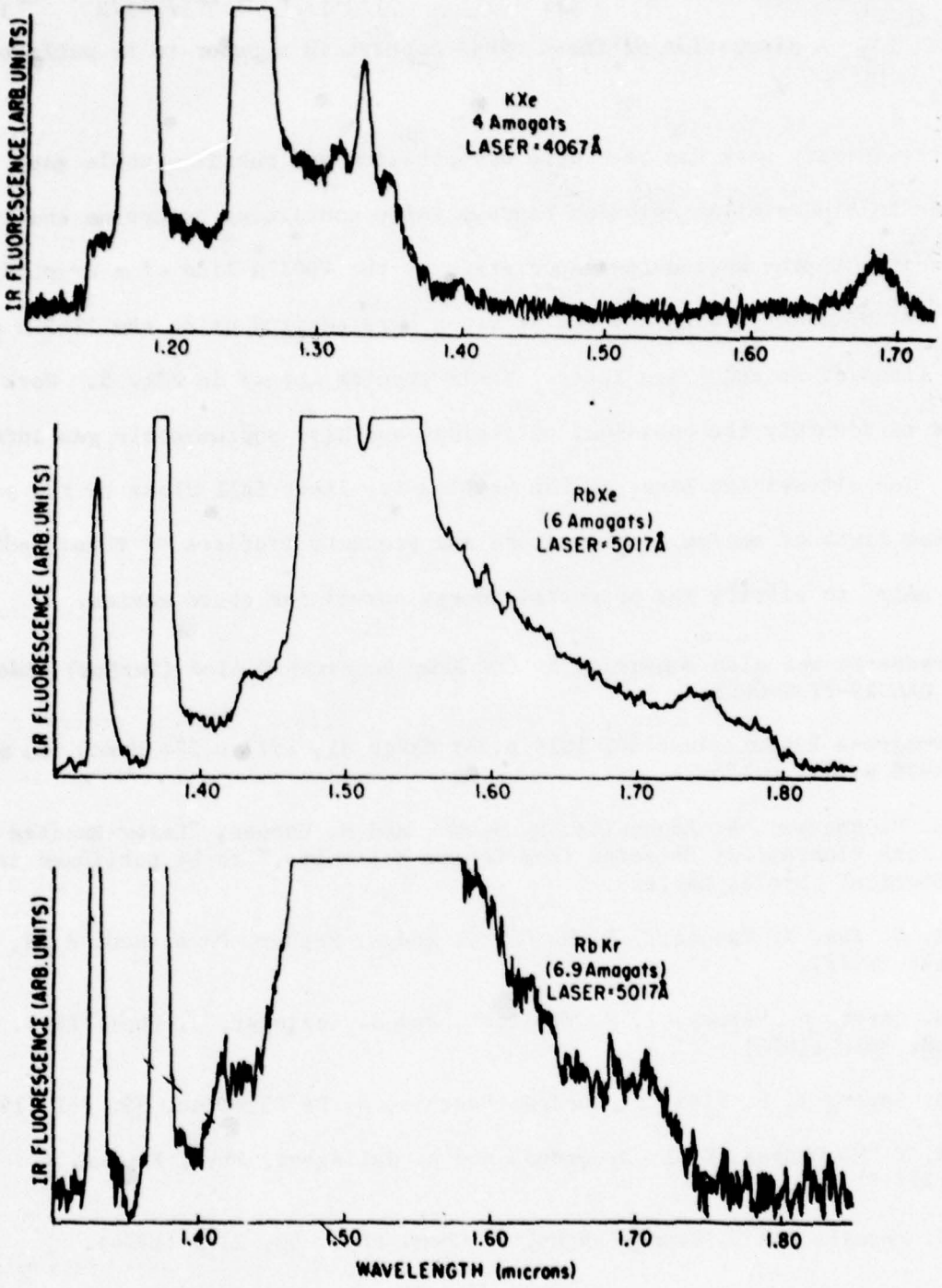

Figure 5: a. KXe infrared spectra
b. RbKr and RbXe spectra

C. SPIN EXCHANGE AND RELAXATION IN Na NOBLE GAS MIXTURES*

(M.Hou, B. Suleman, N. Bhaskar, W. Happer)

It has been shown[1] that very efficient transfer of angular momentum can take place in collisions between spin polarized alkali atoms and the heavy noble gas nuclei. We are trying to apply this spin exchange polarization method using sodium to polarize the xenon nuclei:

$$Na(\uparrow) + Xe(\downarrow) \rightarrow Na(\downarrow) + Xe(\uparrow)$$

i.e. the optically pumped sodium atom transfers its polarization to the unpolarized xenon nucleus.

The sodium spin depolarization rates in xenon gas are being measured. The experimental set up is shown in Fig. 1; a 1.5 ml 1720 glass cylindrical cell containing Na metal, 600 torr of helium gas, 10 torr of nitrogen, and several torrs of xenon is contained within a resistance-heated oven which maintains the cell temperature at about 280°C. A strong pumping beam is used to establish a large ground-state polarization in the Na vapor. When the strong beam is suddenly removed by a chopper, the subsequent evolution of polarization in the Na vapor is measured by monitoring the absorption of a weak probe beam which has been attenuated by a factor of 10^{-4} to 10^{-6} from the strong beam and has negligible influence on the relaxation. In order to prevent the photomultiplier from being saturated by the strong beam, we introduce a small angular deviation (less than 5°) between these two beams so that the transmitted pump beam can be blocked and only the probe beam can get through to the photomultiplier. A special chopper blade which gives us four sequences with pump beam and probe beam on and off separately is shown in Fig. 2. By using this chopper blade, we can obtain the following decay

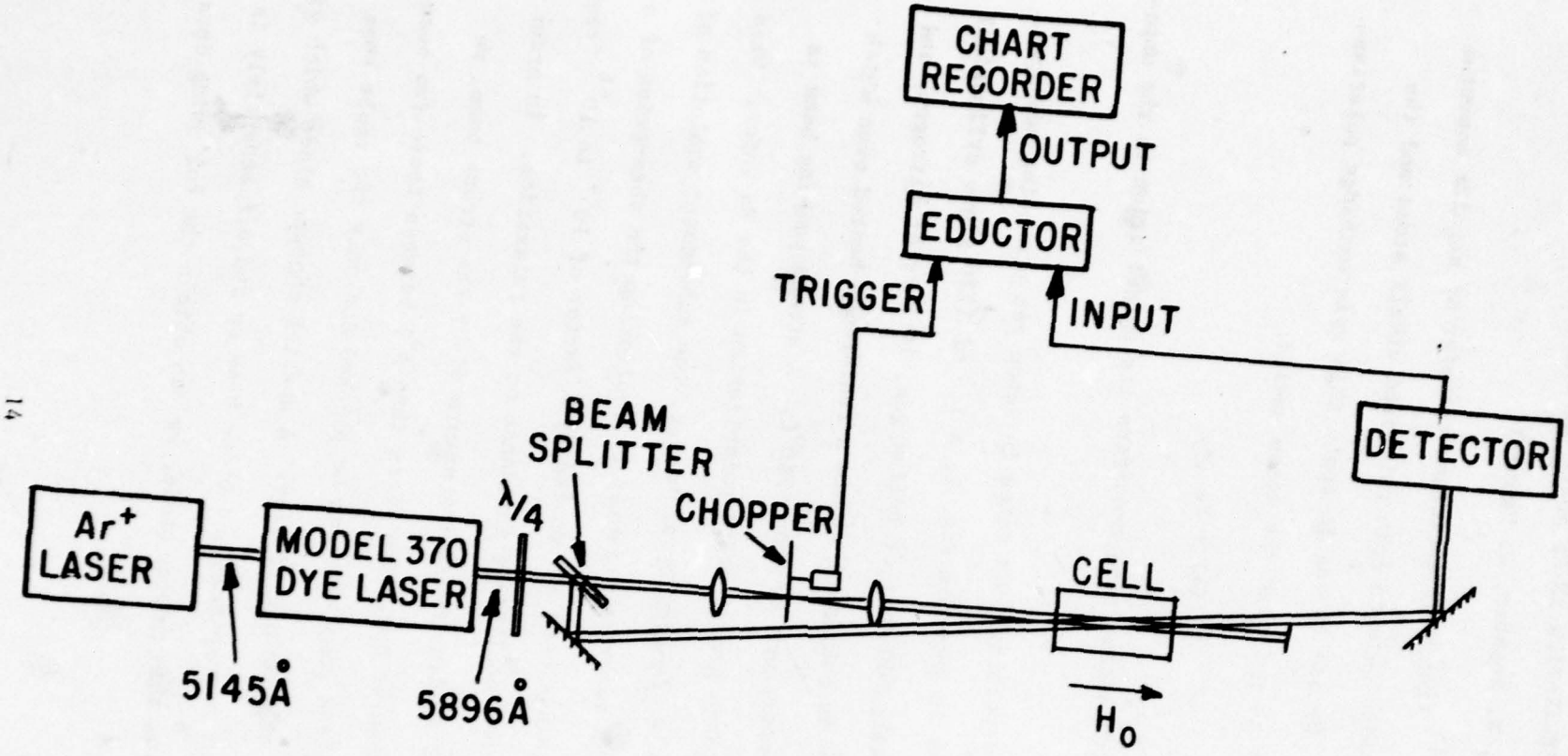
CHART RECORDER
OUTPUT
EDUCTOR
TRIGGER
INPUT
BEAM SPLITTER
λ/4
CHOPPER
DETECTOR
Ar+ LASER
MODEL 370 DYE LASER
CELL
5145Å
5896Å
H0

Figure 1

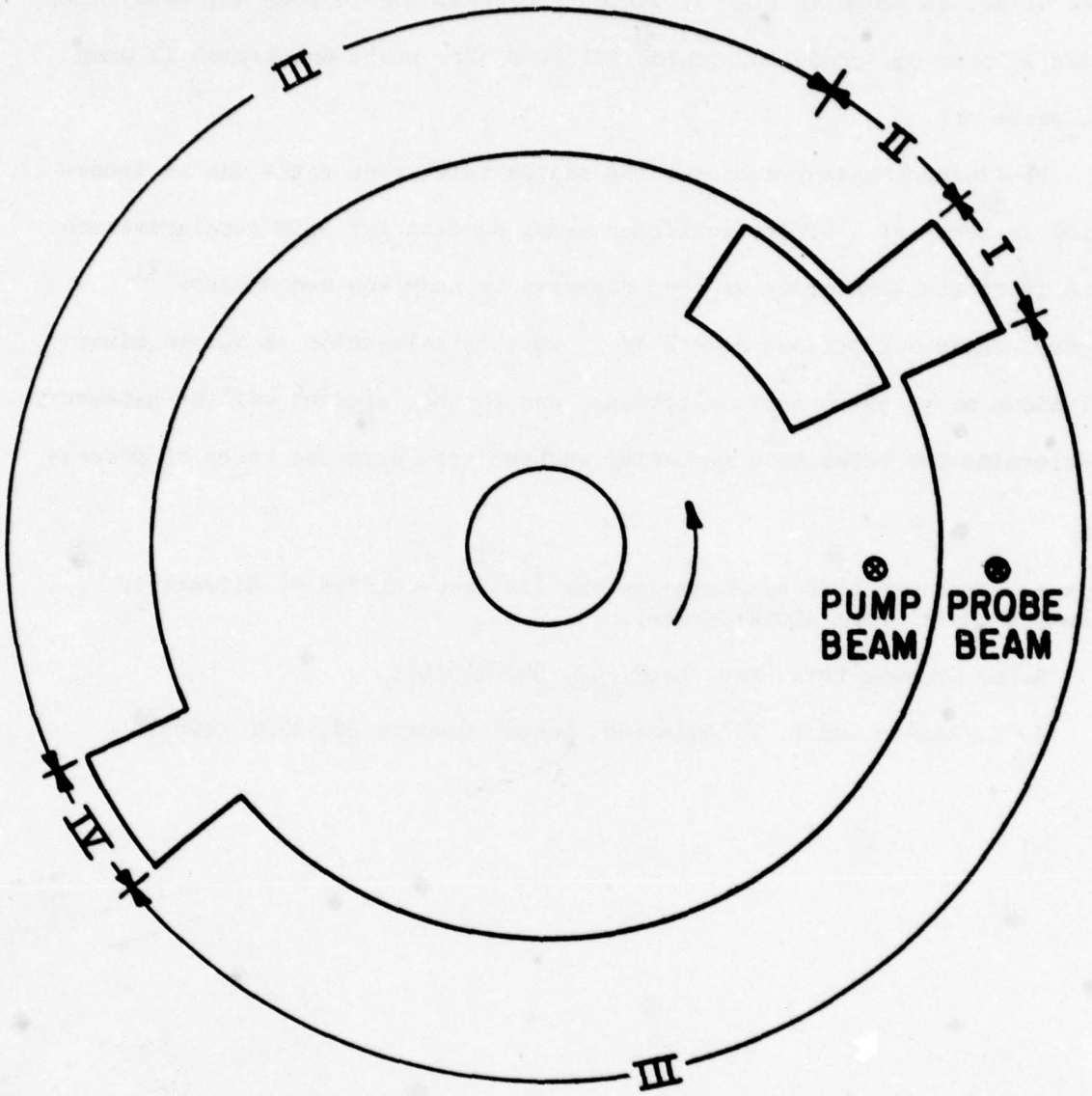

region I: probe off
pump on

region II: probe on
pump on

region III: probe on
pump off

region IV: probe off
pump off

Figure 2

curve of Na, as shown in Fig. 3; region I corresponds to pump on, probe off; region II pump on, probe on, region III pump off, probe on; region IV pump off, probe off.

Preliminary measurements of the sodium relaxation rates can be interpreted in terms of a binary collision cross section for spin depolarization which is of the same order as that reported by Anderson and Ramsey.[2] However, there are serious doubts as to whether relaxation is due to binary collisions or to three body collisions, and further studies will be necessary to determine the relaxation mechanism and the spin exchange rates of process (1).

*This research was also supported by the Air Force Office of Scientific Research under Grant AFOSR-74-2685.

(1) B. C. Groves, Phys. Rev. Lett. 40, 391 (1978).

(2) A. T. Ramsey and L. W. Anderson, Nuovo Cimento 32, 1151 (1964).

Na + He(600 T) + N_2(10T) + Xe(1.0T)

Temp. = 233°C

time scale ~ 10 msec/inch

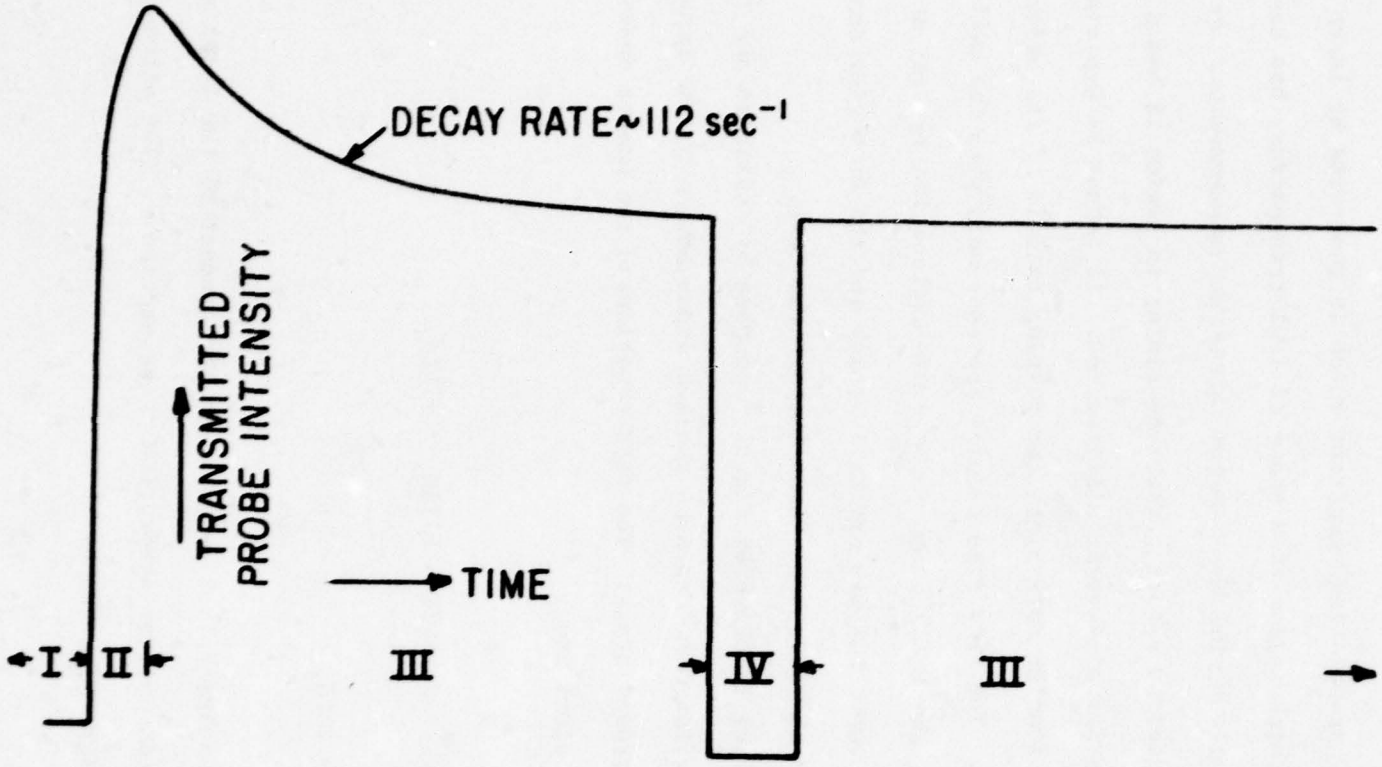

Figure 3

D. PROPAGATING OPTICAL PUMPING WAVEFRONTS*

(M. Hou, B. Suleman, N. Bhaskar, W. Happer)

A spatially propagating wavefront which is generated by laser pumping of an optically thick medium to a state of 100% transparency has been discovered unexpectedly during the Na spin relaxation measurements. As shown in Fig. 3 of the previous report, the slow rising in region II has a time constant of the order of several milliseconds. It cannot be explained as an indication of pumping rate since the pumping rate is of the order of 10^4 to 10^5 sec^{-1}. The slow rise becomes apparent only when the cell temperature is high, about 225^oC and above. Our explanation is that at high temperatures the vapor becomes optically thick and the slow rise shows the rate at which the pump beam burns through the cell.

A simple model is shown by Fig. 1. Suppose by collision and radiative decay a fraction f of spin-up excited atoms decays to the spin-up sublevel of the ground state. The rate equations of the number densities of the ground state atoms are

$$\frac{\partial}{\partial t} N_{\downarrow} = -2RN_{\downarrow} - (1 - f)2RN_{\downarrow} = -2RfN_{\downarrow} \tag{1}$$

$$\frac{\partial}{\partial t} N_{\uparrow} = 2RfN_{\downarrow} \tag{2}$$

where the mean pumping rate R is equal to the product of the local photon flux I and the mean optical absorption cross section σ. The attenuation of the pumping light is given by

$$\frac{\partial I}{\partial z} = -2N_{\downarrow}\sigma I \tag{3}$$

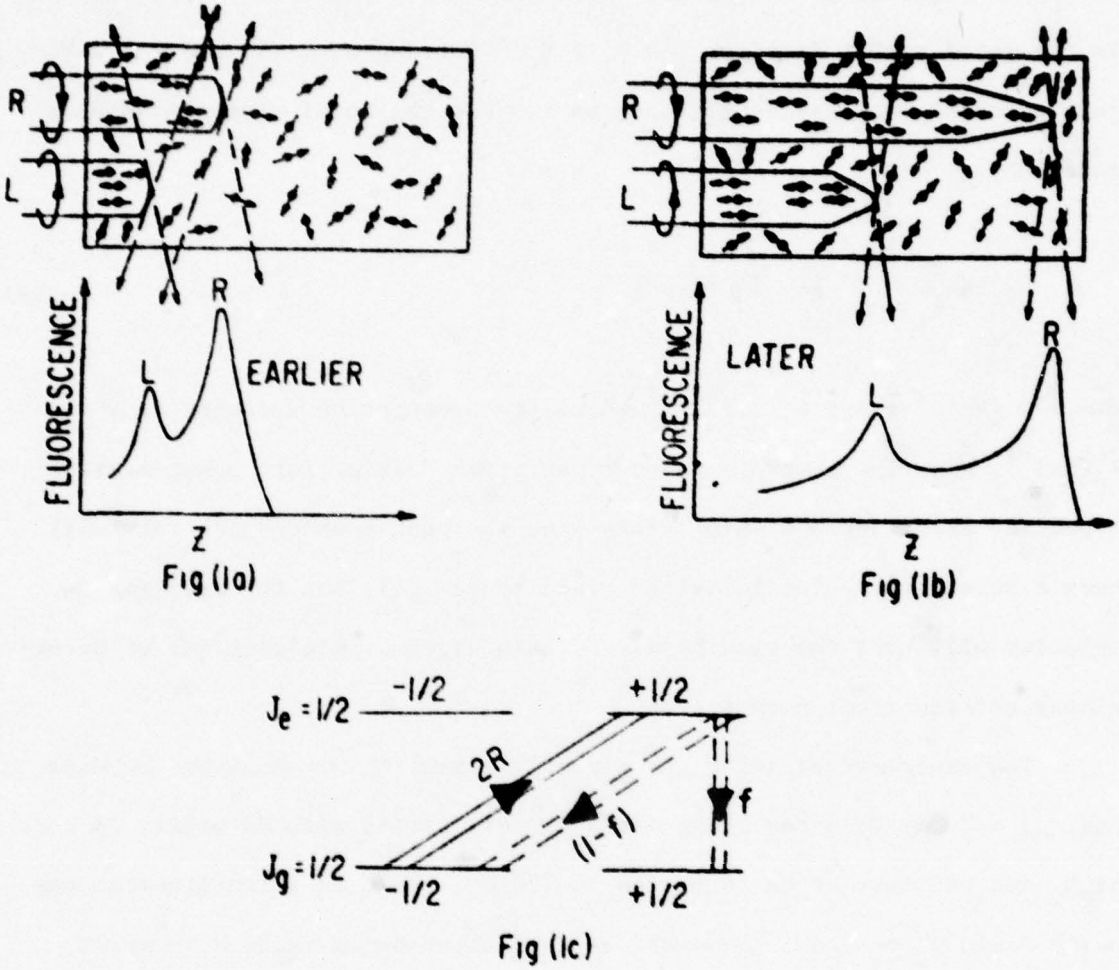

Figure 1: Simple model for propagating optical pumping wavefronts.

The boundary conditions are that $I(z=0) = I_o$, the incident light intensity, and that the atoms are initially unpolarized, i.e. $N_\downarrow(t=0) = N/2$, where N is the total number density, $N = N_\uparrow + N_\downarrow$. Solving eqs. (1) and (3) subject to these boundary conditions, we can get the local photon absorption rate $2RN_\downarrow$.

$$2RN_\downarrow \approx \frac{R_o}{4} \operatorname{sech}^2 \frac{\alpha}{2} (z-vt) \tag{4}$$

when $z >> (N6)^{-1}$ and $t >> (2fR_o)^{-1}$ where the propagation velocity is $v = I_0(Nn)^{-1}$, n is the absorbed photons per atom. Taking into consideration hyperfine structure and spin relaxation, the photon absorption rate will have a more complicated form than given by eq. (4), but the propagation velocity will have the same form. So this gives us a direct way of determining the important parameter n.

The experimental setup for directly measuring the velocity is shown in Fig. 2: a 70 mm long and 12 mm diameter cell filled with Na metal, 10 torr of N_2 and 600 torr of He is heated to 225^oC ~ 275^oC in a longitudinal magnetic field H_o of about 10 Gauss. A wollaston prism is used to split the laser beam into two, one is left, the other right circularly polarized. By rotating the prism the relative intensities of the two beams can be adjusted to any desired value. A lens is used to project an image of the cell onto the face of the photomultiplier. A narrow slit in the focal plane is used to isolate the fluorescence from a small region of the cell. The entire cell can be scanned by moving the slit and photomultiplier parallel to the cell axis. The picture shown in Fig. 3 is taken at different position z. It shows the delay time for the beam to reach the detected position and gives a direct measurement of velocity, which agrees with the prediction of eq. (4).

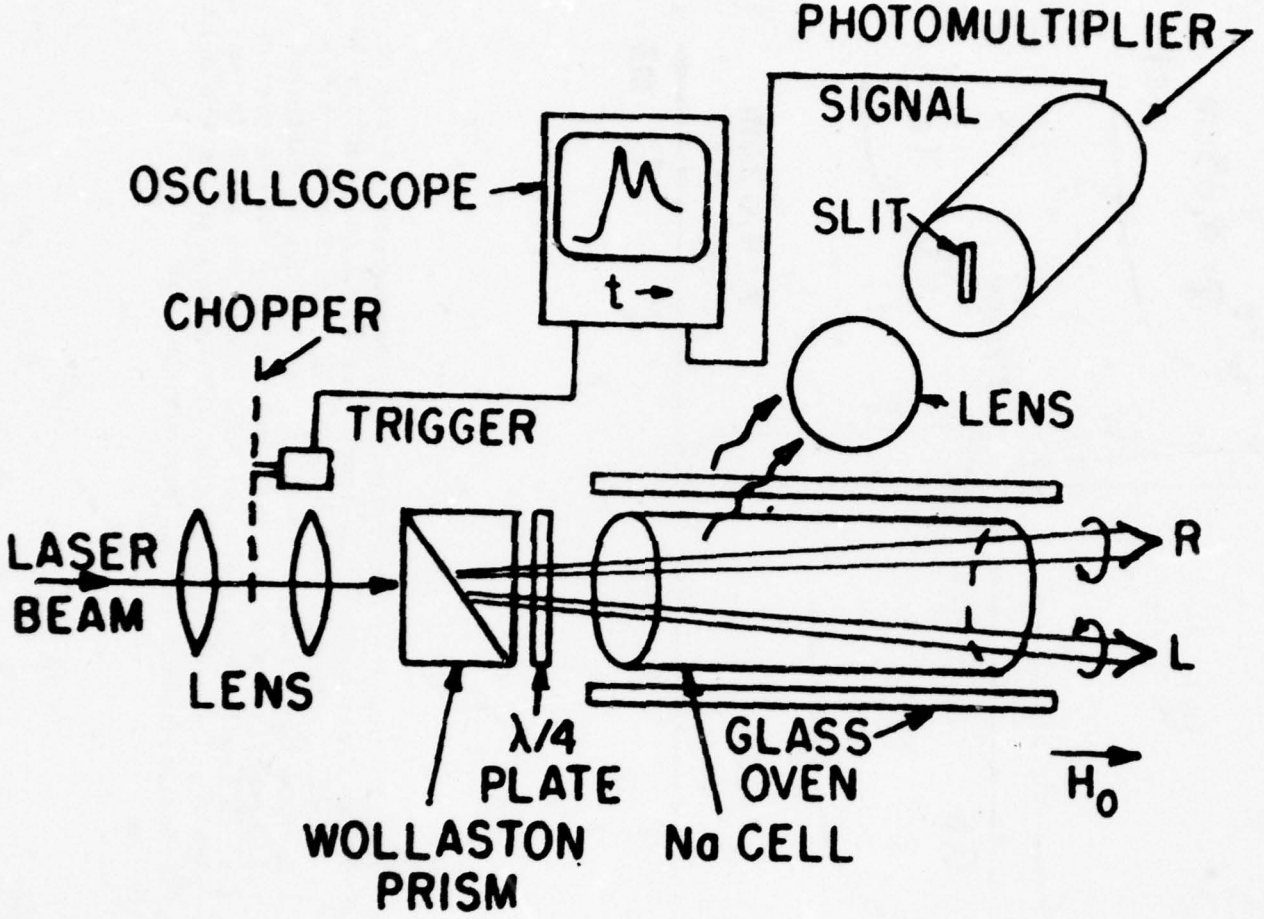

Figure 2: Apparatus

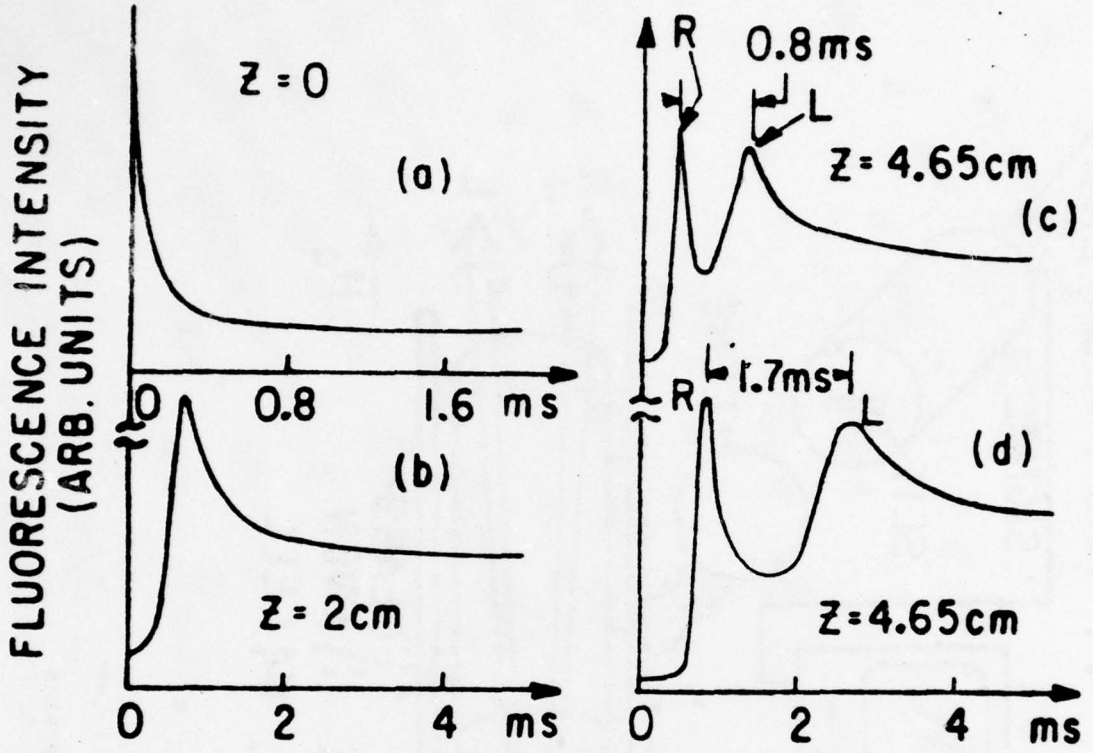

Figure 3: Experimentally measured fluorescence for arrangement of Fig. 2. Power of the laser beam at the input face z = 0 is typically 40 mW. (a) Beam L alone at input face z = 0. (b) Beam L alone at z = 2 cm from input face. (c) Both L and R beams of different initial intensities are launched simultaneously and observed at z = 4.65 cm from input face. (d) Same conditions as in (c) except both L and R are attenuated by 50% before entering the cell. The vertical scales in (a)-(d) are not the same.

*This research was also supported by the Air Force Office of Scientific Research under Grant AFOSR-74-2685.

E. MAGNETIC CIRCULAR DICHROISM (MCD) OF ALKALI VAPORS*

(B. Suleman, W. Happer)

The possible use of alkali dimers in high power tuneable dye lasers as suggested by York and Gallagher,[1] has generated considerable interest in the study of alkali spectra. Na_2 has already been shown to lase on many transitions.[2] However, not very much is known about the transition moments and coupling schemes of alkali dimer bands, especially in the visible. An example of such absorption bands for Cs_2 is shown in Fig. 1. The unusually narrow bands near 7100 Å are believed to originate from $^3\Sigma$ ground state. However, an unambiguous assignment of the bands of Fig. 1 still does not exist. Similarly there is a large number of excimer bands in alkali-noble gas systems for which the transition moments and coupling schemes are not known. No direct measurement of these quantities has been reported yet. Experimental data on MCD of these bands can yield information regarding coupling schemes and transition moments.

The phenomenon of MCD is illustrated in Fig. 2. In isotropic media that are not optically active, the absorption coefficients (k_+, k_-) of left and right circularly polarized light (σ_+, σ_-) are identical, i.e. $k_+ = k_- \Rightarrow \Delta k = 0$. In the presence of a longitudinal magnetic field k_+ and k_- do not remain symmetric and $\Delta k \neq 0$. This preferential absorption of one sense of polarization is called MCD.

It is customary to identify three different contributions[4] A, B and C to the MCD. The A contribution is due to the Zeeman splitting of the degenerate initial and final states of the transition. The perturbation of the wave functions of the system give rise to the term B. The component C is due to unequal population in the Zeeman split sublevels of lower states, which is caused by the lining up of the ground state spins in the presence

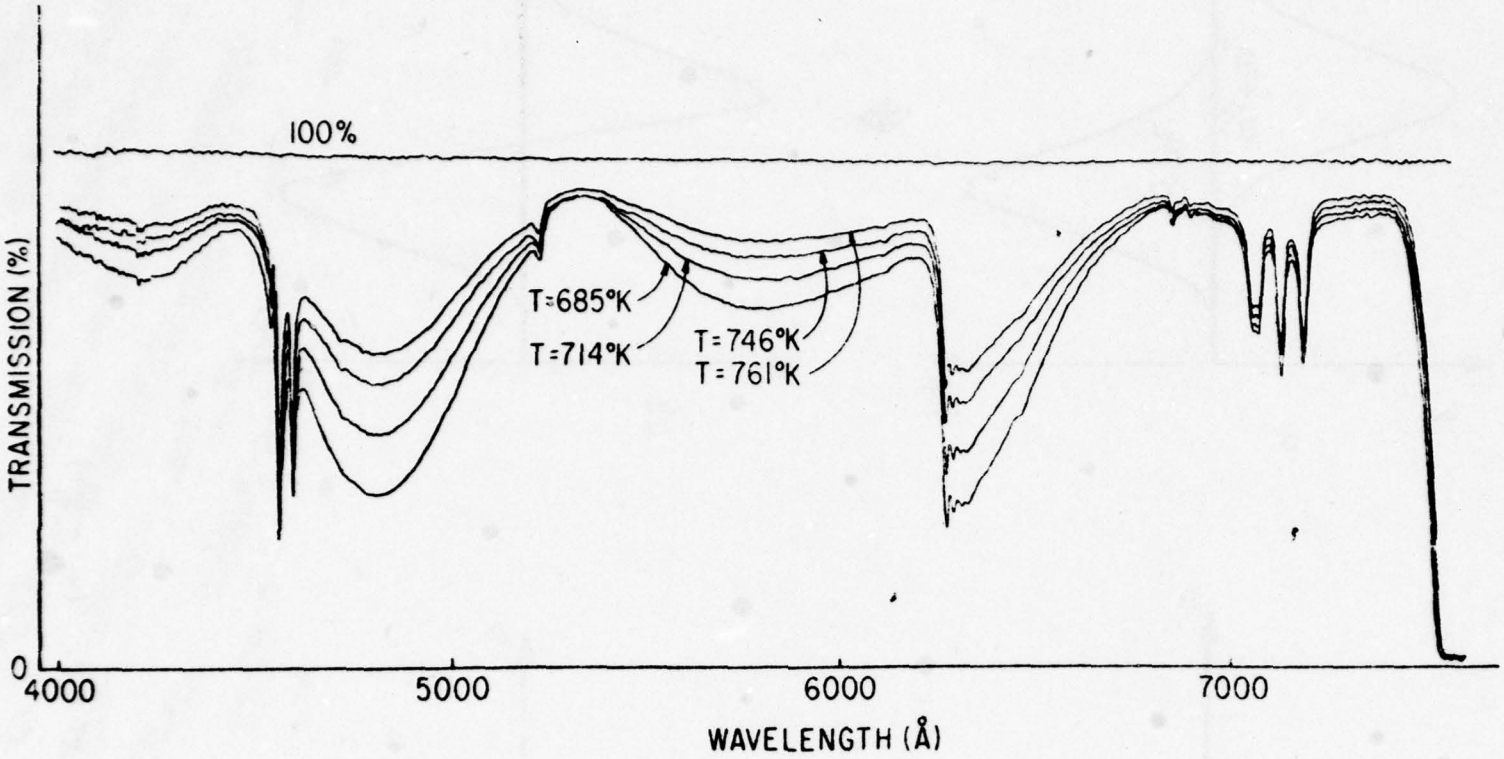

Figure 1:

Absorption spectrum of Cs_2 molecules. These curves were taken for T_1 = 660°K. T_2 was varied between 685°K to 761°K.

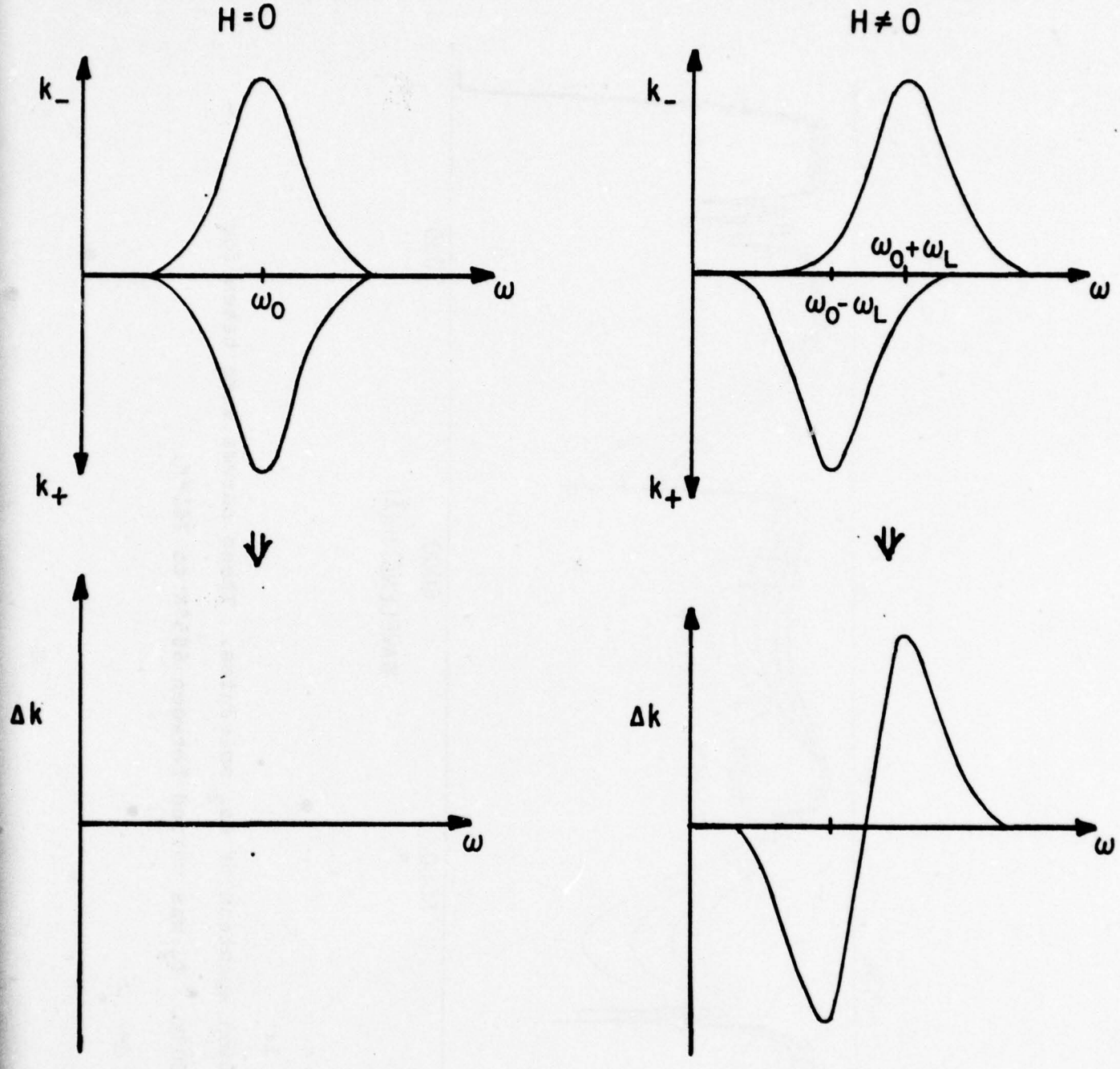

Figure 2: Illustration of MCD. ($\omega_L = \frac{\beta H}{\hbar}$)

of an external magnetic field. If $f(\omega)$ is the band shape of the transition in the absence of a magnetic field H, then the MCD for bands like those in Fig. 1 can be written as

$$\Delta k = \eta[-A \frac{\partial f}{\partial \omega} + (B + \frac{C}{KT})f] \beta H \qquad (1)$$

where β is the Bohr magneton and η is a constant. B is usually small and can be neglected.

In the case of a $\Sigma \rightarrow \Sigma$ transition A = C = 0 and there should be no MCD as indicated in Fig. 3a. The coefficient A is non-zero only when either ground or excited state has a degeneracy which can be lifted with a magnetic field. The MCD for a $\Sigma \rightarrow \Pi$ or $\Pi \rightarrow \Pi$ transition is shown in Fig. 3b. The C terms exist only when ground state is paramagnetic (for example $^2\Sigma$ or $^1\Pi$). Increasing randomization of spins with increasing temperature is a characteristic of paramagnetic C term and its effect for different T is shown in Fig. 3c. A non-zero C term proves the existence of a paramagnetic ground state.

The MCD of alkali vapors has not yet been measured because of their highly corrosive nature and very small signal. The ratio of MCD to zero field absorption is

$$\frac{\Delta k}{k} \sim \frac{\beta H}{\Delta \omega_o} \sim 3 \times 10^{-5} \qquad (2)$$

at 1000 gauss where $\Delta\omega_o$ is the band width. To detect such a small signal we are using modulation technique of lock-in amplifiers. Although we have not yet made any measurements, we have almost completed setting up an experiment which is shown in Fig. 4. A tungsten ribbon lamp is used to

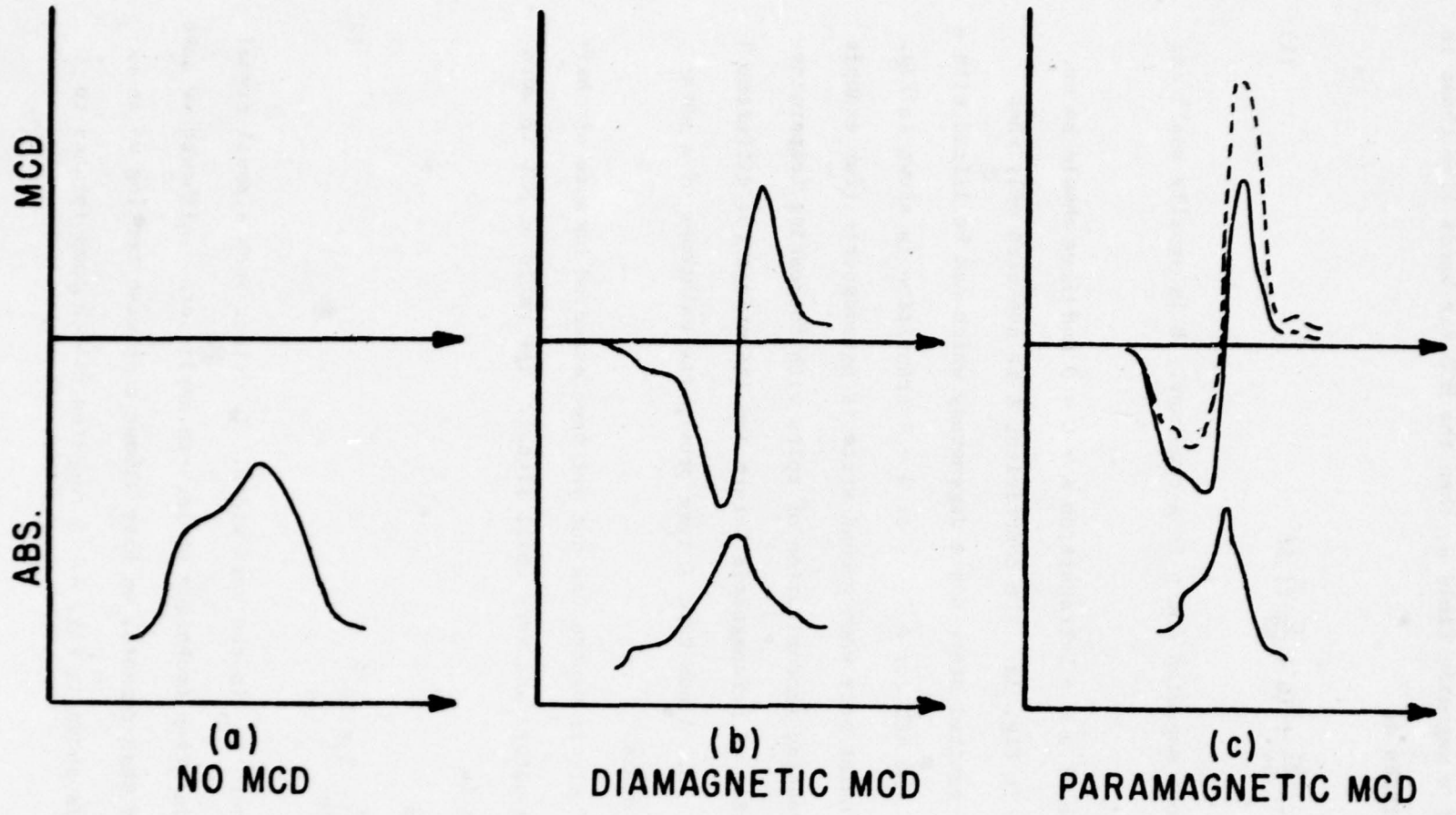

Figure 3: MCD curves (top) for three different cases. The dotted curve is for low temperature. Absorption curves are shown at the bottom.

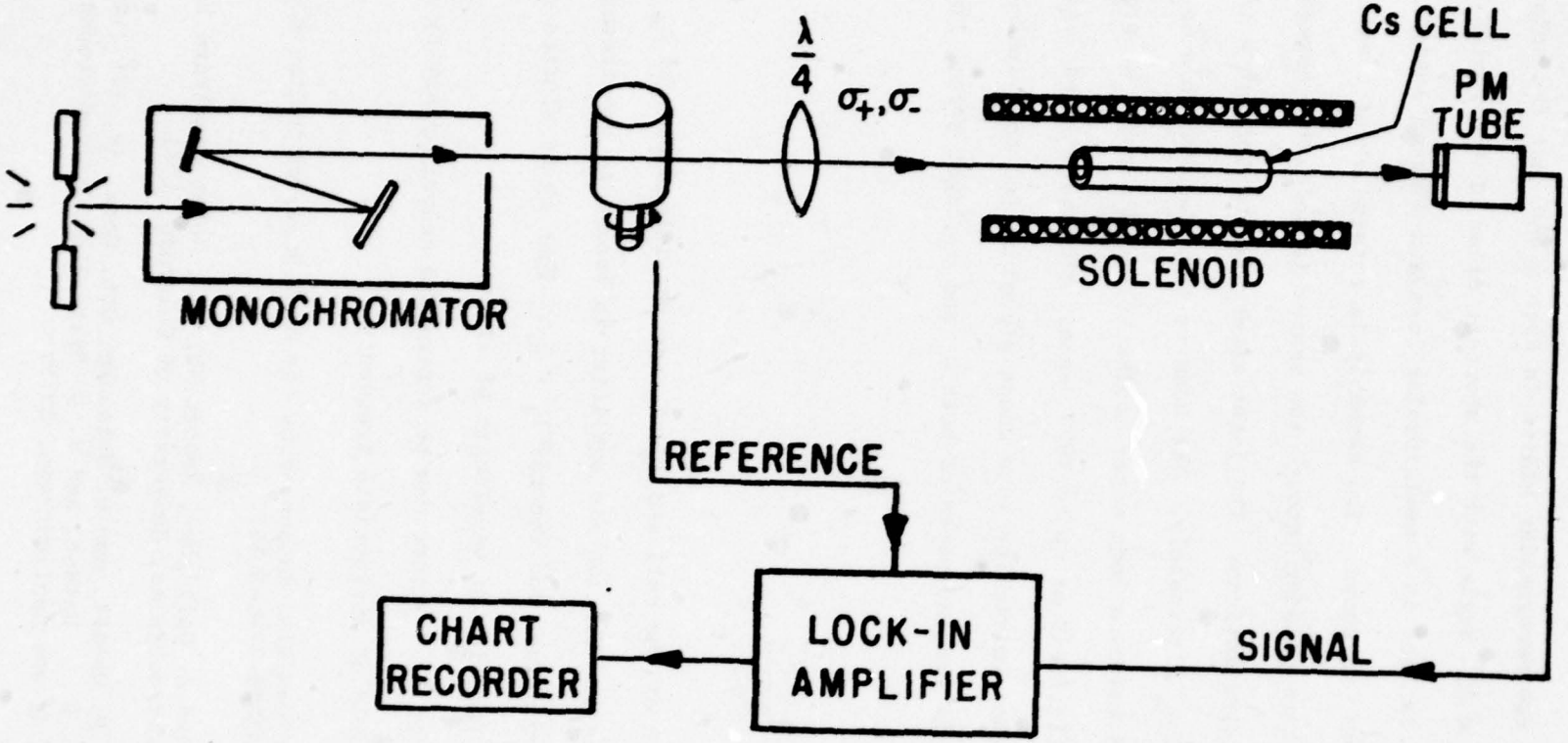

Figure 4: Experimental Arrangement.

illuminate the slit of a monochromater. The monochromatic light passes through a "rotating polariser".[5] This is shown in Fig. 5. A polaroid sheet is cut in two rectangular plates in such a way that the polarization direction makes a 45^{o} angle with the shortest sides of the plates. Each of these plates is bent in a semicircular form and mounted inside an aluminum cylinder as shown. The assembly is rotated about a vertical axis. A light beam passing through the center is modulated between two perpendicular polarizations. The light after passing through a $\lambda/4$-plate gives us σ_+ and σ_- alternately. The beam is then focused in a Cs_2 cell which is placed inside a long water cooled solenoid capable of producing an axial magnetic field of up to 3000 Gauss. The transmitted light is detected by a photomultiplier tube whose signal is fed to a lock-in amplifier. If I_o is the intensity of both σ_+ and σ_- light before the cell, then

$$\Delta k = \frac{I_+ - I_-}{I_o \ell} \tag{3}$$

ℓ is the length of the cell and I_+, I_- are the intensities of σ_+ and σ_- transmitted light. The lock-in amplifier is locked to the frequency of the rotating polarizer and records $I_+ - I_-$. Then Δk is plotted on a chart recorder as a function of wavelength of light.

The effect of "C" term can be determined unambiguously by applying a microwave field of appropriate frequency.

*This research was also supported by the Army Research Office (Durham) under Grant DAAG29-77-G-0015.

(1) G. York and A. Gallagher, Report No. 111, Joint Institute for Laboratory Astrophysics, University of Colorado, 1971.

(2) H. Itoh, H. Uehiki, and H. Matsuoka, Opt. Comm. 18, 271 (1971); M. Henesian, R. L. Herbst, and R. L. Byer, IEEE/OSA Conference on Laser Engineering and Applications, 1975.

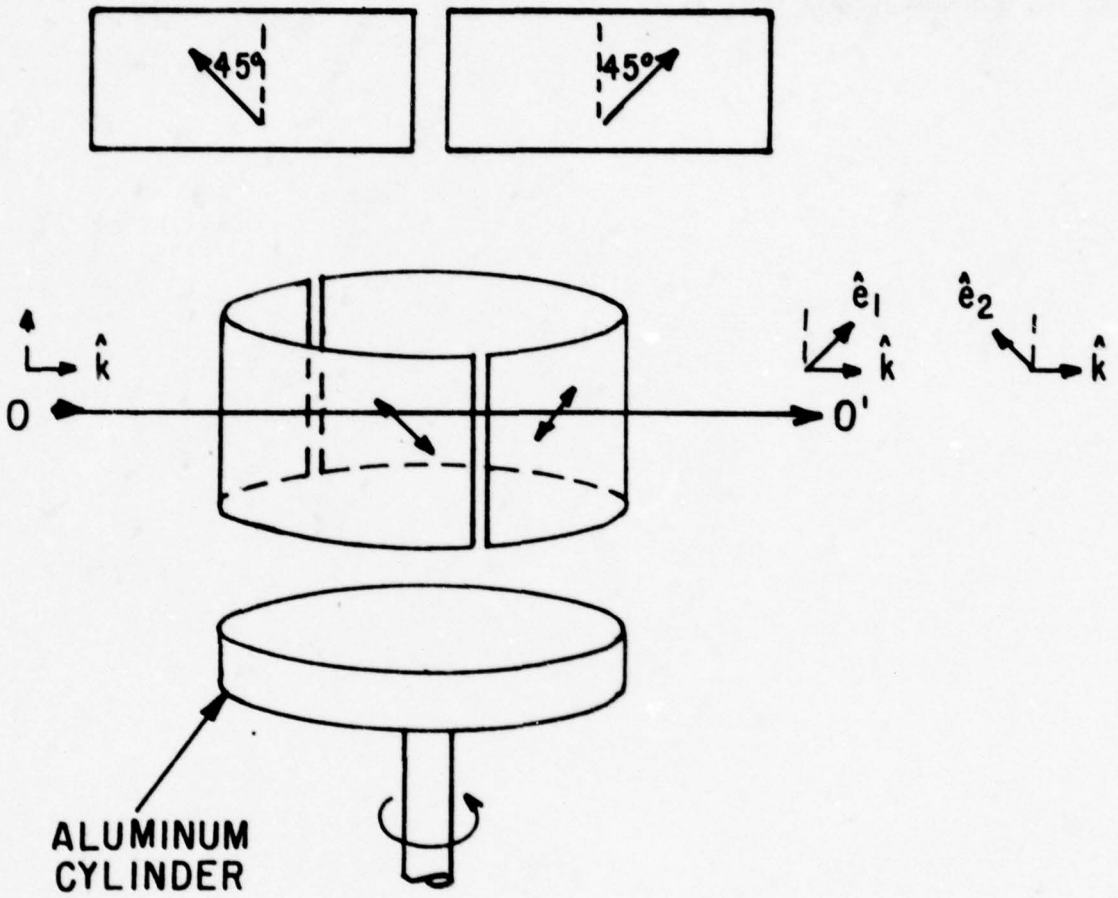

Figure 5: Exploded view of Polarizing Rotator OO' is the path of light along $\hat{k}$. Unpolarized incident light is polarized along $\hat{e}_1$ and $\hat{e}_2$ alternatively after passing through the center of cylindrical sheets.

(3) R. Gupta, W. Happer, J. Wagner, and E. Wennmyr, J. Chem. Phys. 68, 799 (1977).

(4) A. D. Buckingham and P. J. Stephans, Am. Rev. Phys. Chem. 17, 399 (1966).

(5) G. Rinzema, Appl. Opt. 9, (1970).

F. INFRARED ABSORPTION OF ALKALI MOLECULES*

(N. D. Bhaskar, E. Zouboulis, A. Vasilakis, W. Happer)

We have recently discovered new infrared absorption in potassium, rubidium and cesium saturated vapors out to at least 2.5μ. Chertoprud has reported absorption beyond the edge of the A band (1.1μ) in saturated potassium vapor.[1] He has ascribed this absorption to an intercombination transition ($X^1\Sigma_g^+ \rightarrow {}^3\Sigma_u^+$). We have recently completed studies of the temperature dependence of the new infrared absorption bands and these studies show clearly that Chertoprud's assignment, while plausible, cannot be correct. We believe the absorption from 1.1μ to 1.6μ to be the ${}^3\Sigma_u^+ \rightarrow {}^3\Sigma_g^+$ transition in the alkali dimer molecule. This is the analog of the ultraviolet emission continuum of the H_2 molecule. The absorption from 1.6μ to 2.0μ cannot be explained by dimers; however, it seems to be consistent with absorption from potassium trimers.

It is known that the absorption coefficient $\alpha_n(\lambda,T)$ for a cluster of n alkali atoms can be written as[2]

$$\alpha_n(\lambda,T) = C(\lambda)\exp[-(nE + V)/RT] \qquad (1)$$

where E is the latent energy of vaporization, n is an integer which is equal to the number of atoms in the cluster and V is the potential for which an electronic transition of wavelength λ is possible. Note that E can be written in terms of the latent heat ℓ as $E = \ell - RT$ where T is the temperature at which $\alpha_n(\lambda,T)$ is measured.

The slope of the graph log α vs. 1/T gives us the activation energy ($E(\lambda) = nE + V$). In the case of potassium $E = \ell - RT = 18.4$ Kcal at $T = 943^oK$. In Fig. 1C the activation energy of potassium as compared to 2E and

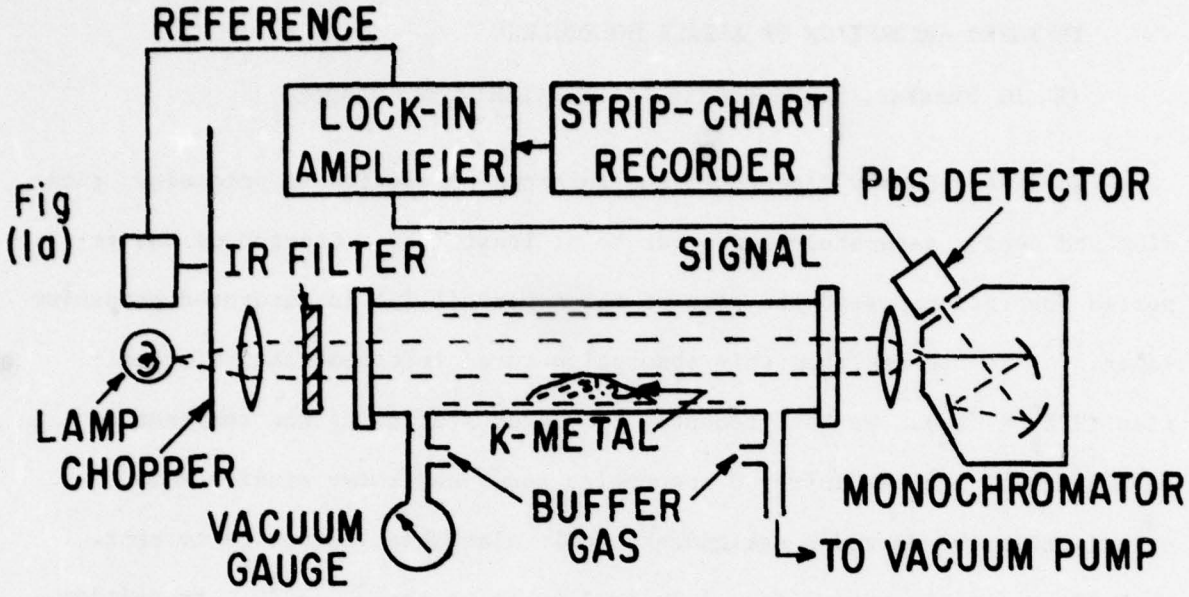
REFERENCE
LOCK-IN AMPLIFIER
STRIP-CHART RECORDER
PbS DETECTOR
IR FILTER
SIGNAL
LAMP
CHOPPER
K-METAL
VACUUM GAUGE
BUFFER GAS
MONOCHROMATOR
TO VACUUM PUMP

Fig (1a)

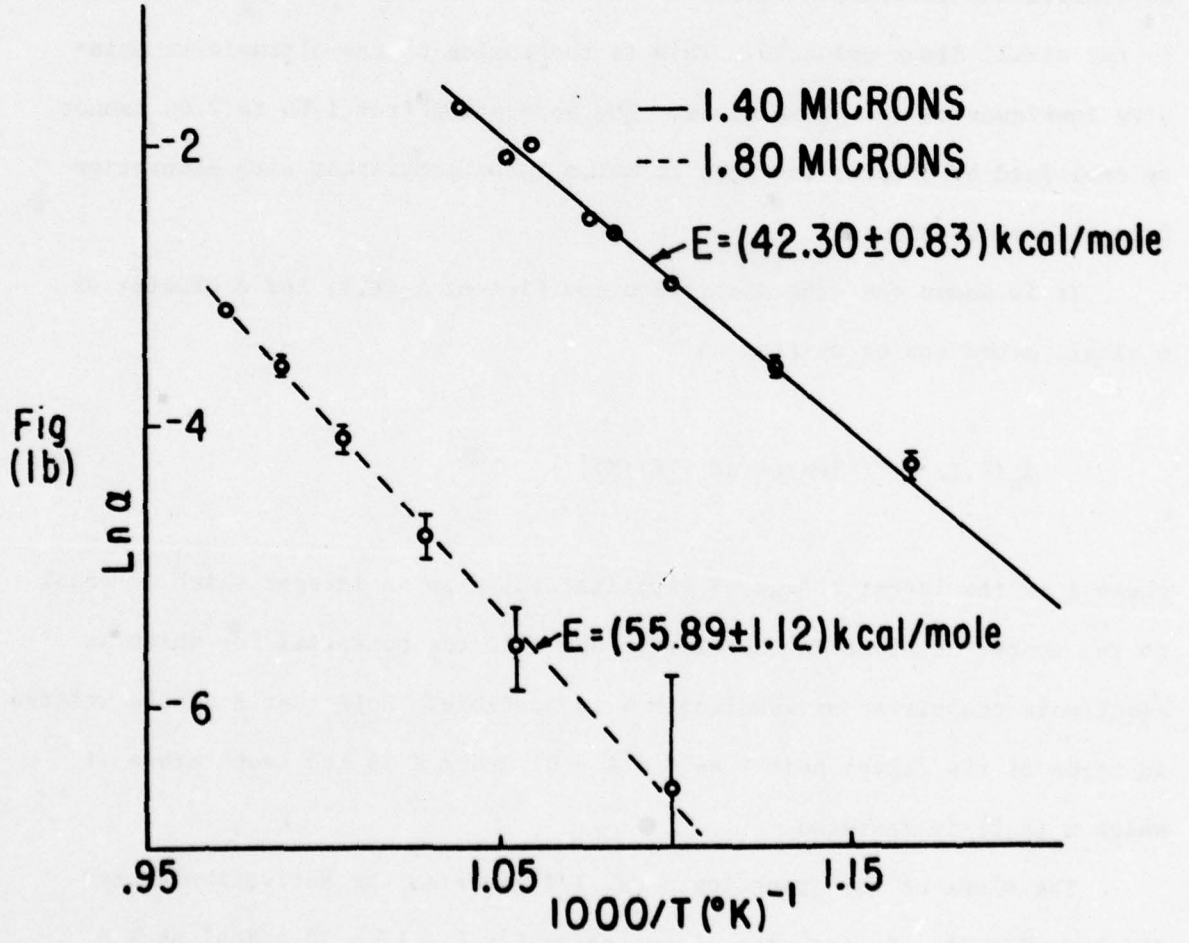
— 1.40 MICRONS
--- 1.80 MICRONS
E=(42.30±0.83) k cal/mole
E=(55.89±1.12) k cal/mole
-2
-4
-6
Ln α
.95
1.05
1.15
1000/T (°K)⁻¹

Fig (1b)

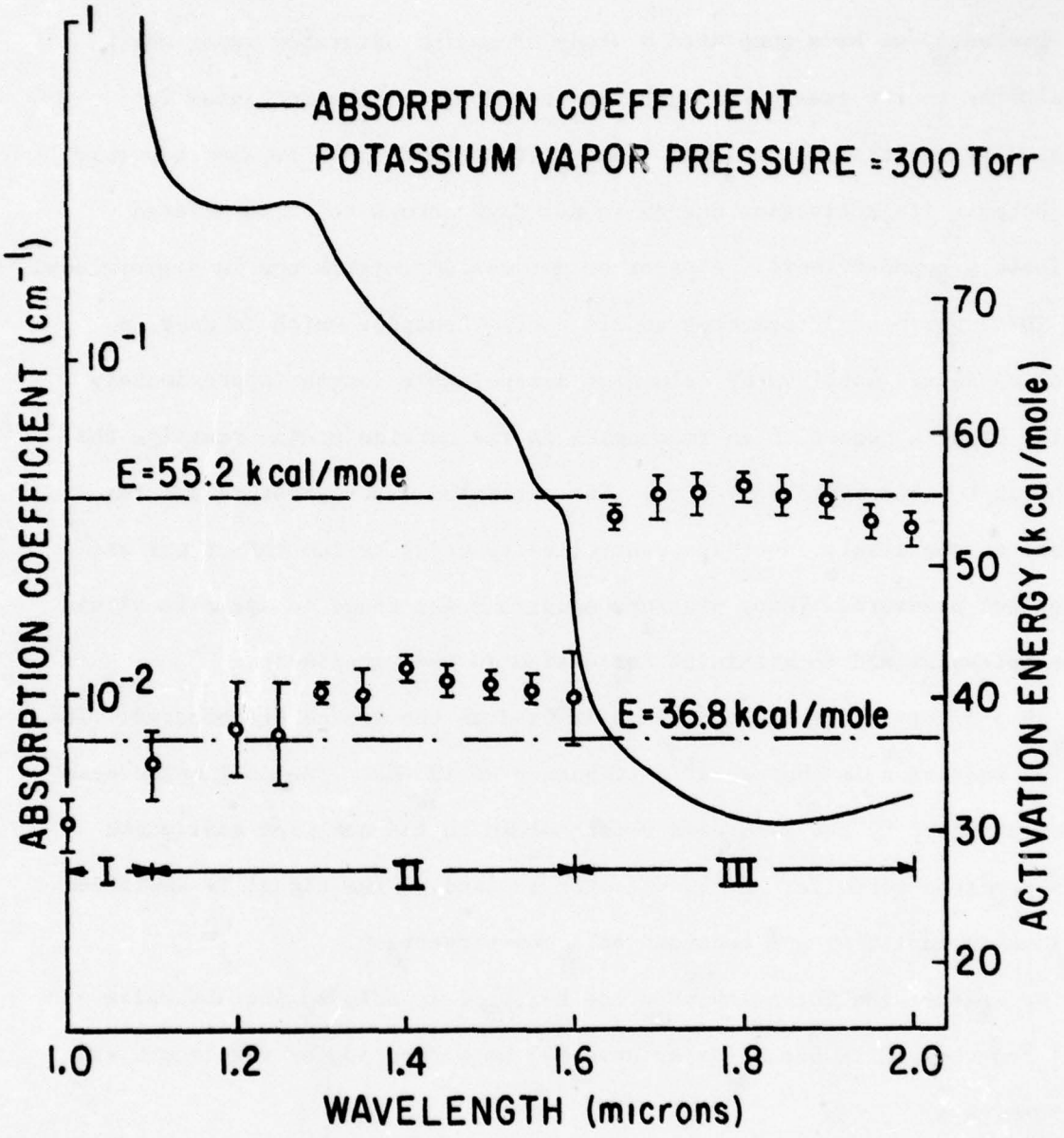
ABSORPTION COEFFICIENT
POTASSIUM VAPOR PRESSURE = 300 Torr
ABSORPTION COEFFICIENT (cm⁻¹)
1
10⁻¹
10⁻²
E=55.2 k cal/mole
E=36.8 kcal/mole
I
II
III
70
60
50
40
30
20
ACTIVATION ENERGY (k cal/mole)
1.0
1.2
1.4
1.6
1.8
2.0
WAVELENGTH (microns)

Fig. 1C:

3E is plotted as a function of λ.

Presently we have completed a study of cesium saturated vapor which also absorbs in the same wavelength region. However, the mechanism for this absorption is still unclear. The region beyond 1.92μ is also a puzzle to us because its activation energy is not high enough to be associated with loosely bound trimers. A paper on our cesium work is now in preparation.

The experimental apparatus consists of a heatpipe which is used to produce an alkali metal vapor column of determinable length (approximately 20 cm). Using a series of thermocouples on the outside of the heatpipe the length can be determined to ± 1 cm. The saturated vapor pressure and temperature of the alkali vapor are controlled by using helium buffer gas at the desired pressure. Vapor pressure equations are found to agree to within 1% for potassium and to within 5% for cesium in our experiment.

An ordinary quartz halogen lamp is used as the source of infrared. The infrared radiation is chopped at a frequency of 193 Hz. The collimated beam is then absorbed by the saturated vapor column in the heatpipe and imaged into a spectrometer slit. A PbS detector is used and the signal is amplified by a lock-in amplifier and recorded on a chart recorder.

We measure the intensity when the heatpipe is cold T_o (no absorbing vapor) and when it is hot T (vapor absorbs) as a function of wavelength and we determine α.

$$\alpha(\lambda,T) = Z^{-1} \ell n \left[\frac{I_o(\lambda,T_o)}{I(\lambda,T)} \right] \qquad (2)$$

As mentioned earlier, graphing log α vs. 1/T yields the activation energy which contains the information on $V(\lambda)$ and on nE. At present we are studying sodium in the infrared beyond 1.0μ up to 2.5μ. (We hope that in the case of sodium beyond the expected $^3\Sigma_u^+ \rightarrow {}^3\Sigma_g^+$ absorption we will see the trimers which

did not show up clearly in our cesium data.) In addition to this experiment we plan to go back to cesium in the future to clear up the mystery in its activation energy. A two temperature oven is being designed in the high temperature side of which pressure (P) and temperature (T) can be varied independently. If the absorption is proportional to the number density cubed, it is due to trimers. If it is proportional to the number density squared, then it is due to dimers. Other possible experiments in the future include studying rubidium and lithium in the infrared.

*This work was also supported by the Army Research Office (Durham) under Grant DAAG29-77-G-0015.

(1) V. E. Chertoprud, Teplofisfika Vysokikh Temperatur 14, 216 (1976).

(2) N. D. Bhaskar, E. Zouboulis, T. McClelland, and W. Happer, Phys. Rev. Lett. 42, 640 (1979).

G. OPTICAL PUMPING OF ALKALI VAPORS WITH SECOND RESONANCE LIGHT AND THE SPIN-EXCHANGE BOTTLENECK*

(J. Liran, J. Pietras, J. Camparo, W. Happer)

Our interest in ground state optical pumping of alkali atoms using second resonance excitation stems mainly from our concurrent interest[1]-[3] in the photochemical production of "laser snow" through the reaction

$$A^* + H_2 \longrightarrow AH + H \qquad (1)$$

A^* = alkali atom excited to second resonante

discovered in our laboratory in 1975.[4] By optically pumping a particular alkali vapor in the presence of H_2 with second resonance light, one can use radiofrequency spectroscopy to control the photochemical reaction in (1). For example, imagine optically pumping the Cs atoms in a cell containing Cs vapor and H_2 gas (plus buffer gas). At the point of complete spin polarization, the Cs vapor becomes transparent to the pumping light, and the production of laser snow ceases, since the reaction in (1) cannot occur. By applying RF or microwave magnetic resonance fields to depolarize the Cs, the Cs atoms can again be made to absorb the light, and the production of laser snow will resume. In this way, one can actually control the photochemistry of (1). Extending these ideas a step further, this scheme can also be used as a means of isotope separation in alkali metals. For instance, imagine optically pumping natural Rb (72% - Rb^{85}; 28% - Rb^{87}) in the presence of H_2 (plus buffer gas) so both isotopes are completely spin polarized. By applying RF or microwave magnetic resonance fields tuned to the resonance of one isotope (e.g. Rb^{85}), atoms of that isotope will depolarize and so be made to absorb the pumping light. Hence, those atoms (Rb^{85}) will react as in (1) to form laser snow. The isotopically (Rb^{85})

enriched snow could then be collected by electrostatic precipitators since the snow is highly charged.

Another reason for interest in optical pumping with second resonance light follows from the fact that the alkali vapors are much less optically thick to second resonance light than to first resonance light ($\sim$ a factor of 100) for a particular atomic density. Thus, optical pumping with the second resonance line permits one to study alkali vapors of much larger densities - a region where some interesting phenomena have been observed.[5]-[7]

We have recently been successful in optically pumping Cs using the second resonance - D_1 excitation ($6S_{1/2} \rightarrow 7P_{1/2}$) of the atom. This has been greatly facilitated by our success in maintaining a workable laser, tunable in the blue part of the spectrum. Our laser consists of a Spectra Physics model 375 dye laser containing Stilben - 3 dye, pumped by a Spectra Physics model 171-19 Ar+ laser operating in the U.V. Tuning of the dye laser is done by a three plate birefringent filter (Spectra Physics model 573). This laser yields a typical output power of 200 mW at 4593 Å for 2.8N of U.V. and a linewidth of $\sim$40GHz. It allows us to tune directly onto the second resonance -D_1 line of Cs (4593 Å) without the necessity of large pressure broadening of the atomic line (as done previously).[4]

The experimental arrangement used in optically pumping Cs and measuring the degree of spin polarization is shown in Fig. 1. Linearly polarized light at 4593 Å emerging from the dye laser is circularly polarized by a quarter wave plate. This light passes into a Corning 1720 - aluminosilicate glass cell containing Cs metal, N_2 "quenching" gas ($\leq$ 200 torr), and He buffer gas ($\sim$ 760 torr). The cell is heated by a resistance coil, and its temperature ranges between 80°C and 180°C. In order to eliminate instrumental scattering, the number of excited Cs atoms is measured by D_1 first resonance

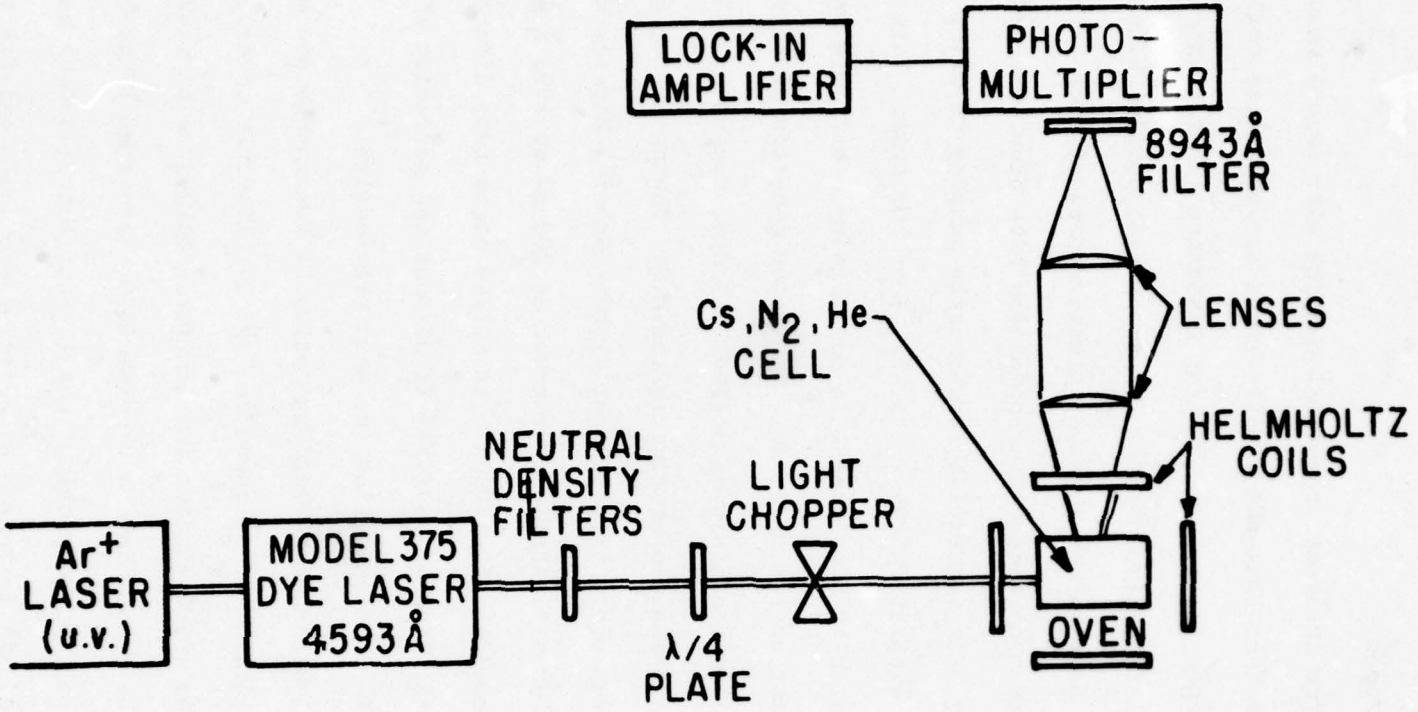

Figure 1: Cs optical pumping by second resonance excitation - experimental set-up

fluorescence (8943 Å). The fluorescence at 90° to the laser beam is focused onto a RCA-8853 photomultiplier equipped with a 8943 Å interference filter. The photomultiplier signal is averaged by a PAR model HR-8 lockin amplifier. A set of Helmholtz coils is present to supply a longitudinal magnetic field (∿1G) along the light when optically pumping, or to create a transverse depolarizing field. The degree of spin polarization is calculated by measuring the fluorescence signal when optically pumping, F_p, and the fluorescence when no polarization is present, F_{Np}, i.e.

$$2 \langle S_z \rangle = \frac{F_{Np} - F_p}{F_{Np}} \qquad (2)$$

where $\langle S_z \rangle$ is the average z-component of electron spin. A set of neutral density filters was used for measuring the degree of polarization as a function of pumping light power.

Earliest optical pumping signals were observed in a cell containing Cs + N_2(10T) + He (739T) at temperatures between 95°C - 160°C (where the flourescence signal is easily measurable and the vapor is not to optically thick). For these conditions, it was expected that 100% spin polarization would be achieved, since the estimated optical pumping rate, R(∿ $10^4 sec^{-1}$ at 200 mW), exceeds the estimated spin depolarization rate (∿ 100 sec^{-1}, due to collisions with He buffer gas and diffusion from the beam). Furthermore, 10T-N_2 was expected to quench the fluorescence sufficiently so no radiation trapping would hamper the degree of polarization. (For 10T-N_2, the quenching rate is ∿2.5 times the fastest radiative decay rate: $6P_{3/2} \rightarrow 6S_{1/2}$.) The results of the spin polarization measurements for this cell, as a function of dye laser power, for a number of temperatures are shown in Fig. 2. As indicated by the graphs, the polarization seems to

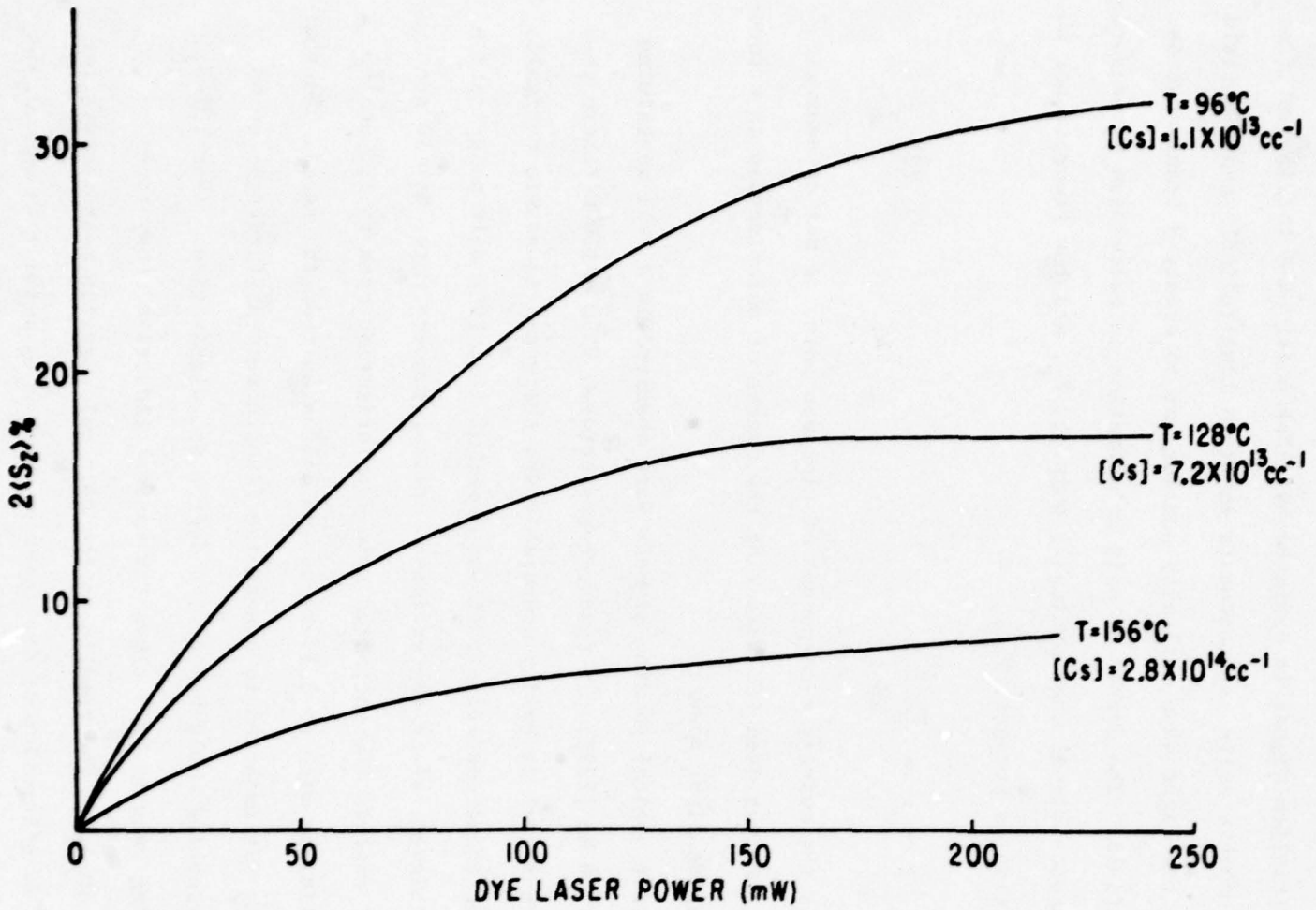

Figure 2: Percent polarization vs. dye laser power for cell: Cs + N_2(10T) + He(739T) (average data curves)

have a saturating effect with laser power (pumping rate), where the level of polarization reached at a particular laser power - say 200 mW - is strongly temperature dependent, and far below the 100% polarization expected. Since radiation trapping is a possible mechanism for such a saturation of the polarization below 100%, cells with higher N_2 pressures were tried. The results for cells with 97T N_2 and 200 T-N_2 are shown in Figs. 3 and 4, respectively. These graphs indicate that the results for 97T-N_2 and 200T-N_2 agree exactly, while when compared to the previous 10T-N_2 results, an increase in polarization for similar temperatures and laser powers is obvious. Furthermore, the saturation of the polarization with laser power is less pronounced in the higher N_2 pressure results, although still present.

In an effort to understand these results, we considered two possible mechanisms for the bottleneck to 100% polarization: radiation trapping and spin-exchange. According to our calcualtions the N_2 pressures in all our cells efficiently quench the excited state, so that the effect of trapping should be negligible. That trapping is negligible at N_2 pressures $\leq$ 100T is shown by the complete similarity of the results of Fig. 3 and 4.) To more fully understand the effect of spin-exchange on our opticalpumping experiments we formulated a rate equation for the density matrix, and then numerically solved for the steady state solution.

As a model we considered repopulation pumping of an alkali ground state using D_1 circularly polarized light in the presence of electron spin randomization (due to buffer gas collisions) and rapid spin-exchange. Thus the rate equation consists of three terms, expressions for which were found in the literature.[6][8] In steady-state we have the matrix equation:

$$\frac{d}{dt}\rho ij=0=\sum_{k,\ell}\left[R_p R_{ij,k\ell}+\gamma E_{ij,k\ell}+\frac{1}{\tau}(E_{ij,k\ell}+\langle S_z\rangle Q_{ij,k\ell})\right]\rho k\ell \qquad (3)$$

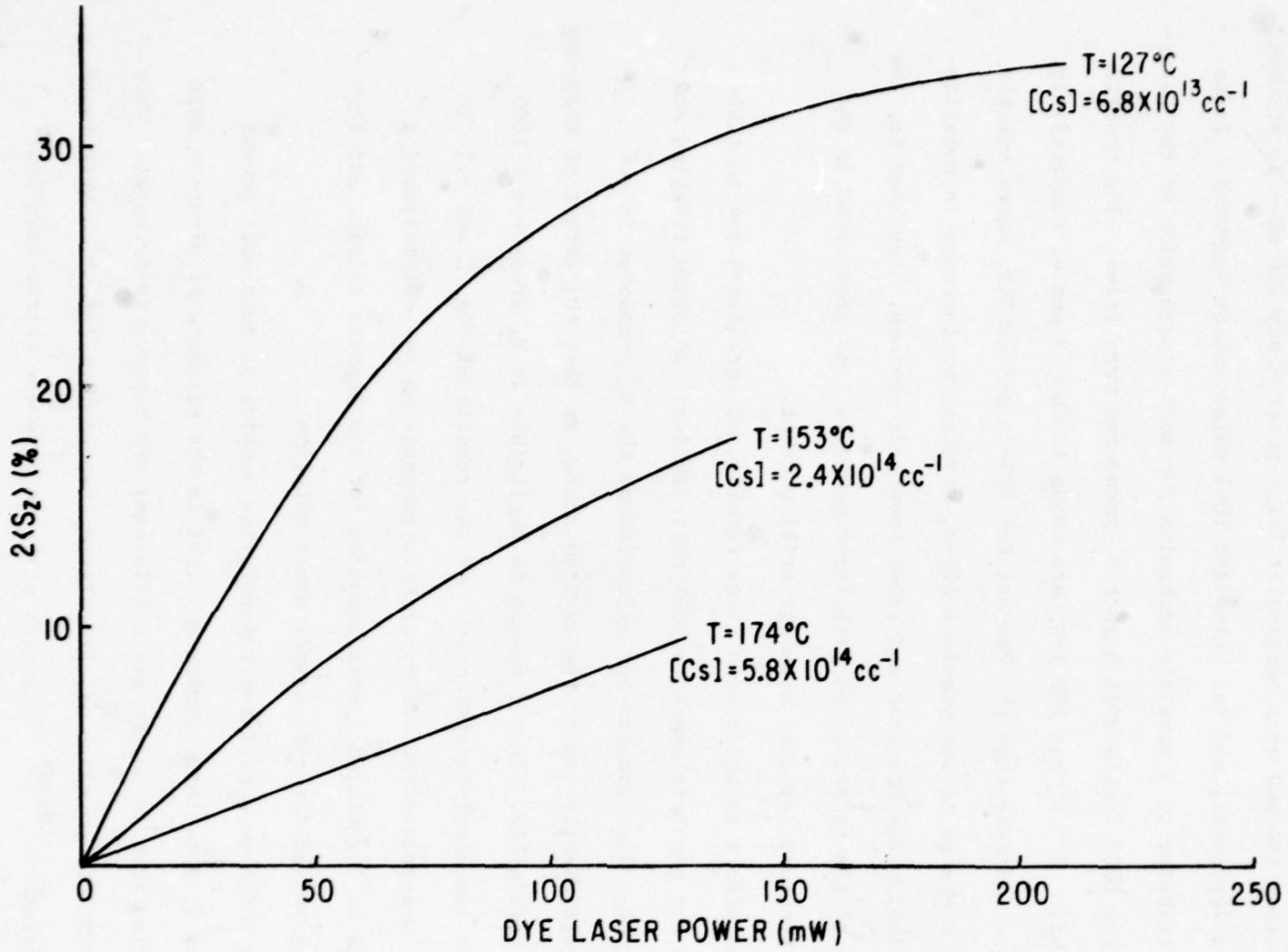

Figure 3: Percent polarization vs. dye laser power for cell: Cs + N_2(97T) + He(630T) (average data curves)

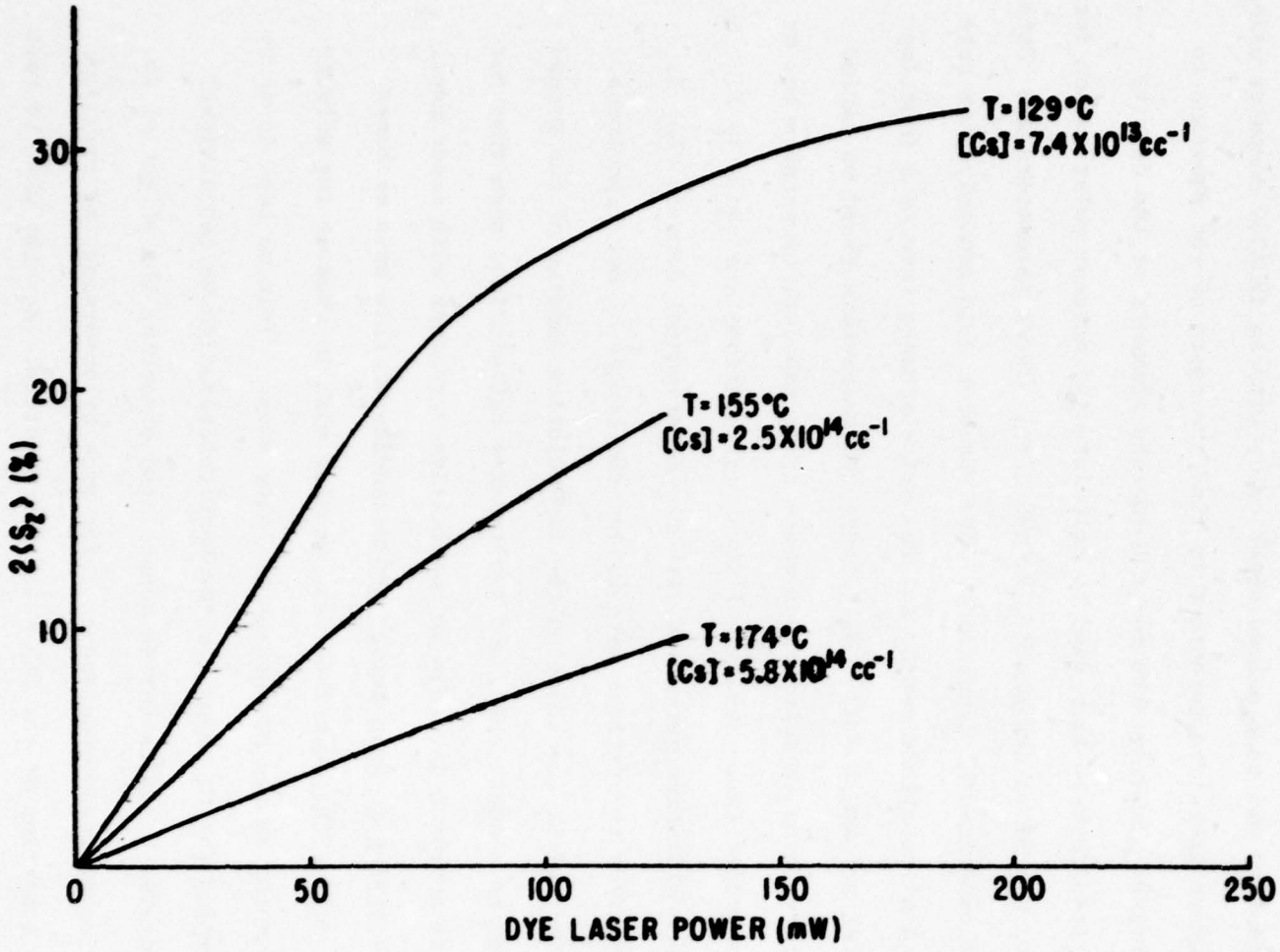

Figure 4: Percent polarization vs. dye laser power for cell: Cs + N_2(200T) + He(530T) (average data curves)

where R_p, γ, and $1/\tau$ represent the pumping rate, electron spin randomization rate, and spin-exchange rate respectively.

This equation was then solved numerically with an IBM/360 computer using a Newton-Rapheson iterative technique to find the roots of the equation to within the desired accuracy--the roots being the elements of the density matrix. The results were then used to calculate the percent polarization for various values of the parameters R_p, γ, and $1/\tau$. These parameters are determined by the experimental conditions. The electron spin randomization rate is fixed for a given alkali metal, and the spin-exchange rate is a function of alkali metal and temperature. With these two parameters fixed we varied the pumping rate so as to cover cases where R_p is smaller, comparable to, or larger than γ and/or $1/\tau$. Results of these calculations are shown in Fig. 5. Fig. 5a shows qualitative agreement with the experimental data of Fig. 3, while Fig. 5b gives theoretical data beyond the limits of our experiment.

The effect of N_2 quenching on the repopulation pumping of the ground state has also been considered, and preliminary calculations show that our density matrix approach is again in qualitative agreement with experiment.

Besides trying to gain better understanding of this spin exchange "bottleneck" during the next interval, we also wish to observe the effects of optical pumping on the production of laser snow. This we hope to do by optically pumping the Cs atoms (to the best polarization we can achieve) in a cell containg H_2 (plus buffer gases), and observing the effect of Cs optical pumping on the production of laser snow by observing the spectral intensity of a portion of the CsH molecular spectrum. We also wish to test the isotopical selectivity of the laser snow by selectively exciting one isotope of Rb to its second resonance level in a cell containing natural Rb plus H_2 gas, with hope of forming isotopically enriched snow. This work will

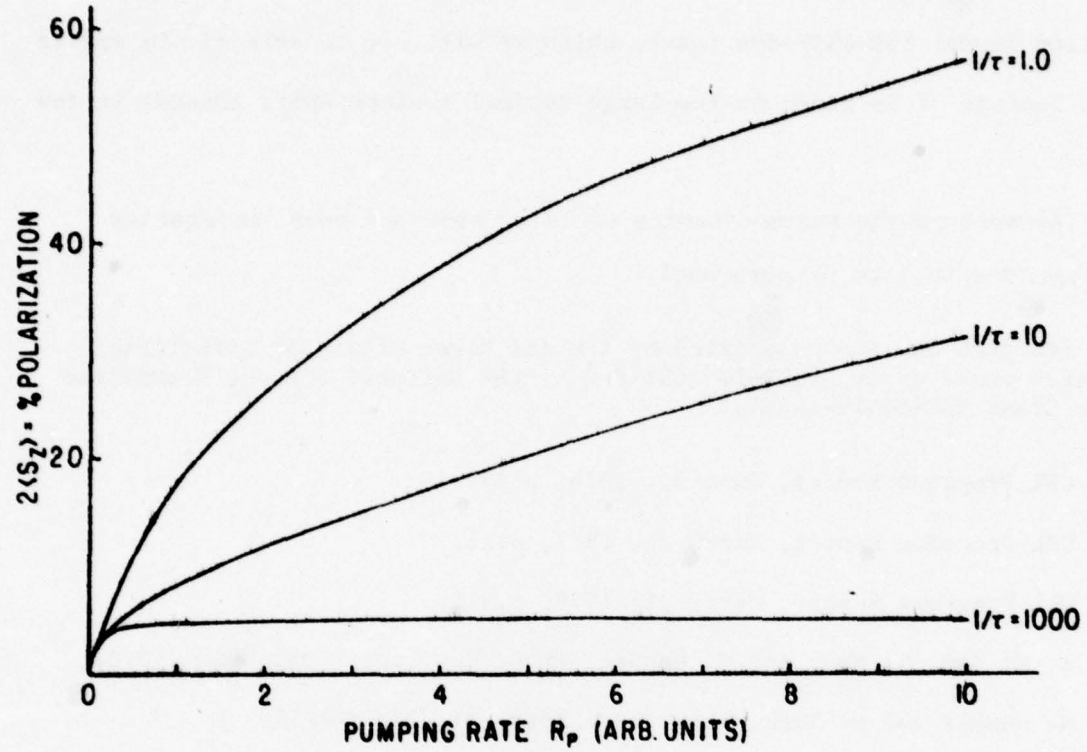

Figure 5a

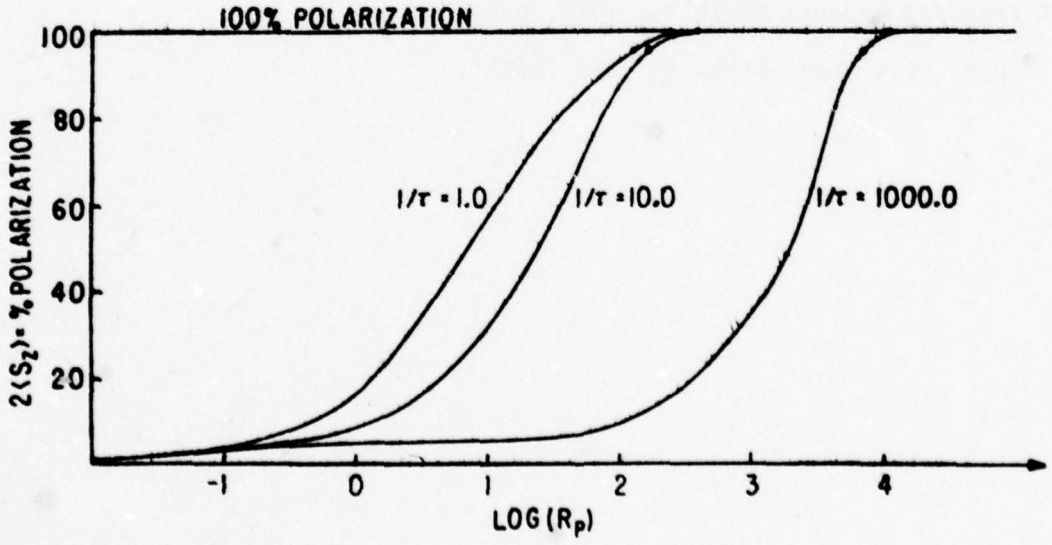

Figure 5b

Theoretical curves of percent polarization vs. pumping rate

soon be possible upon arrival of our newly purchased single mode Coherent Radiation (model 599-D3E) dye laser, which we will use to selectively excite either isotope of Rb based on the large optical isotope shift present (a few GHz).

The work on the thermodynamics of laser snow has been temporarily postponed, due to lack of personnel.

*This research was also supported by the Air Force Office of Scientific Research under Grant AFOSR-74-2685 and by the National Science Foundation under Grant NSF-ENG76-16424.

(1) CRL Progress Report, June 30, 1976, p.27

(2) CRL Progress Report, March 31, 1977, p.26.

(3) CRL Progress Report, March 31, 1978, p.315.

(4) A. C. Tam, G. Moe, and W. Happer, Phys. Rev. Lett. 35, 1960 (1975).

(5) W. Happer and H. Tang, Phys. Rev. Lett. 31, 273 (1973).

(6) W. Happer and A. C. Tam. Phys. Rev. 16, 1877 (1977).

(7) CRL Progress Report, March 31, 1977, p.1.

(8) W. Happer, Rev. Mod. Phys. 44, 169 (1972).

H. SPECTROSCOPY OF THE 5D STATE OF Cs^{133}*

(A. Sharma, W. Happer)

We have undertaken to observe the hyperfine structure of the 5D state of Cs^{133} and determine the quadrupole moment Q of its nucleus. The best currently known value[1] of the quadrupole moment, to our knowledge, is -.0036 (13) barns. The accuracy of this result is indeed very poor as the corresponding value for most of the other alkali atoms is known to a relatively much higher precision . The quadrupole moment of Cs^{133} is unusually small compared to that for other atoms and as such, the contribution that this makes to the hyperfine splitting is not much different from the natural line width of most of the states. Almost all of the measurements to determine the quadrupole moment of Cs^{133} have been done on one of its P states. The life time for the 6P and 7P states is respectively 3×10^{-8} sec. and 10^{-7} sec. The idea in working with the 5D state is that its life time is 10^{-6} sec. and therefore the natural linewidth much smaller. We thus hope to determine Q of Cs^{133} to a much higher accuracy.

The 5D state has its own special problems. We intend to populate it by using an argon ion laser to excite Cs^{133} to its 7P state and letting it cascade down to the 5D state. We will apply radiofrequency to the 5D state and observe resonances in the perturbed fluorescence as the atoms decay to the 6P states. The three wavelengths corresponding to this transition are 3.01 μm; 3.48 μm; 3.61 μm; all of which lie in that range of the infrared spectrum where the solid state detectors have a relatively bad signal to noise ratio. We intend trying a lead sulphide detector cooled to liquid nitrogen temperature. Also the gas cells must have a sapphire window as ordinarily glass and quartz are opaque in this region due to the presence of water

vapor absorption band around the wavelengths of interest. For the same reason, we are using lenses made of zinc sulphide which has a 70% transparency to these wavelengths. Also one must be careful to avoid absorption of the signal by atmospheric water vapor. A schematic diagram of the experimental set up is given in Fig. 1.

*This research was also supported by the Army Research Office (Durham) under Grant DAAG29-77-G-0015.

(1) H. Bucka, H. Kopfermann, and E. W. Otten, Ann. Physik 4, 39 (1959).

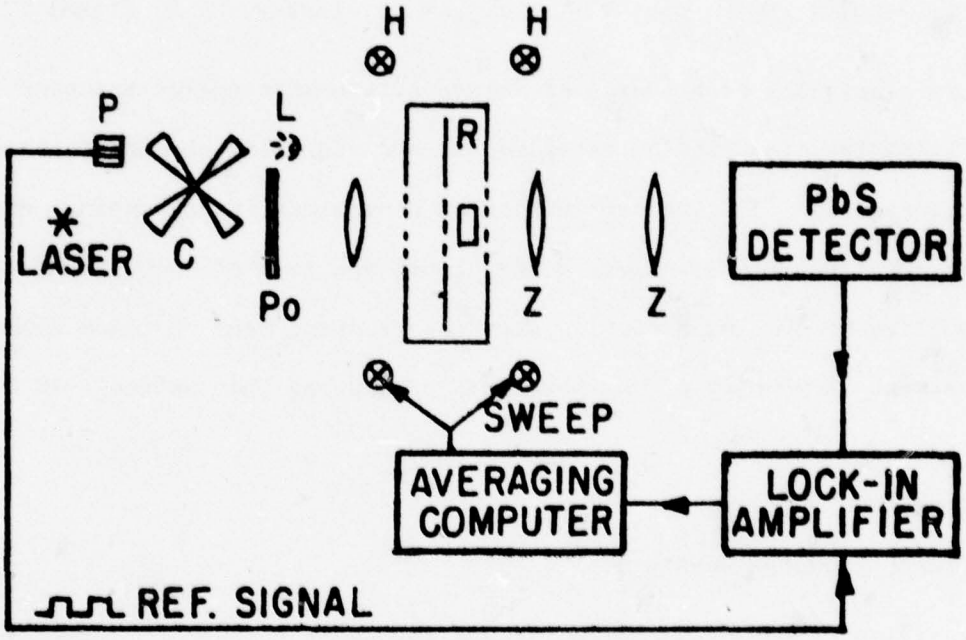

P	Photocell	H	Helmholtz Coils
C	Chopper	R	Resonance Cavity
P_o	Polarisers	Z	ZnS Lens
L	Lamp		

Figure 1

II. RELAXATION AND ENERGY TRANSFER IN SMALL POLYATOMIC MOLECULES

A. RELAXATION, INFRARED MULTIPHOTON PHOTODISSOCIATION, AND VIBRATIONAL TEMPERATURES IN LASER PUMPED COF_2*

(K. Casleton, Y. V. C. Rao, R. Sheorey, M. I. Lester, G. W. Flynn)

COF_2 is a uniquely rich source of data for intermode energy transfer studies, multiphoton dissociation experiments, and vibration-electronic energy transfer processes.[1] [2] The combination of convenient laser pumping, strong IR emission, and a relatively dilute energy level spectrum all contribute to the desireability of COF_2 as a model system for studying many of these fundamental processes. A summary of our progress in studying this molecule is as follows:

a) Energy Transfer

The energy transfer events

$$COF_2(\nu_2) + M \rightleftharpoons COF_2(\nu_6) + M + 199\ cm^{-1} \quad (1)$$

$$COF_2(\nu_6) + M \rightleftharpoons COF_2(\nu_3,\nu_5) + M + 167\ cm^{-1} \quad (2)$$

$$COF_2(\nu_2) + M \rightleftharpoons COF_2(\nu_3,\nu_5) + M + 366\ cm^{-1} \quad (3)$$

require on the average 500, 175, and $\geq$ 1500 COF_2/COF_2 collisions, respectively. Event (1) is one of the slowest intermode energy transfer events known for a polyatomic and is particularly remarkable when compared to (2) which is noticeably more efficient. Overall V-T/R relaxation

$$COF_2(\nu_3) + M \longrightarrow COF_2(0) + M + 583\ cm^{-1} \quad (4)$$

requires 2300 collisions on the average for M = COF_2.

b) Multiphoton Dissociation

We have observed infrared multiphoton photodissociation of COF_2 via

$$COF_2 + n\hbar\nu \longrightarrow COF + F$$

The F atoms were detected by adding H_2 or CH_4 to the system and observing infrared chemiluminescence[3][4] from HF*

$$F + RH \longrightarrow R + HF\ (v \geq 0) \qquad (5)$$

$$HF(v \geq 1) \longrightarrow HF(v - 1) + h\nu(\lambda \sim 2.5\mu) \qquad (6)$$

We find that F atoms are produced and appear to have a thermal (ambient) velocity distribution. Under the proper conditions the process is purely optical since no ions have been detected.

c) Vibrational Temperature Measurements

We have used the cold gas filter method[5] to make a preliminary measurement of the C=O stretch (ν_1) peak vibrational temperature under strong laser excitation conditions. Though these studies require further experimental data, the peak temperatures in the COF_2 mode appear to exceed 1500 ^oK before loss of energy from ν_2 via step (1) occurs. (The ν_1 and ν_2 modes are brought into rapid equilibrium (30 collisions) via

$$2COF_2(\nu_2) \rightleftharpoons COF_2(\nu_1) + COF_2(0) \qquad (7)$$

after laser pumping of ν_2.)

If ν_1 can be made very hot, vibrational energy transfer from high lying levels of this mode (e.g. (7-10) ν_1) to electronic states of other atoms or molecules should be possible via a collisional vibration/electronic energy exchange process.

*This research was also supported by the National Science Foundation under Grant NSF-CHE-77-24343. The laser chemistry work is being transferred to DOE contract ER-78-S-02-4940.

(1) K. Casleton and G. Flynn, J. Chem. Phys. 67, 3133 (1977).

(2) Progress Report #28, Columbia Radiation Laboratory, March 31, 1978 pp. 46-66.

(3) J. Preses, R. Weston, and G. W. Flynn, Chem. Phys. Lett. 48, 425 (1977).

(4) C. R. Quick, Jr and C. Wittig, Chem. Phys. Lett. 48, 420 (1977).

(5) R. McNair, S. Fulghum, G. Flynn, M. J. Feld, and B. Feldman, Chem. Phys. Lett. 48, 241 (1977).

B. ENERGY TRANSFER IN $SO_2/^{18}O_2$ MIXTURES*

(M. I. Lester, G. W. Flynn)

The infrared laser-induced fluorescence technique has been successfully used to monitor state-to-state energy transfer processes in simple polyatomic molecules. The rates of these vibrational to vibrational (V-V) and vibrational to translational/rotational (V-T/R) processes yield information on the mechanisms for efficient vibrational energy exchange, storage and relaxation. In this work, the rates of vibrational energy transfer from SO_2 to $^{18}O_2$ and $^{16}O_2$ have been studied. A comparison of the rate for crossover to each of the oxygen isotopes is important in probing the methods of vibrational energy equilibration since only the energy gap between reacting species has been changed.

The symmetric stretching mode (ν_1) of SO_2 was excited by a standard Q-switched CO_2 laser which has previously been described in detail.[1] Laser-induced fluorecence emanating from the asymmetric stretch (ν_3) of SO_2 at $\lambda = 7.4\ \mu$ has been studied in the presence of large amounts of $^{18}O_2$ and $^{16}O_2$. The overall characteristics of SO_2 ν_3 fluorescence in $SO_2/^{18}O_2$ mixtures was different from that seen to date for pure SO_2,[2][3] SO_2/rare gas mixtures,[2][3] and $SO_2/^{16}O_2$ mixtures.[3] In the SO_2 systems previously investigated, the fluorescence consisted of a single exponential rise and fall. In the case of $SO_2/^{18}O_2$ mixtures, a single exponential rise followed by a <u>double</u> exponential decay was observed.

The fluorescence rise in $SO_2/^{18}O_2$ mixtures corresponds to the filling of ν_3 from the pump mode by rapid collisional energy transfer. The appearance of a fast component to the decay may be attributed to an energy sharing process with $^{18}O_2$. The decay then slows as the coupled $SO_2/^{18}O_2$ vibrational

manifolds relax to ambient conditions. No similar evidence for a V-V energy crossover from SO_2 to $^{16}O_2$ has been observed by the fluorescence technique.

The rate of the fast decay process has been measured at fixed $SO_2/^{18}O_2$ mole fraction ratios as a function of total pressure. A plot of this rate versus pressure data for a $SO_2/^{18}O_2$ partial pressure ratio ($P_{SO_2}/P_{^{18}O_2}$) of 1/5.74 has a slope of 3.2 ± 0.2 msec^{-1}torr^{-1}. The corresponding slope for $P_{SO_2}/P_{^{18}O_2} = 1/2.50$ was found to be 4.3 ± 0.3 msec^{-1}torr^{-1}. The error estimates are 2σ values from the least-square fits.

The microscopic rate coefficients for energy crossover from SO_2 to $^{18}O_2$ can be determined from the observed rate coefficients of the ν_3 fluorescence. This deconvolution process must be based on an appropriate kinetic model for the coupled $SO_2/^{18}O_2$ system. The dominant energy transfer mechanism for pure SO_2 gas has been determined to be[2]

$$SO_2(\nu_1) + M \rightleftharpoons SO_2(\nu_3) + M - 210 \text{ cm}^{-1}\text{(fast)} \qquad (1)$$

$$SO_2(\nu_1) + M \longrightarrow SO_2(2\nu_2) + M + 120 \text{ cm}^{-1} \text{ (slow)} \qquad (2)$$

The stretching modes ν_1 and ν_3 equilibrate quickly compared to the relaxation rate of these modes through the bending mode (ν_2). Thus, for a relatively long time a metastable steady state is established in the ν_1 and ν_3 modes.

With the addition of $^{18}O_2$, the vibrationally hot SO_2 stretching modes can energy transfer to $^{18}O_2$ via the translationally endothermic process

$$SO_2(\nu_3) + {}^{18}O_2(0) \underset{k_b}{\overset{k_f}{\rightleftharpoons}} SO_2^{(0)} + {}^{18}O_2^{(1)} - 107 \text{ cm}^{-1} \qquad (3)$$

Based on the assumption that the equilibration of the stretching manifold is much faster than the rate of $SO_2/^{18}O_2$ crossover, the observed fast decay rate, γ_{OBS}, for $SO_2(\nu_3)$ fluorescence at a specific mole fraction of $^{18}O_2 (X_{^{18}O_2})$

would be[4][5]

$$\frac{\gamma_{OBS}}{P_{TOTAL}} = F_3 k_f X_{^{18}O_2} + k_b (1 - X_{^{18}O_2})$$

where F_3 is the fraction of vibrationally excited SO_2 population in the ν_3 asymmetric stretch. Detailed balancing of equation (3) yields a relationship of $k_b = 1.673\ k_f$ at room temperature . The rate of the fast exponential decay at the mole fraction mixtures studied predict to excellent agreement an experimental value of $k_f = 6.5 \pm 0.6$ msec^{-1}torr^{-1} for the molecular rate constant. This is equivalent to gas kinetic rate of approximately 1300 collisions. The corresponding k_b value is 10.9 ± 1.0 msec^{-1}torr^{-1} or 800 gas kinetic collisions.

Thermal lensing measurements,[6][7] which are a sensitive probe of the translational temperature of a gas following laser excitation, have been made on specific mole fraction mixture of SO_2 with $^{18}O_2$ and Ar. Some additional cooling has been observed in the case of $SO_2/^{18}O_2$ sample. The extra translational cooling indicates that the crossover to oxygen occurs by the proposed endoergic path (3).

In addition to the laser-induced infrared fluorescence technique described here, V-V and V-T/R energy transfer rates for small polyatomics have also been measured by ultrasound dispersion methods. A sound absorption study in $SO_2/^{16}O_2$ mixtures indicates a V-V coupling between the asymmetric stretch, ν_3, of SO_2 and the fundamental mode in $^{16}O_2$.[8] The rate of energy transfer reported, $M_\mu P_{01}(3,4,\mu)$, is 0.26 msec^{-1}torr^{-1} or approximately 33,000 gas kinetic collisions. This rate is 30 times slower than the rate reported here for energy transfer from $SO_2(\nu_3)$ to the $^{18}O_2$ isotope. This rate is much slower than the overall relaxation rate of $SO_2(\nu_3)$ as measured

by fluorescence in $SO_2/^{16}O_2$ systems.[3]

Theoretical calculations are now in progress to calculate the probability of energy transfer for the $SO_2(\nu_3)/^{18}O_2$ and $SO_2(\nu_3)/^{16}O_2$ systems. Order of magnitude probabilities have been predicted by a simple SSH-breathing sphere calculation.[9]-[11] The range parameter for the short-range potential α, was assigned a value of 5.0×10^{-8} cm^{-1} as in the case of other SO_2 calculations.[12] Values of the breathing sphere parameters, as defined in Stretton[11] are 0.015, 0.111, and 0.125 amu^{-1} for the $SO_2(\nu_3)$, $^{18}O_2(1)$, and $^{16}O_2(1)$ fundamentals, respectively. The SSH model predicts a rate of 1700 gas kinetic collisions for energy crossover to $^{18}O_2$ and a corresponding rate of 9400 collisions to $^{16}O_2$. The agreement between theory and experiment is extremely good for energy transfer to $^{18}O_2$. However, a large discrepency exists between SSH theory and the ultrasound results for $^{16}O_2$.

Future work includes application of the vibrational energy transfer theory of Sharma and Brau[13][14] to SO_2/O_2 systems. The theory is based on the role of long-range forces in causing vibrational-rotational energy transfer. In this case the long range interaction is caused by the instantaneous dipole moment of SO_2 with the quadrupole moment of oxygen. The Sharma-Brau theory is expected to give a more accurate theoretical prediction of the probability of energy-transfer from SO_2 to O_2 than possible by SSH-theory.

*This research was also supported by the National Science Foundation under Grant NSF-CHE-77-24343.

(1) E. Weitz, G. W. Flynn, and A. M. Ronn, J. Chem. Phys. 56, 6060 (1972).

(2) D. Siebert and G. W. Flynn, J. Chem. Phys. 62, 1212 (1975).

(3) G. A. West, R. E. Weston, and G. W. Flynn, J. Chem. Phys. 67, 4873 (1977).

(4) J. Preses, G. W. Flynn, and E. Weitz, J. Chem. Phys. 69, 2782 (1978).

(5) T. L. Cottrell and J. C. McCoubrey, Molecular Energy Transfer in Gases (Butterworths, London, 1961) p. 31-32.

(6) F. R. Grabiner, D. R. Siebert, and G. W. Flynn, Chem. Phys. Lett. 17, 189 (1972).

(7) D. R. Siebert, F. R. Grabiner, and G. W. Flynn, J. Chem. Phys. 60, 1564 (1974).

(8) B. Anderson, F. D. Shields, and H. E. Bass, J. Chem. Phys. 56, 1147 (1972).

(9) R. N. Schwartz, Z. I. Slawsky, and K. F. Herzfeld, J. Chem. Phys. 20, 1951 (1952).

(10) F. I. Tanczos, J. Chem. Phys. 25, 439 (1956).

(11) J. L. Stretton, Trans. Faraday Soc. 61, 1053 (1965).

(12) B. L. Earl, A. M. Ronn, and G. W. Flynn, Chem. Phys. 9, 307 (1975).

(13). R. D. Sharma and C. A. Brau, Phys. Rev. Lett. 19, 1273 (1967).

(14) R. D. Sharma and C. A. Brau, J. Chem. Phys. 50, 924 (1969).

C. ENERGY TRANSFER MAP FOR OCS *

(M. Mandich, G. Flynn)

Vibrational energy transfer maps in simple molecules contribute to the understanding of molecular interactions, guide explorations into laser enhanced chemical reactivity, and can lead to improved operation of gas lasers. A partial mapping for OCS, well known as both an infrared and chemical laser,[1,2] has been attempted by several laboratories with considerable disagreement on results.[3]-[7] The results reported here resolve some of these differences and add much new information towards a complete energy transfer mapping of OCS.

The technique of laser induced fluorescence is used to probe the redistribution of an initial excitation of the OCS (020) level pumped by a Q switched CO_2 laser operating at P(22) of the 9.6μ band (power = .75 - 1.0 mJ/pulse). The time dependent population deviations are thus measured for the (100), (010), (001) and (120) levels. The experimental apparatus has been described previously;[8] however, several recent acquisitions (including a Biomation 8100 transient recorder interfaced to a Tracor Northern NS-575A-2 digital signal averager and a highly sensitive HgCdTe (77K) detector) have been invaluable in detecting the weak OCS fluorescence and resolving multiple exponentials in the data.

The measured (100) fluorescence is composed of a single exponential rise and fall. These rates, including rare gas cross sections are tabulated in Table I. The weak (010) fluorescence has been observed and consists of a single very rapid rise followed by a multiple exponential decay. Strong (001) fluorescence, which may consist of 'hot-band' fluorescence (e.g. (011) → (010)), has been recorded anew showing that the risetime is single exponential (when precautions are taken to filter out (004) and (120) fluor-

TABLE I

11.7μ Fluorescence Data

Risetimes (rates in $msec^{-1}$ $torr^{-1}$)		Fall Times
Species	Rate	Rate
OCS-OCS	7.3	1.4
OCS-^{4}He	20	10
OCS-Ne	3.1	.51
OCS-Ar	1.8	.17
OCS-Kr	1.2	.05
OCS-Xe	1.4	.04

escences) but that the fall time is clearly multiple exponential. Finally, (120) fluorescence was also observed and shows a rapid rise followed by a rapid fall characteristic of a hot-band pumped level.

In theory, the entire vibrational energy transfer map of a molecule can be deduced from the rates of energy flow in and out of a single vibrational mode. Usually, a few processes predominate in a fluorescence signal and can be unambiguously assigned to the appropriate energy transfer steps. In the case of OCS, fluorescence data has been gathered from the strongly emitting (001) state, which contains, however, less than one percent of the total excited state population. Positioned rather high up in the vibrational state manifold, the (001) state population has many routes of escape adding additional decay rates to the few predominating rates. Most probably, this has been the source of ambiguity in measuring the vibrational-translational energy transfer rate from (001) data. A quick calculation shows that 99% of the upper state population resides in the three level system composed of (100), (010) and (020). The population deviations in higher levels, notably (001), have negligible amplitudes in the kinetic behavior of this system which can be written:

$$OCS(0) \xrightarrow{P(22)9.6\mu} OCS(020) \tag{1}$$

$$OCS(020) + OCS(0) \underset{k_{12}}{\overset{k_{21}}{\rightleftharpoons}} 2OCS(010) \tag{2}$$

$$OCS(020) + OCS \underset{k_{-a}}{\overset{k_a}{\rightleftharpoons}} OCS(100) + OCS + 188\ cm^{-1} \tag{3}$$

or

$$OCS(010) + OCS \underset{k_{-a}}{\overset{k_a}{\rightleftharpoons}} OCS(100) + OCS - 239\ cm^{-1} \tag{4}$$

$$OCS(010) + OCS \underset{k_{-VT}}{\overset{k_{VT}}{\rightleftharpoons}} OCS(000) + OCS + 520\ cm^{-1} \tag{5}$$

From these equations with six rate constants, three eigenvalues are expected. Three rates have in fact been measured: the up-the-ladder rate (k_{12}) (this is the rise of (010)) which is nearly gas kinetic, the V-V crossover from the ν_2 manifold to (100) (this is the rise of (100)) which is 7.3 $msec^{-1}$ $torr^{-1}$ and the V-T decay of the overall excited state population (this is the fall of (100)) which is 1.4 $msec^{-1}$ $torr^{-1}$. The V-V crossover step is probably via (020) → (100) as evidenced by the rare gas cross section data and the lack of an observed cooling in a thermal lensing study.[9]

With this three level kinetic scheme established, the rate information from other fluorescence data becomes useful. The fast, single exponential rise (55 $msec^{-1}$ $torr^{-1}$) of the (001) level can be assigned to a kinetic step:

$$OCS(040) + OCS \underset{k_{-b}}{\overset{k_b}{\rightleftharpoons}} OCS(001) + OCS + 39\ cm^{-1} \qquad (6)$$

The hot-band fluorescence behavior of the (120) level supports this claim and directly refutes previous claims for a

$$OCS(120) + OCS \rightleftharpoons OCS(001) + OCS - 170\ cm^{-1} \qquad (7)$$

type mechanism.[5] The multiple exponential fall of the (001) fluorescence includes a fast decay followed by a slower decay. The rate of the fast decay compares, within experimental error, favorably to the rate of rise of (100). This rate is expected in the decay of (001) from Eq. (6) since a filling of (100) would bleed population from the entire ν_2 manifold which alone feeds (001). The slower portion of the fluorescence decay is not merely one rate as reflected by conflicting results; it undoubtedly represents a convolution of many slow rate processes which affect the decay of (001) population.

Clearly, the additional new fluorescence data brings the vibrational energy transfer map of OCS within close reach. A power dependent study of the V-T decay rate of (100) will discriminate finally between mechanism (3) and mechanism (4); this experiment will be performed soon with our recently acquired CO_2 TEA laser.

*This work was also supported by the National Science Foundation under Grant NSF-CHE-77-24343.

(1) H. R. Schlossberg and H. R. Fetterman, Appl. Phys. Lett. 26, 316 (1975).

(2) D. Kligler, H. Pummer, W. Bischel, and C. K. Rhodes, J. Chem. Phys. 69, 4652 (1978).

(3) D. R. Siebert and G. W. Flynn, J. Chem. Phys. 64, 4973 (1976).

(4) K. Hui and T. Cool, J. Chem. Phys. 65, 3536 (1976).

(5) B. H. Hopkins, A. Baronavski, and H. Chen, J. Chem. Phys. 59, 836 (1973).

(6) J. D. Hancock, D. F. Starr, and W. H. Green, J. Chem. Phys. 61, 3017 (1974).

(7) A. Hairi and C. Wittig, J. Chem. Phys. 67, 4454 (1977).

(8) R. D. Bates, Jr., G. W. Flynn, J. T. Knudtson and A. M. Ronn, J. Chem. Phys. 53, 3621 (1970).

(9) D. R. Siebert, F. R. Brabiner, and G. W. Flynn, J. Chem. Phys. 60, 1564 (1974).

D. INFRARED LASER INDUCED FLUORESCENCE IN CH_3COF*

(J. Ahl, G. W. Flynn)

Though the vibrational relaxation of simple polyatomic molecules has been extensively studied, there appears to be a lack of information on the relaxation processes of molecules with a number of very low lying vibrational states, and in particular, of molecules with a torsional degree of freedom We have studied one such case, the molecule acetyl fluoride, CH_3COF.

The CH_3 rocking mode of acetyl fluoride was pumped with a Q-switched CO_2 laser and the laser-induced fluorescence observed. Several modes are easily observable: the C-H stretch at 3.3 μ, the C=O stretch at 5.4μ and the C-C stretch at 8.44 μ. In all cases, the fluorescence was observed to be quite similar with a very fast rise followed by a double exponential decay. The fast decay exhibits a bimolecular rate constant of $\gtrsim 10^6$ $sec^{-1}torr^{-1}$, while the slow decay is attributed to the decay of black body radiation due to the diffusion of translationally hot gas out of the detector viewing volume.

Since we are <u>not</u> looking at fluorescence from the pumped mode, the very fast rise time of observed fluorescence indicates a rapid V-V equilibration is occuring (possibly collisionless), which distributes energy throughout the molecule. It is quite surprising that the initial CH_3 rocking energy is propagated to the C=O and C-F bonds at nearly the same rate as the C-H stretch is pumped.

Simultaneously with the V-V equilibration, very fast V-T processes quench the vibrational excitation at a near gas kinetic rate. A possible explanation for this extremely fast rate is the presence of a number of very low lying modes. These modes provide a near resonant path for the initial excitation to

be converted into translation, with the maximum energy defect occuring for the quenching of the C-C torsion at 208 cm^{-1}. Such rapid V-T rates for low lying states are not particularly surprising.

While it is possible that the case of acetyl fluoride is atypical, it appears that the relaxation of molecules with a dense vibrational manifold having states within kT of the ground state will be extremely fast, with the vibrational energy distributed among the available states on the same time scale as the V-T relaxation.

*This research was also supported by the National Science Foundation under Grant NSF-CHE-77-24343.

III. GENERATION AND CONTROL OF RADIATION

A. RELAXATION AND EXCITATION TRANSFER OF OPTICALLY EXCITED STATES IN SOLIDS*

(Y. C. Chen, K. Chiang, S. R. Hartmann)

There is a great deal of interest in the studying of relaxation and spectroscopic properties of optical transitions of $LaF_3:Pr^{3+}$. Pr^{3+} ion in LaF_3, owing to its lack of an electronic moment, is essentially isolated and behaves in a relatively simple manner which allows convenient analysis. In the past few years a considerable amount of work has been performed in this material. Both the $^3H_4 - {}^3P_o$ transition (4777 Å) and $^3H_4 - {}^1D_2$ transition (5925 Å) are accessible to dye lasers and have been investigated by a wide variety of techniques, including the fluorecence line narrowing,[1][2] optical free decay,[3] photon echoes,[4][5] and optical rf double resonance.[6]

Last year we reported the observation of echo modulation effect in the $^3H_4 - {}^3P_o$ transition, which was in sharp disagreement with simple exponential decay behavior reported by Yamagishi and Szabo.[7] The disagreement hinged on one data point out of 13, the one corresponding to a pulse separation of 240 ns. The full recovery of echo intensity we observed implied a much slower echo relaxation rate than that which they reported. The problem was that the optical delay line used by both groups did not allow convenient and arbitrary variation of the excitation pulse separation. In order to make detailed studies of the echo behavior and to increase the resolution of the echo technique, we decided to improve our experimental technique. We developed a double N_2 laser pumped dye laser system which could be electronically triggered to produce any pulse separation we wanted.

The pulse separation was monitored by an Ortech Model 457 time to pulse height converter, and was determined to an accuracy of 0.1%.

In Fig. 1 (a) and Fig. 2 (a) we present the results obtained with this improved apparatus. The sharp peak at 236 ns confirms our previous result. The extended range and increased resolution of our new apparatus shows the echo behavior to be quite complex. An understandable feature is the regular rephasings which occur every 118 ns and which correspond to the nuclear splittings of 8.47 MHz and 16.7 MHz associated with the ground level of the $^3H_4$ state.[6] The high frequency modulations damp out with a time constant of $\sim$2 μsec. These are followed by low frequency modulations which correspond to the smaller splittings of the excited ^3P_o state. A Fourier transform of the low frequency modulations yields level splittings of 0.73 MHz and 1.12 MHz. Another feature of the data is the relatively slow ($\sim(1.2\ \mu\text{sec})^{-1}$) rate at which it decays. This corresponds to a linewidth of 70 kHz and is a factor three narrower than the nmr linewidth of 200 kHz reported by Erickson for the double resonance transitions in the $^3H_4$ ground state. This implies that the nuclear linewidths are inhomogeneous. The effect of this inhomogeneity is to damp out the high frequency modulation with time constant of 800 ns and twice 800 ns depending on which particular terms are singled out.[8] Our data indicates that the low frequency modulations have much smaller (20 kHz) damping rates. The 20 kHz linewidth associated with the ^3P_o nuclear splittings is understandable based on a second moment calculation for the Pr-F interaction[8] and the experimentally determined inhomogeneous broadening of the electric quadrupole interaction.[9] The much larger (200 kHz) inhomogeneous broadening associated with the nuclear splittings of the $^3H_4$ state is interpreted as being due to the enhanced nuclear magnetism of the Pr nucleus in that state.[10]

The effective hamiltonians of $LaF_3:Pr^{3+}$ can be written as

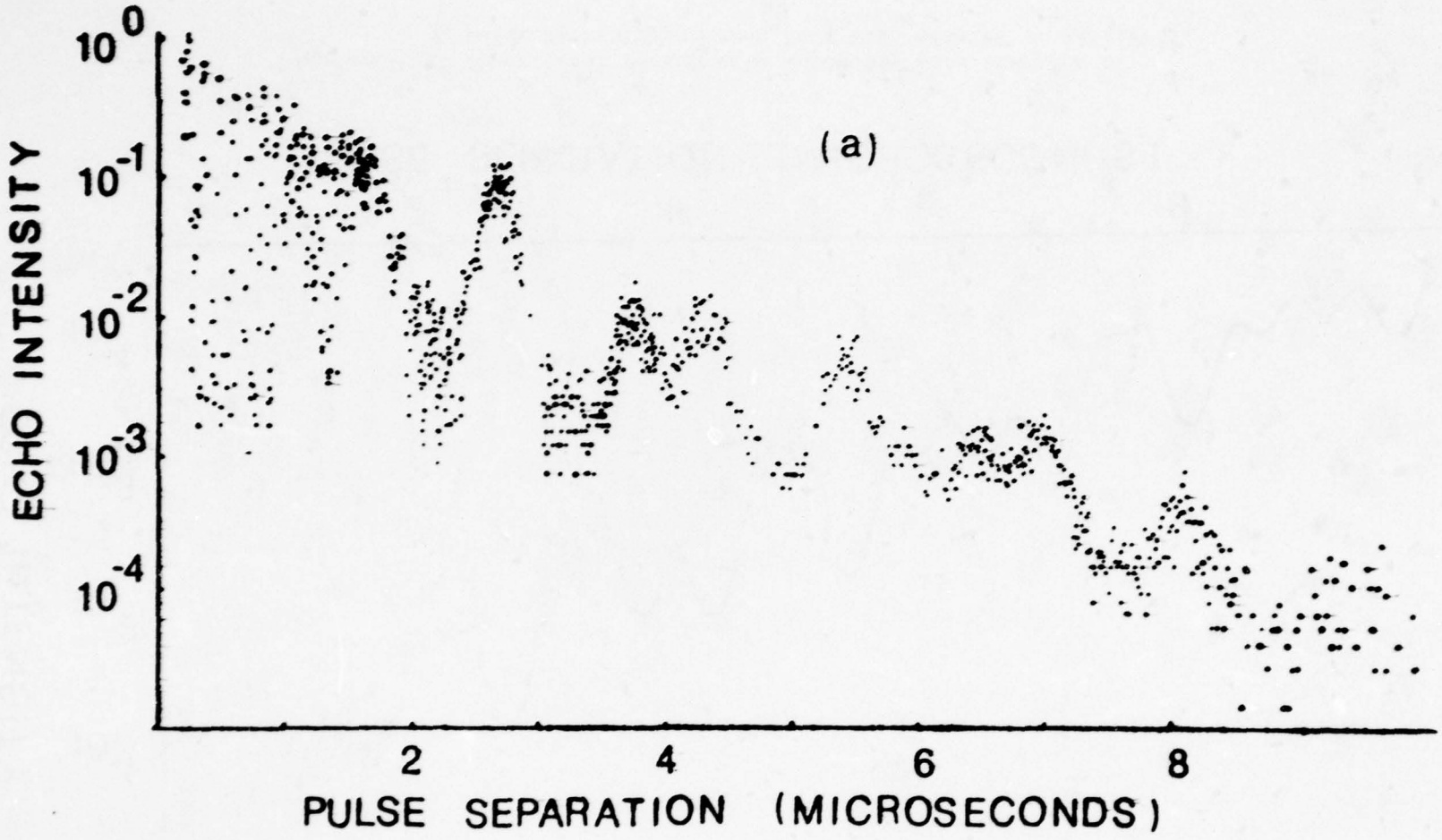

Figure 1(a): Experimental photon echo intensity as a function of pulse separation, taken in a 0.03 atomic% of $LaF_3:Pr^{3+}$.

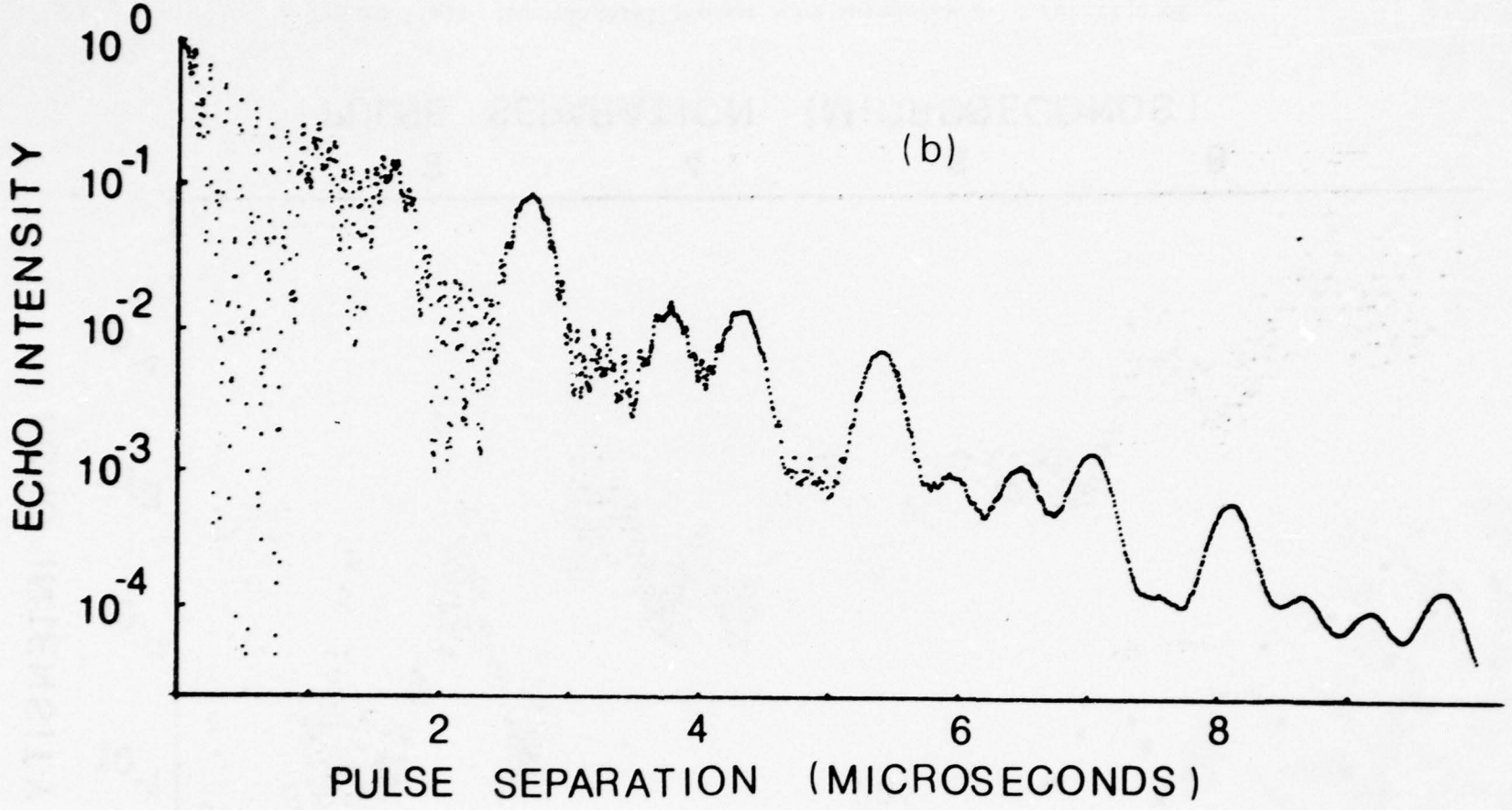

Figure 1(b): Theoretical photon echo intensity as a function of pulse separation, taken in a 0.03 atomic% of $LaF_3:Pr^{3+}$.

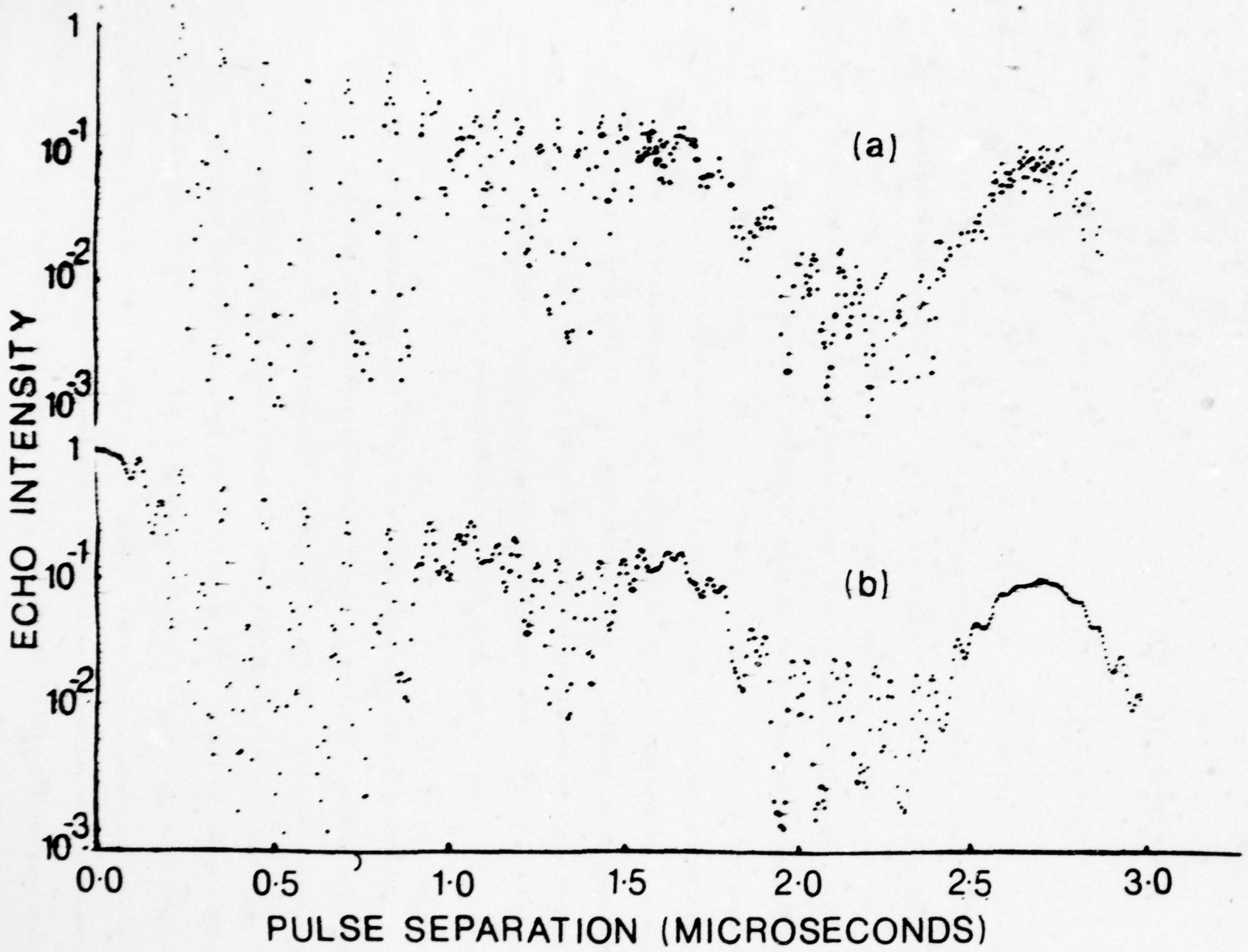

Figure 2: Experimental (a), and theoretical (b) photon echo intensity as a function of pulse separation in the region from 200 ns to 3.0 μsec.

$$H_G = P_g(I_z^2 + \quad _G(I_x^2 - I_y^2)) \qquad \text{for the } {}^3H_4 \text{ state}$$

$$H_E = P_E(I_{z'}^2 + \quad _E(I_{x'}^2 - I_{y'}^2)) \qquad \text{for the } {}^3P_o \text{ state}$$

where $P_G = \pm$ 4.185 MHz, $\eta_G = 0.035$, $P_E = \pm$ 0.29 MHz, $\eta_E = 0.168$. The interaction parameters are determined based on the Fourier transform of the echo modulation data. The (x,y,z) and (x', y',z') systems are principal axes of the electric quadrupole interaction of the Pr nucleus. For the ${}^3H_4$ state, the hamiltonian represents the combination of the electric quadrupole interaction and the second order hyperfine interaction.[10] The relative orientation of the (x,y,z) and the (x',y',z') axes has strong influence on the theoretical echo modulation pattern and therefore provides a means of determining it. The site symmetry of Pr^{3+} requires one of principal axes to be parallel to the two fold axis, $\hat{C}_2$. We find that the best agreement with the experimental results is obtained if $\hat{x}$(or $\hat{y}$) $\| \hat{x}' \| C_2$, and $30^\circ < \cos^{-1}(|\hat{z}\cdot\hat{z}'|) < 35^\circ$. The corresponding theoretical calculations are shown in Fig. 1(b) and Fig. 2(b). The agreement between the theory and the experiment is excellent.

An additional interesting discovery we would like to mention is the variation of echo relaxation rate at different positions within the ${}^3H_4$ - ${}^3P_o$ absorption profile. In Fig. 3 we present the results of the measurement of the homogeneous linewidth made in a 5.0 atomic % sample using wide band (10GHz) pulse dye lasers. The linewidth varies from about 500 kHz near the line center to less than 60 kHz at a detuning of 200 GHz. Similar effect has also been observed in a 1.0 atomic % sample. It seems to indicate a correlation between the echo relaxation rate and the inhomogeneity of the crystal field which broadens the optical transition. However this site dependent relaxation

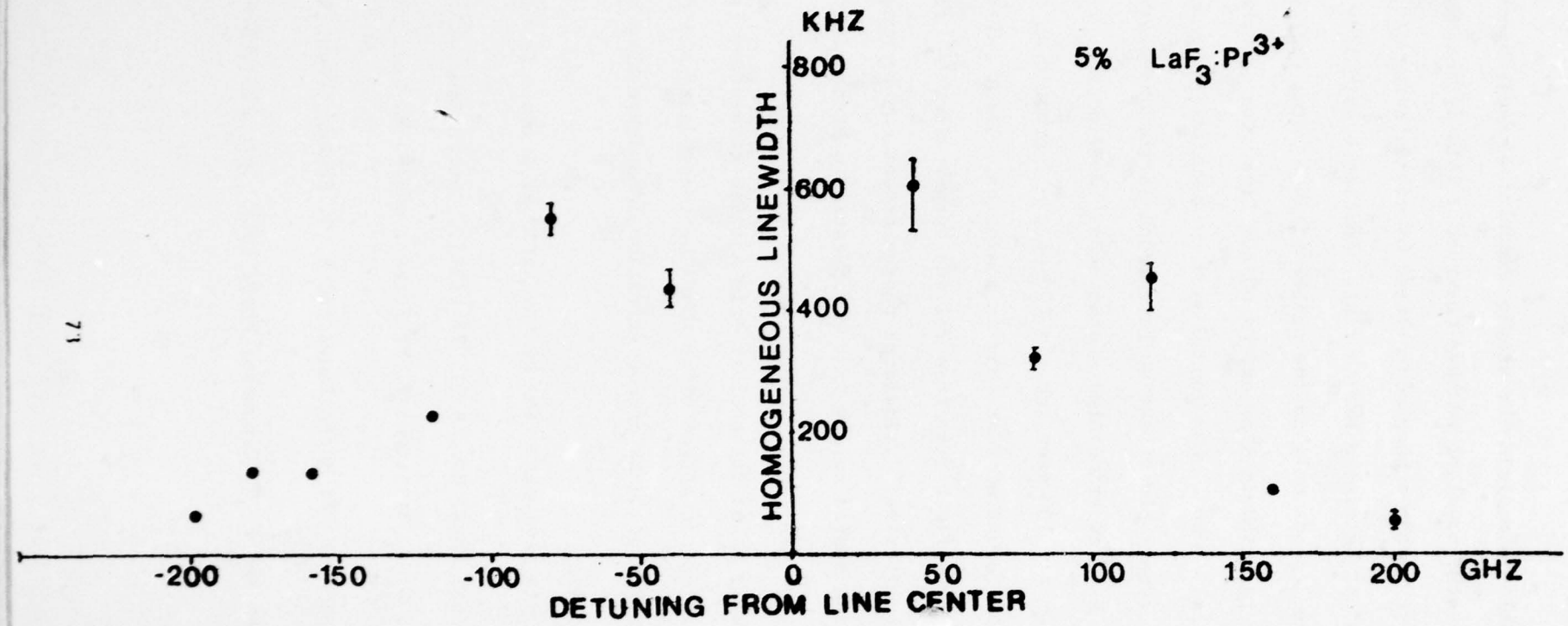

Figure 3: Variation of the homogeneous linewidth of the $^3H_4$-^3P_o transition at different positions in the absorption profile.

would not be able to explain the simple exponential decay behavior (see Fig. 2) of the echo envelope we have observed. This is because the overall decay pattern of photon echoes contributed by atoms having different relaxation rates can not be simple exponential. Another possibility is that echo relaxation rate depends only on the number of ions being excited. If so, the relaxation rate should also depend on the linewidth and the power of the excitation pulses. More experimental work is necessary to unravel this effect.

Another remarkable effect we have found is the observation of a very long-lived three-pulse stimulated photon echo. We find that three excitation pulses at t = 0, t = 100 nsec and t = 100 nsec + T produce an echo at t = 200 nsec + T for values of T as long as 3 minutes. These latter echoes have a signal-to-noise ratio better than 2:1 and appear after 10^6 times the excited state's 47 μsec lifetime. Stimulated photon echoes can be produced with phase information stored solely in the population distribution of the ground state levels. Our experiment demonstrates this dramatically. Our stimulated echoes most likely relax via nuclear spin lattice relaxation induced by paramagnetic impurities, an effect which should be temperature and concentration dependent. No measurements of concentration dependence have been made yet.

*This research was also supported by the National Science Foundation under Grant NSF-DMR77-05995.

(1) E. Erickson, Phys. Rev. B 11, 77 (1975); Optics Comm. 15, 246 (1975).

(2) R. Flach, D. S. Hamilton, P. M. Selzer, and W. M. Yen, Phys. Rev. Lett. 35, 1034 (1975).

(3) A. Z. Genack, P. M. Macfarlane, and R. G. Brewer, Phys. Rev. Lett. 37, 1078 (1976).

(4) Y. C. Chen and S. R. Hartmann, Phys. Lett. 58A, 201 (1976).

(5) Y. C. Chen, K. Chiang and S. R. Hartmann, Optics Comm. 26, 269 (1978).

(6) L. E. Erickson, Optics Comm. 21, 147 (1977).

(7) A. Yamagishi and A. Szabo, Optics Lett. 2, 160 (1978).

(8) Y. C. Chen, K. Chiang and S. R. Hartmann, Optics Comm. to be published.

(9) L. O. Anderson and W. G. Proctor, Z. Krist, 127, 366 (1968).

(10) B. Bleaney, Physica, 69, 317 (1973).

B. SPONTANEOUS AND INDUCED COHERENT RADIATION GENERATION AND CONTROL IN ATOMIC VAPORS*

(T. Mossberg, R. Kachru, K. Leung, E. Whittaker, S. R. Hartmann)

Our research is oriented toward the attainment of two complementary objectives: 1) to advance the basic understanding of the generation of coherent radiation in atomic vapors, and 2) to utilize coherently generated radiation to study atomic processes occurring within such vapors. With respect to the first objective, we have discovered a number of important properties of the three-excitation pulse stimulated photon echo.[1] Among other things we have found that in contrast to all other known echo effects the stimulated echo can be generated via the information stored in a single atomic state. This has a number of important consequences which will be discussed below. We have also continued our work on the two-photon (Raman) echo.[2] We have observed the two-photon echo on the $6^2P_{1/2} - 6^2P_{3/2}$ transition of atomic Tl vapor. We have found that the polarizations of the excitation pulses can be arranged in such a fashion that it is not necessary to use optical shutters to observe the echo. With regards to the second objective we have employed the tri-level echo effect[3] to make extensive measurements[4] of the foreign-gas-induced relaxation of the 3S-nS and 3S-nD superposition states in atomic sodium vapor. We have been able to extend our measurements to superpositions involving upper states (nS or nD where $4 \leq n \leq 34$) which are well into the Rydberg regime. Our work represents the first comprehensive study of foreign-gas-induced relaxation of coherent superpositions involving levels coupled only by two-photon transitions.

The excitation pulses which produce the stimulated photon echo are shown in Fig. 1a. We assume that pulses 1 and 2 are both parallel to $\hat{z}$ and are resonant with the $|0\rangle - |1\rangle$ transition, where $|0\rangle$ is a thermally populated

FIG. 1a

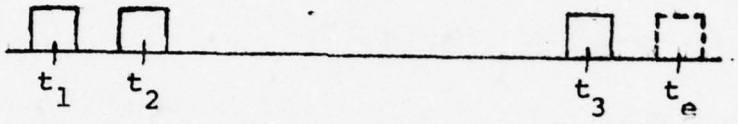

FIG. 1b

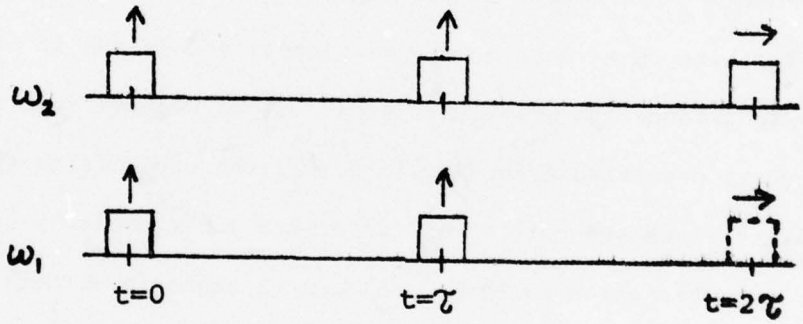

FIG. 1c

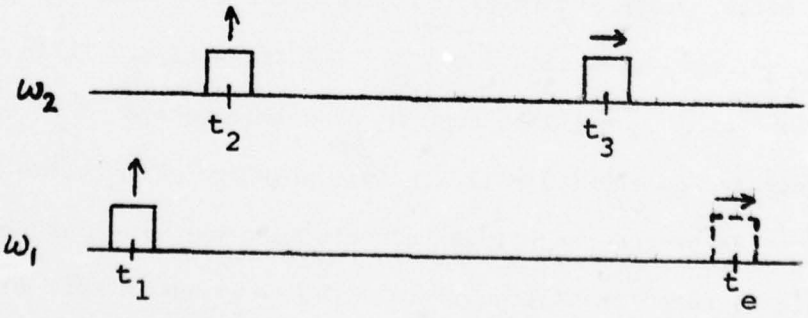

Figure 1

AD-A071 664 COLUMBIA RADIATION LAB NEW YORK F/G 5/1
RESEARCH INVESTIGATION DIRECTED TOWARD EXTENDING THE USEFUL RAN--ETC(U)
MAR 79 G W FLYNN DAAG29-77-C-0019
UNCLASSIFIED NL

2 OF 2
AD A071664

END
DATE FILMED
8-79
DDC

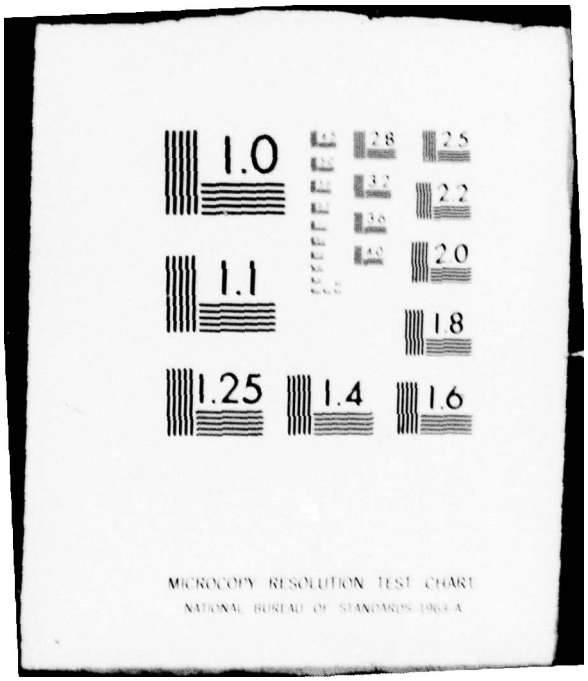
1.0
1.1
1.25
1.4
1.6
2.8
3.2
3.6
4.0
2.5
2.2
2.0
1.8
MICROCOPY RESOLUTION TEST CHART
NATIONAL BUREAU OF STANDARDS 1963-A

ground state and $|1\rangle$ is an initially unpopulated excited state. If both pulses have an area of $\pi/2$, it can be shown that after pulse 2 both states are populated and that the distribution of the z-component of velocity (z-velocity, v_z) of the atoms in each state is modulated with v_z according to

$$n'(v_z) = C_o \exp(-mv_z^2/2k_bT) f(k_1 v_z t_{21}/2) \qquad (1)$$

where C_o is a constant, $t_{ij} = t_i - t_j$, $f \equiv \sin^2$ for state $|0\rangle$, $f \equiv \cos^2$ for state $|1\rangle$, m is the mass of the "echo" atom, k_b is the Boltzmann constant, T is the absolute temperature, and $\vec{k}_1$ is the wavevector of pulses 1 and 2. The exponential envelope represents the thermal distribution of v_z initially found in $|0\rangle$. The third pulse acts on the z-velocity modulation in either state <u>separately</u> to produce the stimulated echo. If, as we have described above, both states are populated according to Eq. 1, the echo fields generated from atoms in either state separately will interfere constructively and make the echo larger than that which would be produced by atoms in either state separately. Since the z-velocity distribution of Eq. 1 does not indicate the sense along $\hat{z}$ in which pulses 1 and 2 were travelling, pulse 3 and the echo it generates can propagate along either $\pm \hat{z}$. Since the modulated z-velocity distribution in either state separately is sufficient to produce an echo the third pulse does not need to excite the $|0\rangle - |1\rangle$ transition. It is only necessary that one of $|0\rangle$ or $|1\rangle$ be coupled to a third state $|2\rangle$. An echo will then be generated on the $|i\rangle - |2\rangle$ transition where $|i\rangle$ represents $|0\rangle$ or $|1\rangle$. These facts concerning the stimulated echo were not previously recognized. It should be noted that because state $|0\rangle$ (a ground state) does not radiatively decay, the stimulated echo resulting from the modulated z-velocity distribution in $|0\rangle$ can be produced for <u>very long</u> t_{32}. By utilizing the characteristics of the stimulated echo discussed above, it is possible to

produce a stimulated echo which (as a function of foreign-gas pressure) decays during t_{32} only as a result of the thermalization of the z-velocity distribution of atoms in a single state. We term collisions which modify the atomic velocities "velocity-changing collisions" (VCC). Detailed analysis of the effect of VCC reveals[1] that for fixed excitation pulse separations the intensity of the stimulated echo varies with foreign-gas pressure P as

$$I_e(P) = I_o \exp\{-2(n_o/P_o)v_r \sigma t_{32}[1-\int_{-\infty}^{\infty} \exp(-ik_e \Delta v_i t_{e3}) f(\Delta v_i) d(\Delta v_i)]P\} \exp\{-\beta P\} \quad (2)$$

where n_o is the foreign-gas density at pressure P_o, $v_r = (8k_b T/\pi\mu)^{1/2}$ where μ is the echo atom - foreign-gas atom reduced mass, σ is the total VCC cross section, $\vec{k}_e$ is the wavevector of the third pulse and the echo, Δv_i is the z-velocity change in a single collision, and $f(\Delta v_i)$ is the collision kernel, i.e. the probability distribution of the Δv_i. The $\exp(-\beta P)$ term, which represents the decay due to collisions during the intervals t_{21} and t_{e3}, can be independently measured allowing the VCC-induced decay during t_{32} to be determined. The only unknowns in Eq. 2 are σ and $f(\Delta v_i)$. For large t_{e3} the integral involving $f(\Delta v_i)$ becomes zero and σ can be unambiguously determined. Using the value of σ obtained for large t_{e3}, it is possible to determine $f(\Delta v_i)$ through stimulated echo decay measurements for short t_{e3}. Note that the σ determined here is the same absolute elastic scattering cross section laboriously obtained in atomic-beam experiments. Unlike atomic-beam experiments, stimulated echo experiments can measure the absolute σ for short-level excited states as well as ground states. We have performed detailed stimulated echo measurements in Na and have measured[1] both the Na(3S)-He and Na($3P_{1/2}$)-He scattering cross section. In the case of Na(3S)-

He scattering our data has allowed us to infer the form of $f(\Delta v_i)$, which surprisingly turns out to be of Lorentzian form rather the the commonly assumed Gaussian form. Fig. 2 shows the results of our Na(3S)-He measurements. Here we have defined $\sigma_{eff} \equiv \sigma[1 - \int_{-\infty}^{\infty} \exp(-ik_e \Delta v_i t_{e3}) f(\Delta v_i) d(\Delta v_i)]$. The solid [broken] curve in Fig. 2 was generated from Eq. 2 assuming a Lorentzian [Gaussian] kernel. More details of our work can be found in Ref. 1. It is clear that measurements of the collisionally-induced decay of the stimulated echo will provide important new information concerning atomic collision physics.

The excitation pulses necessary to produce the two-photon echo are shown (solid lines) in Fig. 1b. The sum or difference of ω_1 and ω_2 is equal to the energy difference between states coupled by a two-photon transition. In our experiments ω_1 and ω_2 are separately resonant with single-photon transitions, i.e. we produce the two-photon echo via a resonant intermediate state. While a resonant intermediate state lowers the power requirements for producing the two-photon echo, it introduces the necessity of preventing single-photon coherent transients, e.g. photon echoes, produced at both ω_1 and ω_2 from obscuring the two-photon echo. In our original experiment this was accomplished by a difficult non-collinear excitation scheme in which the two-photon echo was spatially separated from the single-photon transients. We have subsequently recognized that by using linearly polarized excitation pulses oriented as shown by the arrows in Fig. 1b we can eliminate (on transitions involving states of suitable angular momenta) single-photon transients using simple polarization selective detection. Equally importantly, this excitation arrangement allows us to eliminate both of the excitation pulses at the echo frequency (which tend to saturate the detector and prevent the echo

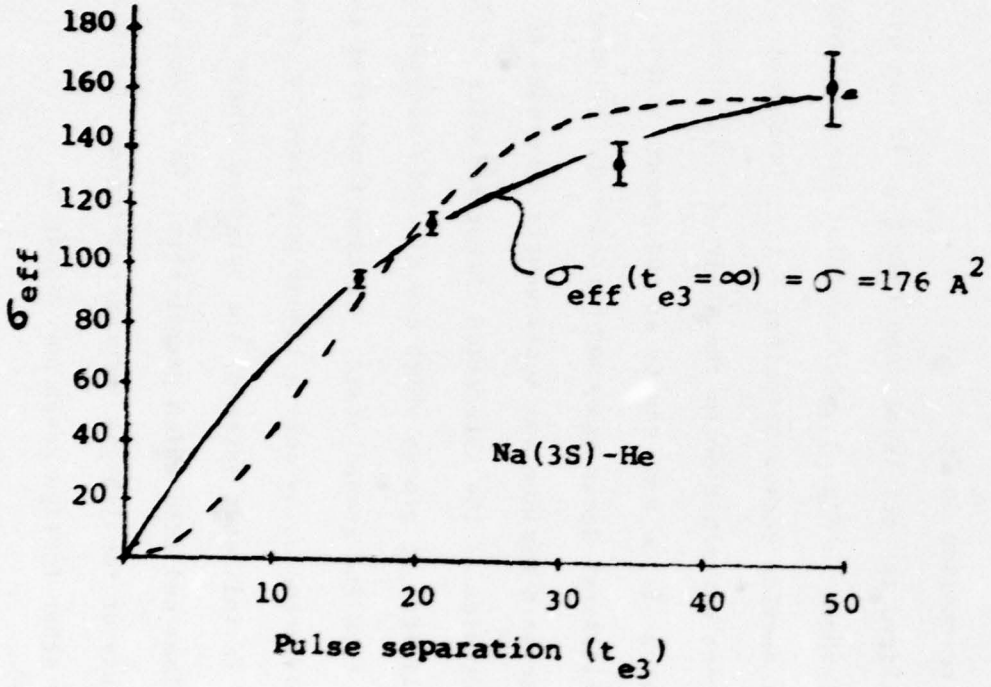
180
160
140
120
100
80
60
40
20
σ_{eff}
$\sigma_{eff}(t_{e3}=\infty) = \sigma = 176\ A^2$
Na(3S)-He
10
20
30
40
50
Pulse separation (t_{e3})

Figure 2

from being seen) without recourse to optical shutters. As a result we are able to see two-photon echoes using convenient collinear excitation pulses with only a glan-prism polarizer and band-pass filter to prevent detector saturation. By making the two-photon echo easier to produce and observe we have enhanced its utility. We are currently using the two-photon echo to study collisional relaxation in Tℓ.

We have utilized the tri-level echo (see Fig. 1c for excitation scheme) to obtain the data shown in Fig. 3, where we plot the tri-level echo collisional decay cross section versus principal quantum number n. This data represents a significant contribution to the study of collisional relaxation of highly excited states of the same parity as the ground state. It will be noted that the collisional decay cross section does not increase monotonically with n. Instead it reaches a maximum and subsequently decreases to an asymptotic limit. Previous studies of the relaxation characteristics of highly excited states have been limited to states which are directly accessible via single-photon absorption from the ground state. We have found that the tri-level echo can also be detected using only a linear polarizer to prevent detector saturation. Fig. 1c indicates (arrows) the relative linear polarizations of the excitation pulses and echo which permit this. We intend to extend our tri-level echo study of foreign-gas-induced relaxation of the alkali S and D Rydberg states to other foreign gases and higher n.

*This research was also supported by the Office of Naval Research under Contract N00014-78-C-0517.

(1) T. Mossberg, A. Flusberg, R. Kachru, and S. R. Hartmann, (submitted to Phys. Rev. Lett.)

(2) A. Flusberg, T. Mossberg, R. Kachru, and S. R. Hartmann, Phys. Rev. Lett. 41, 305 (1978).

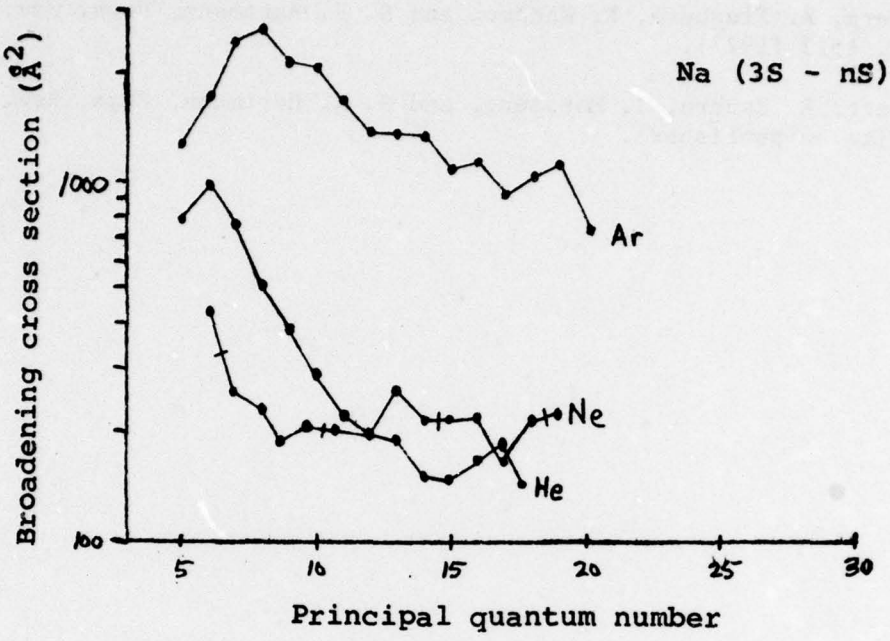

Figure 3. Broadening of Na Rydberg states by He, Ne, and Ar.

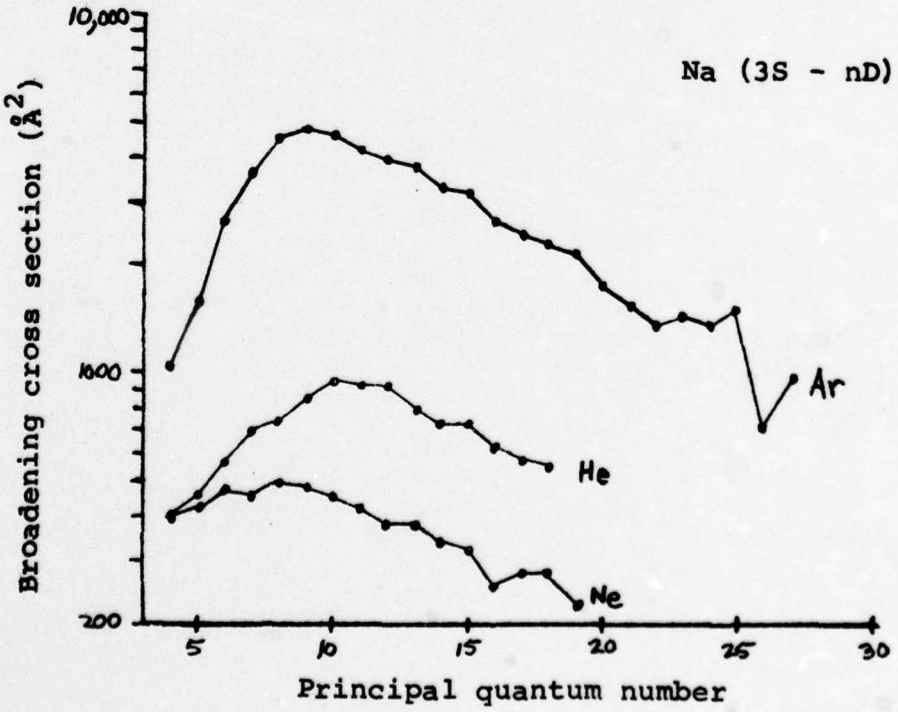

(3) T. Mossberg, A. Flusberg, R. Kachru, and S. R. Hartmann, Phys. Rev. Lett. 39, 1523 (1977).

(4) A. Flusberg, R. Kachru, T. Mossberg, and S. R. Hartmann, Phys. Rev. A. 4/79 (to be published).

IV. QUANTUM DETECTION AND SENSING OF RADIATION

A. NONLINEAR HETERODYNE DETECTION AND SENSING IN THE INFRARED AND OPTICAL

(M. C. Teich, R. A. Meyers, M. Elbaum*)

Considerable progress has been achieved in the theoretical analysis of the heterodyne correlation radiometer, the details of which have been recently published.[1] The ideal signal-to-noise ratio (SNR) and minimum-detectable-power (MDP) at the output of the system have been obtained for a number of cases of interest, including sinusoidal signals, and Gaussian signals with both Gaussian and Lorentzian spectra. We have shown that the system exhibits an MDP $\sim(h\nu/\eta_1)\sqrt{\bar{\gamma}\bar{f}/\zeta}$ where $h\nu$ is the photon energy, η_1 is the detector quantum efficiency, $\bar{\gamma}$ is the average linewidth of a typical line, $\bar{f}$ is the mean frequency interval between signal lines, and ζ is the ratio of locally-produced power to the received remotely-radiated power. This result is very encouraging since it indicates that a strong locally radiating sample can increase ζ and thereby decrease the MDP. Our detailed calculations show that small linewidths and closely spaced lines enhance detectability, as does a strongly radiating local sample. Of course, the remote source should be as strong as possible for definitive detection. Correction factors for impurity species will not, it appears, seriously impair operation of the system. For certain choices of parameters, the SNR at the output of the heterodyne correlation radiometer will provide a sufficient confidence level for detection. For situations in which this is not the case, we have shown that further improvement can be obtained by adding a classical radiometer, a balanced mixer, and/or a multi-channel receiver. Though calculated ideal system performance is excellent, the real SNR may be reduced by a variety of deleterious effects in analogy with the conventional system.[2]

We have shown that the technique should operate over a broad frequency

range from the microwave to the optical. For the submillimeter region, it may be possible to use a combination Schottky-barrier-diode/harmonic-mixer that would provide an output at low frequencies as long as the high-frequency beat signals are generated and mixed within the detector. LO harmonics are also readily generated in these devices[3] so that harmonic-mixing heterodyne correlation radiometry could be performed.[4] Josephson junctions, which can sometimes be made to produce their own LO power, and metal-oxide-metal diodes could also be used. An IMPATT solid-state oscillator could conveniently be considered as an LO in these regions since frequency stabilization, which is difficult to achieve in these devices, is not required. At higher frequencies, tunable diode lasers and Schottky-barrier detectors may be useful components.

We have also evaluated the performance of an optical or infrared heterodyne system in estimating the mean intensity of a gaussian random signal, and shown that it depends on the mean number of photocarriers released by the signal radiation in its coherence volume (degeneracy parameter).[5] In a pulsed radar, this parameter can be manipulated by varying the pulse duration while keeping the mean number of signal photocarriers constant. Furthermore, in a number of situations of practical interest, an optimal pulse duration exists, corresponding to a degeneracy parameter of unity. Heterodyne and direct detection are compared for this case, and direct detection is found to be superior in the strong-signal limit.

* Supported by DARPA.

(1) M. C. Teich, Opt. Eng. 17, 170 (1978).

(2) M. M. Abbas, M. J. Mumma, T. Kostiuk, and D. Buhl, Appl. Opt. 15, 427 (1976).

(3) H. R. Fetterman, B. J. Clifton, P. E. Tannenwald, C. D. Parker, and H. Penfield, IEEE Trans. Microwave Theory Tech. MTT-22, 1013 (1974).

(4) P. F. Goldsmith, R. L. Plambeck, and R. Y. Chiao, IEEE Trans. Microwave Theory Tech. MTT-22, 1115 (1974).

(5) M. Elbaum and M. C. Teich, Opt. Comm. 27, 257 (1978).

B. PHOTON COUNTING DETECTION FOR COMMUNICATIONS, RADAR, AND IMAGING*

(P. R. Prucnal, G. Vannucci, M. C. Teich, H. C. Card)

The likelihood-ratio detection of a signal embedded in noise constitutes an important class of classical binary decision problems that has found widespread applicability in the synthesis and analysis of many types of systems.[1] These applications range from optical communications[2]-[19] to radar systems.[18]-[21] For complex signal and noise statistics, it is sometimes difficult or impossible to express the likelihood ratio in closed form, however. Even for simple signal and noise statistics, direct implementation of the likelihood ratio as an optimum processor may be rather difficult. It may be possible to reduce the likelihood ratio to a simpler, but equivalent processor by using various *ad hoc* geometric arguments or lengthy algebraic manipulations.

We have made excellent progress[22] in deriving a simple processor that is optimum for a broad range of classical binary decision problems involving the likelihood-ratio detection of a signal embedded in noise. The class of problems we have considered encompasses the case of N independent (but not necessarily identically distributed) observations of a nonnegative (or nonpositive) signal random variable embedded in an additive, independent, and noninterfering noise random variable, where the range of the signal and noise is discrete. We have shown that a comparison of the sum of the N observations with a unique threshold comprises optimum processing, provided that the logarithm of the noise probability density does not contain a point of inflection. This condition on the noise probability density is not necessary, but is sufficient, to imply our single-threshold processor and does not depend on the signal probability density. The results are applicable to a spatial array of detectors exposed to a temporal sequence of observations. We have shown by example

that in many cases it is not difficult to test the log of the noise density for a point of inflection analytically. In more difficult cases ,a graphical representation of the noise density with a logarithmic ordinate scale may be useful in revealing a point of inflection. We have applied the results to a generalized photocounting optical communication system and shown that background noise, dark noise, modulation, avalanche multiplication, and channel distortions are easily included in our model.

We had previously[18] derived a limited version of these results for a single observation (N=1) of a nonnegative signal embedded in noise, when the logarithm of the noise density is concave downward. The proof was based on the existence of a nonunique continuous extension of the noise density, so that implementation of the result depended on a proper choice of this continuous extension. No such ambiguity now exists. We have eliminated the need for a continuous extension by applying a finite-difference condition directly to the discrete noise density.

We have also considered a mathematical description for the class of optical experiments in which a pulse of light is generated in which the underlying Poisson photon statistics are modified by an intensity that decays exponentially in time.[23] In some cases, as when the light is weak, it is necessary to use photon-counting techniques to detect this signal. In those situations in which the sampling interval (or time) T is much greater than the decay time, essentially all of the light energy is contained in each sampling interval, so that the photocounting distribution will be Poisson of mean $\langle n \rangle = \eta \bar{I} T$. Here η is the quantum efficiency of the detector, $\bar{I}$ is the time-averaged intensity of the light at the detector, and it is assumed that spatial effects can be ignored.

We have derived the exact photocounting distribution expected when the sampling interval T is not necessarily large in comparison with the decay time τ of the light. We have also derived closed-form expressions for the count mean and variance. The results are valid for the repeated and exhaustive sampling of a single exponentially decaying light pulse, or for sampling from an ensemble of such pulses of identical height when the starting time of the sampling interval is uniformly distributed.

*This research was also supported by the National Science Foundation.

(1) H. L. Van Trees, Detection, Estimation, and Modulation Theory, Part 1 (Wiley, New York, 1968).

(2) B. Reiffen and H. Sherman, Proc. IEEE 51, 1316 (1963).

(3) C. W. Helstrom, IEEE Trans. Inf. Theory IT-10, 275 (1964).

(4) W. K. Pratt, Laser Communication Systems (Wiley, New York, 1969).

(5) Proc. IEEE (Special Issue on Optical Communications), 58 (1970).

(6) E. Hoversten, "Optical Communication Theory," in Laser Handbook, F. T. Arrechi and E. O. Schulz-DuBois, Eds.(North-Holland, Amsterdam, 1972), Vol. 2

(7) M. C. Teich and R. Y. Yen, IEEE Trans. Aerosp. Electron. Syst. AES-8, 13 (1972).

(8) R. Y. Yen, P. Diament, and M. C. Teich, IEEE Trans. Inf. Theory IT-18, 302 (1972).

(9) M. C. Teich and S. Rosenberg, Appl. Opt. 12, 2616 (1973).

(10) S. Rosenberg and M. C. Teich, Appl. Opt. 12, 2625 (1973).

(11) E. V. Hoversten, D. L. Snyder, R. O. Harger, and K. Kiromoto, IEEE Trans. Commun. COM-22, 17 (1974).

(12) D. L. Snyder, Random Point Processes (Wiley, New York, 1975).

(13) R. M. Gagliardi and S. Karp, Optical Communications (Wiley, New York, 1976).

(14) C. W. Helstrom, Quantum Detection and Estimation Theory (Academic, New York, 1976).

(15) S. D. Personick, Bell Syst. Tech. J. 50, 3075 (1971).

(16) S. D. Personick, Proc. IEEE 65, 1670 (1977).

(17) S. D. Personick, P. Balaban, J. H. Bobsin, and P. R. Kumar, IEEE Trans. Commun COM-25, 541 (1977).

(18) M. C. Teich, P. R. Prucnal, and G. Vannucci, Opt. Lett. 1, 208 (1977).

(19) M. C. Teich and B. I. Cantor, IEEE J. Quantum Electron. QE-14, 993 (1978).

(20) G. W. Flint, IEEE Trans. Mil. Electron. MIL-8, 22 (1964).

(21) J. W. Goodman, Proc. IEEE 53, 1688 (1965).

(22) P. R. Prucnal and M. C. Teich, Appl. Opt. 17, 3576 (1978).

(23) M. C. Teich and H.C. Card, Opt. Lett., to be published.

C. MILLIMETER- AND SUBMILLIMETER-WAVE MIXERS USING JOSEPHSON JUNCTIONS*

(A. R. Kerr, P. Thaddeus, Y. Taur)

The Josephson junction has great potential as a very low noise coherent detector at millimeter and submillimeter wavelengths. When operated as a mixer it possesses the unique characteristics of requiring local oscillator power of only a few nanowatts, while being more sensitive than the best cryogenic Schottky diode mixers. The engineering problems which have delayed practical application of the Josephson junction as a receiver front-end are:

(i) Development of a device with an impedance level sufficiently high to be matched to a practical waveguide structure.

(ii) Fabrication of such a device and its mounting structure with the very small dimensions and tolerances required for millimeter and sub-millimeter wavelength operation, and with sufficient mechanical stability for cryogenic cooling.

(iii) Development of appropriate waveguide matching structures in which to mount the Josephson junction.

We have developed a stable, thermally re-cyclable Josephson junction mixer for 115 GHz.[1][2][3] The high sensitivity and low conversion loss of this device promise a gain in overall receiver sensitivity by a factor of $\sim$4 over the best room temperature receivers at this frequency (this corresponds to a reduction in necessary observing time by a factor of 16). Following initial testing in a laboratory dewar, the Josephson mixer is now being mounted in a specially designed receiver using a cryogenically cooled transistor IF amplifier to reduce second-stage noise. This receiver will be installed on the Columbia-GISS 4-foot CO Sky Survey telescope in the near future.

Work on understanding the noise behaviour of Josephson mixers has led to a digital computer simulation of the device, including the effects of thermal noise in the junction resistance. This has given excellent agreement with our

experimental results at 115 GHz,[4] and will be an essential tool in developing the next generation of Josephson junctions and their waveguide coupling structures.

*This research was also supported by the National Aeronautics and Space Administration under Grant NSG-5163 Scope L.

(1) Y. Taur and A. R. Kerr, "A Recyclable Josephson Junction Mixer at 115 GHz," presented at the URSI/USNC Meeting, Boulder, CO, October 1977.

(2) Y. Taur and A. R. Kerr, "Low-Noise Josephson Mixers at 115 GHz Using Recyclable Point Contacts," Applied Phys. Lett. 32, 775 (1978).

(3) Y. Taur and A. R. Kerr, "Progress on Millimeter-Wave Josephson Junctions," AIP Conference Proceedings. No. 44, on Future Trends in Superconductive Electronics, p. 254 (1978).

(4) Y. Taur, "Noise Down-Conversion in a Pumped Josephson Junction," Journal de Physique, 39, C6-575 (1978).

(5) Y. Taur, "Characteristics of a Josephson Junction Harmonic Mixer with External Pumping," IEEE Transactions on Magnetics, Jan. 1979.

V. PHYSICAL PROPERTIES AND EFFECTS OF ELECTRONIC MATERIALS

A. TUNNELING IN ULTRATHIN SiO_2 LAYERS ON SILICON*

(H. C. Card, K. K. Ng)

This work is an extension of the studies of MOS tunneling first reported in the previous progress report (Sec. IV A 1 of progress report 28).

We report here on a basic asymmetry observed in the tunneling probabilities for electrons and holes of ultrathin SiO_2 films in metal-SiO_2-nSi structures. Hole tunneling in this sense implies the tunneling of electrons from the metal into the valence band of the semiconductor. The tunneling transmission coefficient for holes (T_h) is consistently appreciably lower than that for electrons (T_e) when these coefficients are measured on the same sample.

We deal with an n-type semiconductor and the transmission coefficient for majority carriers (electrons), T_e, is first determined from dark measurements of current density and capacitance vs bias voltage V by a method described previously.[1] The sample (which has an optically transparent metal electrode) is then illuminated with photons of energy in excess of the semiconductor energy gap in order to determine the photocurrent density. The photocurrent density is suppressed by the SiO_2 layer (for thickness $d \gtrsim 20$ Å) to an extent that is determined by comparison with an ideal metal-semiconductor structure ($d \to 0$) fabricated at the same time so that the optical transparency of the metal films are identical. The magnitude of photocurrent density is used to determine the transmission coefficient of the SiO_2 film for minority carriers (holes), T_h.

These transmission coefficients are given in the WKB approximation by[1][2]

$$T_e = \exp(-2|K_e|d)$$
$$= J_o h^3 [4\pi q m_{te} k^2 T^2 \exp(-\frac{q\phi_b}{kT})]^{-1} \quad (1)$$

where K_e is the imaginary wavevector for electrons (tunneling through the SiO_2 layer at the energy of the semiconductor conduction band edge $E_c(Si)$), J_o is the measured value of the dark saturation current density due to the majority carrier transport, m_{te} is the transverse effective mass in the semiconductor conduction band, $q\phi_b$ is the (Schottky) barrier height, determined from the capacitance characteristics, and equal to the energy difference between the metal Fermi energy and $E_c(Si)$ for V=0, and by[1][2]

$$T_h = \exp(-2|K_h|d)$$

$$= qD_p\left[L_p q m^* \left(\frac{kT}{2\pi m_{dh}^3}\right)^{\frac{1}{2}} \exp\left(\frac{q\psi_s^o}{kT}\right)\left(\frac{J_{ph}}{J_{sc}} - 1\right)\right]^{-1} \qquad (2)$$

where m_{th}^* is the effective mass for holes with momentum transverse to the barrier, m_{dh} is the density-of-states effective mass in the semiconductor valence band, D_p and L_p are the diffusion coefficient and diffusion length for holes in the Si, ψ_s^o is the Si surface potential for V=0, J_{sc} is the measured photocurrent density for V=0 in the presence of the SiO_2 layer, and J_{ph} is the measured photocurrent density for the same illumination as $d \to 0$ (in the ideal metal-semiconductor structure with no photocurrent suppression). ψ_s^o was determined by capacitance measurements under the illuminated conditions, and L_p was measured for these samples by a method due to Kar.[3]

The results of K_e and K_h vs d are shown in Fig. 1. In the case of K_h for d = 33 Å the result is a gross underestimate because of complications due to photoemission from the metal into the SiO_2 conduction band. The striking observation is that $K_h >> K_e$, in order words that $T_h << T_e$ for all d when these parameters are measured on the same structure. These samples were Au-SiO_2-nSi structures with SiO_2 layers grown in steam at 900°C after initial growth and removal of ≈2000 Å SiO_2 layers and d was determined by ellipsometry measurements.

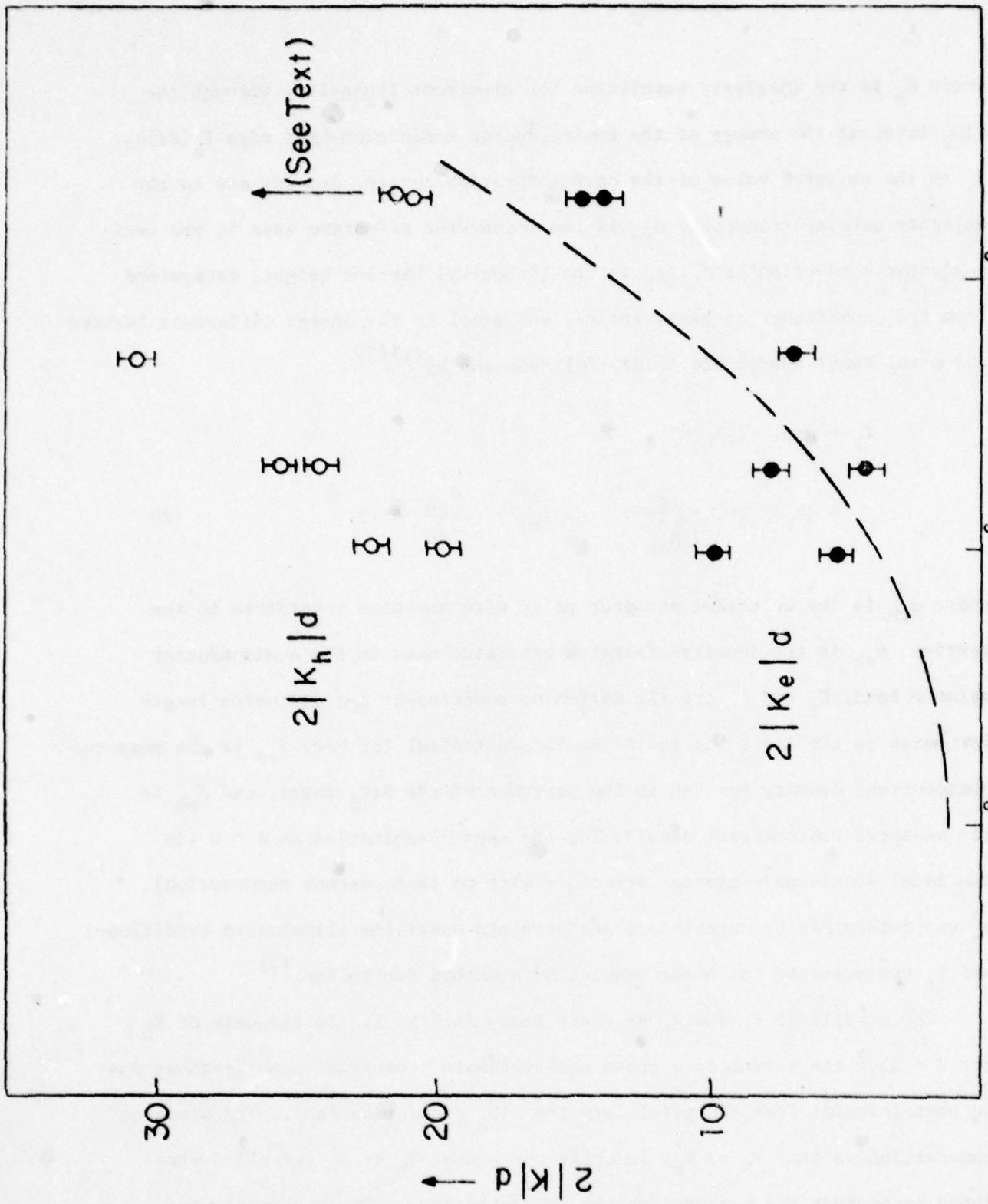

Figure 1: Magnitudes of tunneling exponents for electrons and holes in ultra-thin SiO_2 films illustrating the asymmetry between the (imaginary) wavevectors K_e and K_h. Dotted line shows previous data (Ref. 2) for electrons for comparison.

Let us consider the E-K disperson relation for electrons with energies in the forbidden gap of the SiO_2 film. Assuming a Franz relation[4] we have that

$$\frac{1}{K^2} = \frac{1}{K_c^2} + \frac{1}{K_v^2} = \frac{\hbar^2}{2\, m_c (E-E_g)} - \frac{\hbar^2}{2 m_v E} \tag{3}$$

where m_c, m_v are the effective masses in the conduction, valence bands of the SiO_2.

Photoemission measurements on SiO_2 layers of much greater thickness ($\approx$1000 Å) have shown that $E_c(SiO_2)-E_c(Si) \approx 3$eV, $E_v(Si)-E_v(SiO_2) \approx 4$-5 eV and that $E_g(SiO_2) \approx 9$ eV.[5]-[8] Using these values in Eq. (3) we find that the results of Fig. 1 cannot be obtained with a positive value of both m_c and m_v. It is known however that considerable positive charge (which has as its origin excess Si in the SiO_2) exists in the oxide. This enhances the electron tunneling barrier and reduces that for holes in a way that is consistent with the observations reported here.

This work is being prepared for publication in the Journal of Applied Physics.

*This research was also partially supported by the National Science Foundation under Grant NSF-ENG76-15063.

(1) H. C. Card and E. H. Rhoderick, J. Phys. D: Appl. Phys., 4, 1589 and 1602 (1971).

(2) H. C. Card, Solid St. Commun., 14, 1011 (1974).

(3) S. Kar, Appl. Phys. Lett., 25, 587 (1974).

(4) W. Franz, Handbuch der Physik, Springer, Vol. XVIII, 155 (1956).

(5) R. Williams, Phys. Rev., 140, A 569 (1965).

(6) A. M. Goodman, Phys. Rev., 152, 780 (1966).

(7) T. H. DiStefano and D. E. Eastman, Solid St. Commun., 9, 2259 (1971).

(8) E. Loh, Solid St. Commun., 2, 269 (1976).

(9) R. A. Smith, Semiconductors, Cambridge Univ. Press (1959).

B. CARRIER TRANSPORT ACROSS HETEROJUNCTION INTERFACES

(E. S. Yang, C. M. Wu, H. C. Card)

The transport of carriers from one side of a semiconductor heterojunction to the other is characterized by the quantum-mechanical transmission coefficient (QMT), defined as the ratio of the transmitted to the incident current. The current per unit area from side 1 to side 2 of the junction in the x-direction is given by[1]

$$J_{1\to 2} = \frac{2q}{(2\pi)^3}\iiint\frac{1}{\hbar}\left(\frac{\partial E}{\partial k_x}\right)dk_x dk_y dk_z T(E,k_y,k_z) f_1(E(\bar{k}))\{1-f_2(E(\bar{k}))\} \qquad (1)$$

where k_x, k_y and k_z are the wave vectors in the x, y and z directions respectively. Since heterojunctions used in optical devices are mostly fabricated with a direct-band semiconductor, we assume that the electron effective mass m^* is isotropic. In addition,

$T(E,k_y,k_z)$ = the quantum mechanical transmission coefficient,

E = total kinetic energy

$$= \frac{h^2}{2m^*}\bar{k}^2$$

$$= \frac{h^2}{2m^*}(k_x^2 + k_y^2 + k_z^2)$$

f_1, f_2 = the probability of the carrier occupancy at the energy E in side 1 and side 2, respectively.

Here, electrons are considered as the only carriers and the formulae are valid for holes. Then the net current is the difference of the two current components flowing in opposite directions.

$$J = J_{1\to 2} - J_{2\to 1}$$

$$= \frac{2q}{(2\pi)^3}\iiint\frac{1}{\hbar}\left(\frac{\partial E}{\partial k_x}\right)dk_x dk_y dk_z T(E,k_y,k_z)\{f_1(E(\bar{k})) - f_2(E(\bar{k}))\} \qquad (2)$$

The QMT is defined as the ratio of the transmitted current to the incident, i.e., the probability of a carrier passing through a junction interface. From Crowell's analysis, the QMT of the depletion region of a Schottky barrier depends on the potential height and the material parameter $E_{oo} = 1.8565 \cdot 10^{-11}(N/m_r\epsilon_r)^{1/2}$. The WKB approximation is valid when the carrier's kinetic energy is not near the peak of the potential. In the Schottky diode, electrons are emitted to a region with a larger effective mass (the free electron mass); therefore, the current transport is very sensitive to the value of the effective mass ratio ϕ. In the heterojunction, the carrier transport through the junction is affected by the change of the effective mass which makes the perpendicular kinetic energy to be added or subtracted dependent on the value of ϕ.

The transport equations are examined in the heterojunction interface, being especially concerned with the different masses of carriers in both sides of either an isotype or anisotype heterojunction. The upper and lower limits of the perpendicular component of the kinetic energy are, in general, not infinity and zero, respectively. The general form of the current density is derived by assuming an isotropic effective mass. In the model presented here, the perpendicular component of the kinetic energy is modified by $1/\phi$ so that the perpendicular momentum is conserved when carriers pass through the barrier and the QMT coefficient is modified by the factor $\tilde{n}_1$ (Figs. 1 and 2). For the conservation of the total energy, this modulated perpendicular kinetic energy of $(1/\phi - 1)E_\perp$ plays a role in reducing effectively the barrier height in the calculation of the quantum-mechanical transmission coefficient.

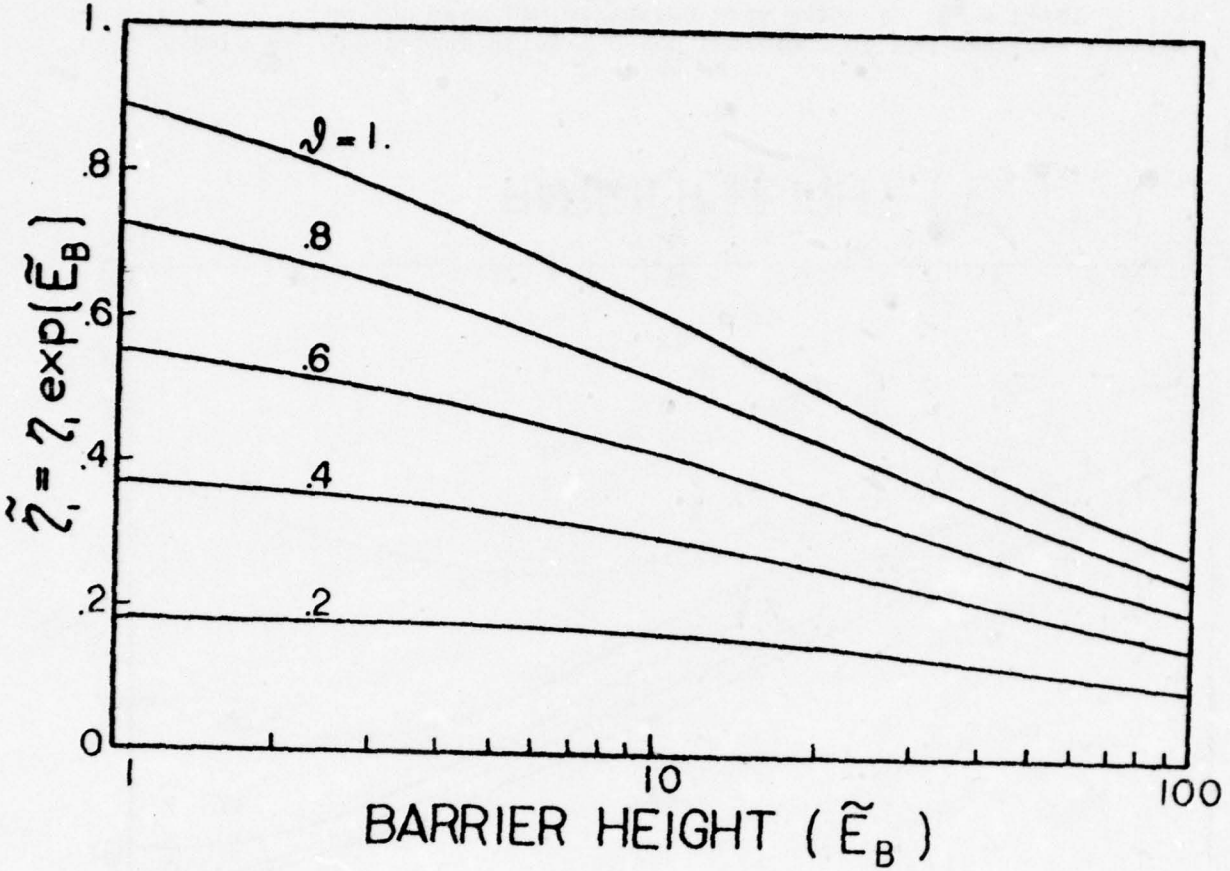

Figure 1: The values of $\tilde{\eta}_1 = \eta_1 \exp(\tilde{E}_B)$ are functions of the barrier with the effective mass ratio ϑ. $\tilde{E}_B = E_B/kT$.

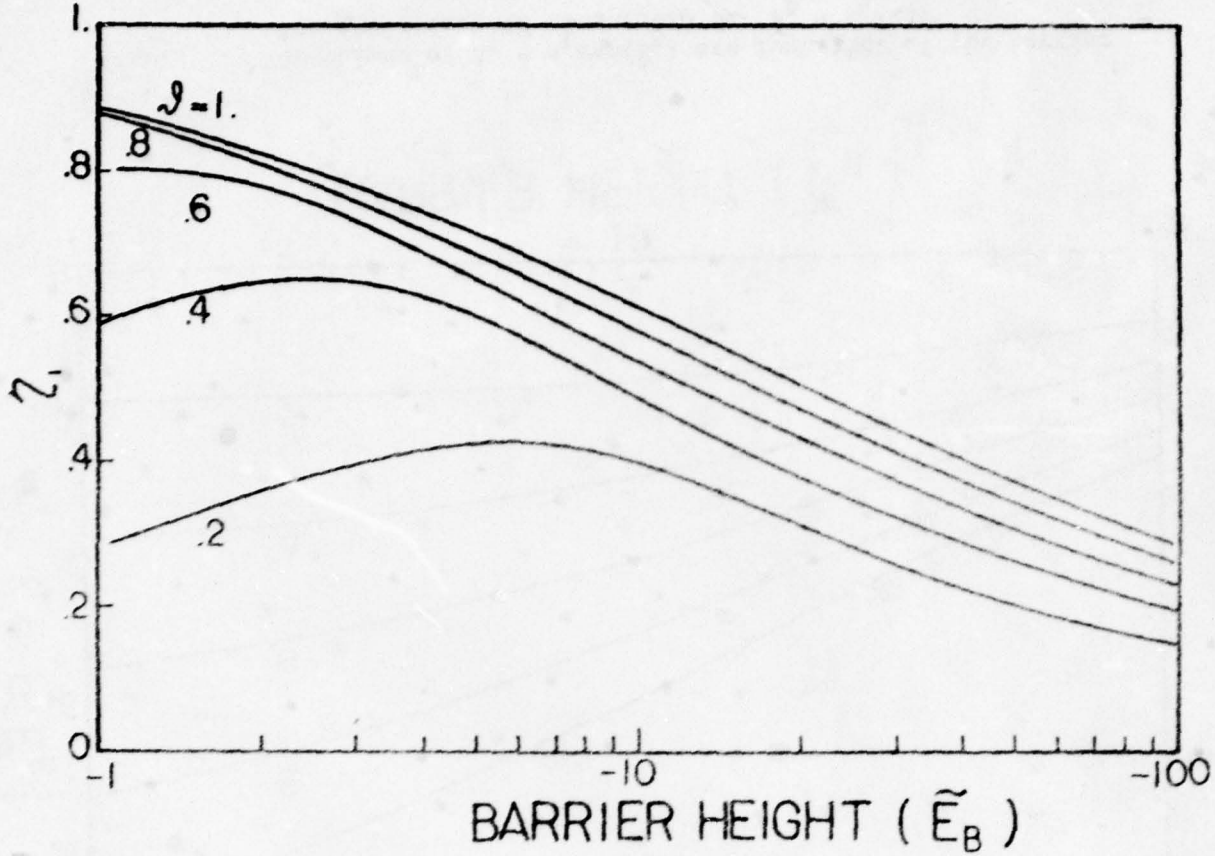

Figure 2: The values of $\tilde{\eta}_1 = \eta$ are functions of the negative barrier height with the effective mass ratio ϑ. $\tilde{E}_B = E_B/kT$.

Since the WKB approximation cannot be used to calculate the quantum-mechanical transmission when the kinetic energy is around the peak of the potential barrier, we have used a combined WKB-numerical method in which the parallel kinetic energy is considered separately in three regions: (i) $E_{\parallel} > E_u$ in which the WKB method is valid, (ii) $E_u > E_{\parallel} > E_\ell$ in which the numerical method is used, and (iii) $E_{\parallel} < E_\ell$ in which the WKB method is employed in the depletion region of side 1 and the numerical method is used in side 2. Referring to Rode's work on the AlGaAs-GaAs DH laser, the $Al_xGa_{1-x}As$-GaAs N-n junction is taken as an example to calculate the current densities under both forward and reverse biasing voltages (Figs. 3 and 4). At high biasing, the forward characteristics show that the quantum-mechanical reflection reduces the current density to sixty percent of its classical value. But at low biasing, it shows that the tunneling current must be considered as the semiconductor of the larger energy-band gap is heavily doped. This transport theory is applicable to the anisotype heterojunction. It has to be considered additionally that the diffusion mechanism appears in series with the T-F emission considered here.

We have also calculated the electrostatic effects of interface states on the carrier transport across p-N and N-p heterojunctions and this is reported in Ref. 2.

(1) C. M. Wu and E. S. Yang, "Carrier Transport across Heterojunction Interfaces," Solid State Electron., in press (1979).

(2) H. C. Card, "Electrostatic Effects of Interface States on Carrier Transport in Semiconductor Heterojunctions," J. Appl. Phys., in press (1979).

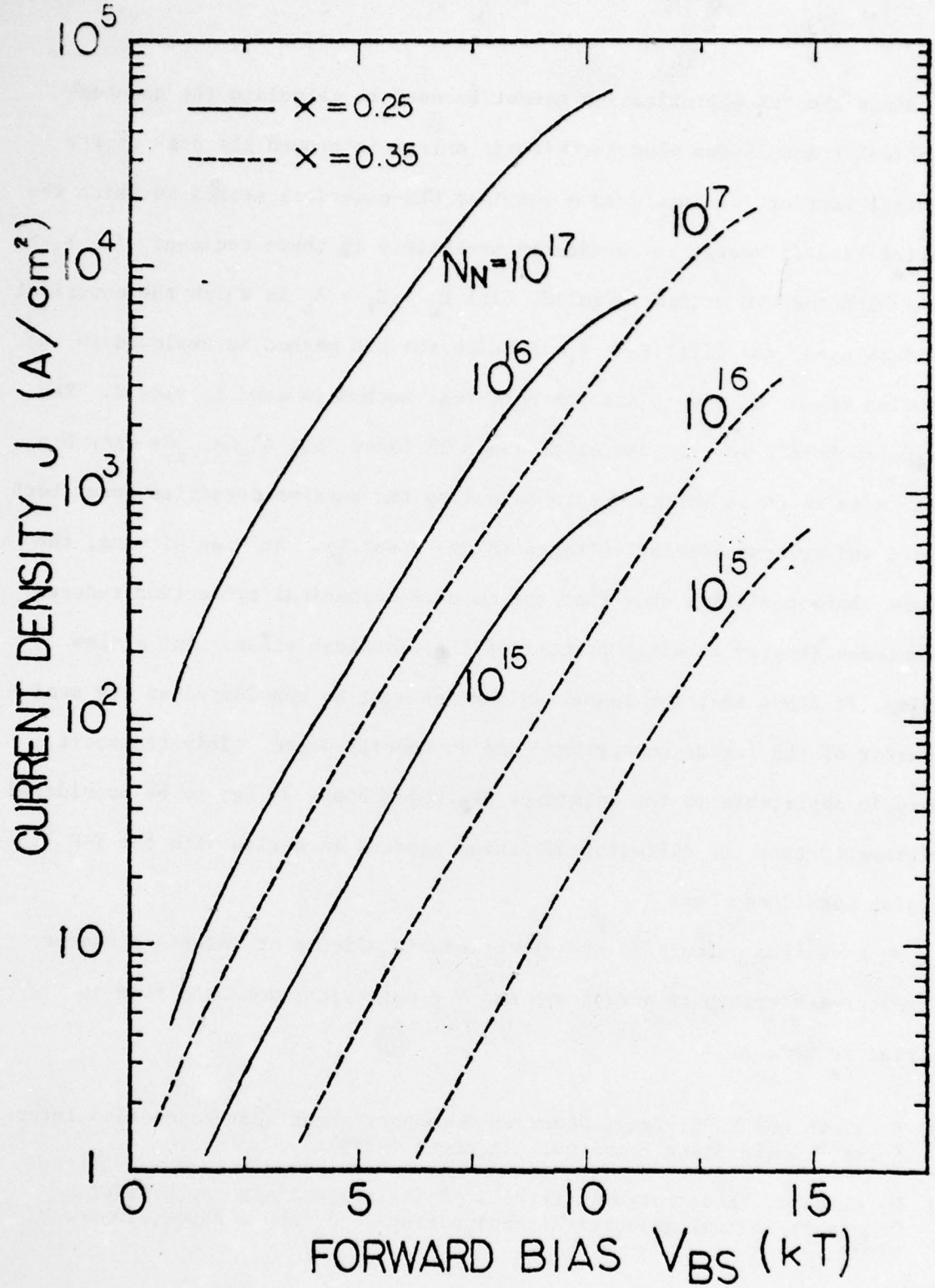

Figure 3: The forward current of the N-n $Al_xGa_{1-x}As$ - GaAs junction under the bias V_{BS}, Nn is the doping of the ternary compound and that of GaAs is $10^{15}cm^{-3}$.

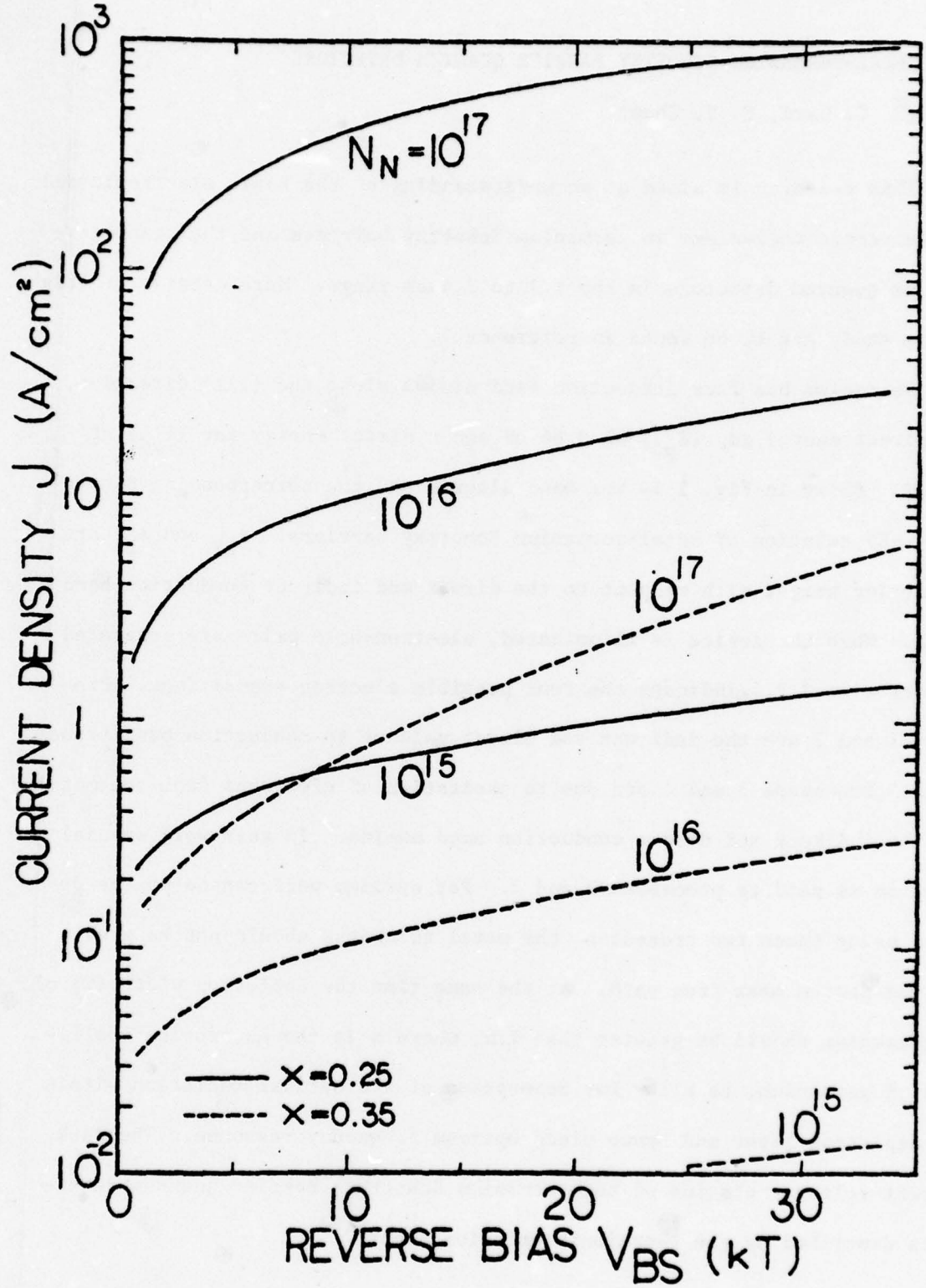

Figure 4: The reverse current of the N-n $Al_xGa_{1-x}As$ - GaAs junction under the bias V_{BS}, N_n is the doping of the ternary compound and that of GaAs is $10^{15}cm^{-3}$.

C. METAL-GERMANIUM SCHOTTKY BARRIER QUANTUM DETECTORS

(H. C. Card, E. Y. Chan)

This research is aimed at an understanding of the basic electronic and optoelectronic mechanisms in germanium Schottky barriers and their applications as quantum detectors in the 1.1 to 1.4 μm range. More details of this initial study are to be found in reference 1.

Germanium has four conduction band minima along the (111) direction, an indirect energy gap (E_{gi}) of 0.66 eV and a direct energy gap (E_{gd}) of 0.81 eV. Shown in Fig. 1 is the band diagram and the corresponding dispersion (E-K) relation of metal-germanium Schottky barriers. ϕ_{B2} and ϕ_{B1} are the barrier height with respect to the direct and indirect conduction band minima. When the device is illuminated, electron-hole pairs are generated and arrows 1,2,3,4 indicate the four possible electron transitions. Processes 1 and 2 are the indirect and direct valence to conduction band transitions. Processes 3 and 4 are due to excitation of electrons from the metal into the indirect and direct conduction band minima. In this work special attention is paid to processes 1 and 2. For optimum performance of the detector using these two processes, the metal thickness should not be greater than the photon mean free path. At the same time the depletion width (W) of the germanium should be greater than $1/\alpha$, where α is the absorption coefficient of germanium, to allow for absorption of the optical radiation within the depletion layer and hence yield optimum frequency response. The dark current-voltage relation of the germanium Schottky barrier quantum detector is described by the thermionic emission theory[3] as

$$I = A^{**}aT^2 \exp\left(\frac{-\phi_b}{KT}\right) \left\{\exp\left(\frac{qV}{nKT}\right)-1\right\} \qquad (1)$$

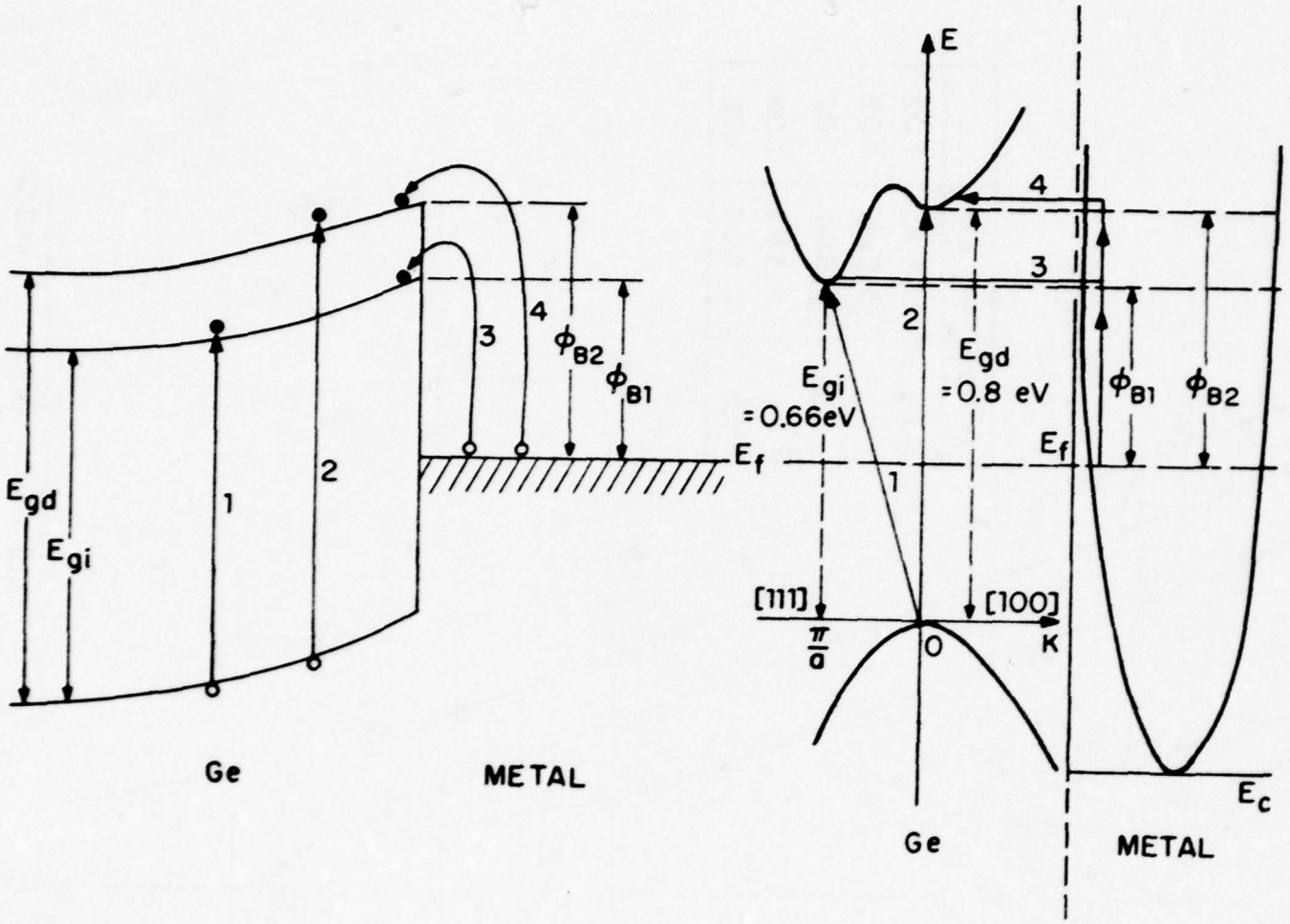

Figure 1: Energy band diagram and dispersion (E-K) relation for metal-Ge Schottky barrier. Arrows 1,2,3 and 4 indicate the four possible electron transition mechanisms.

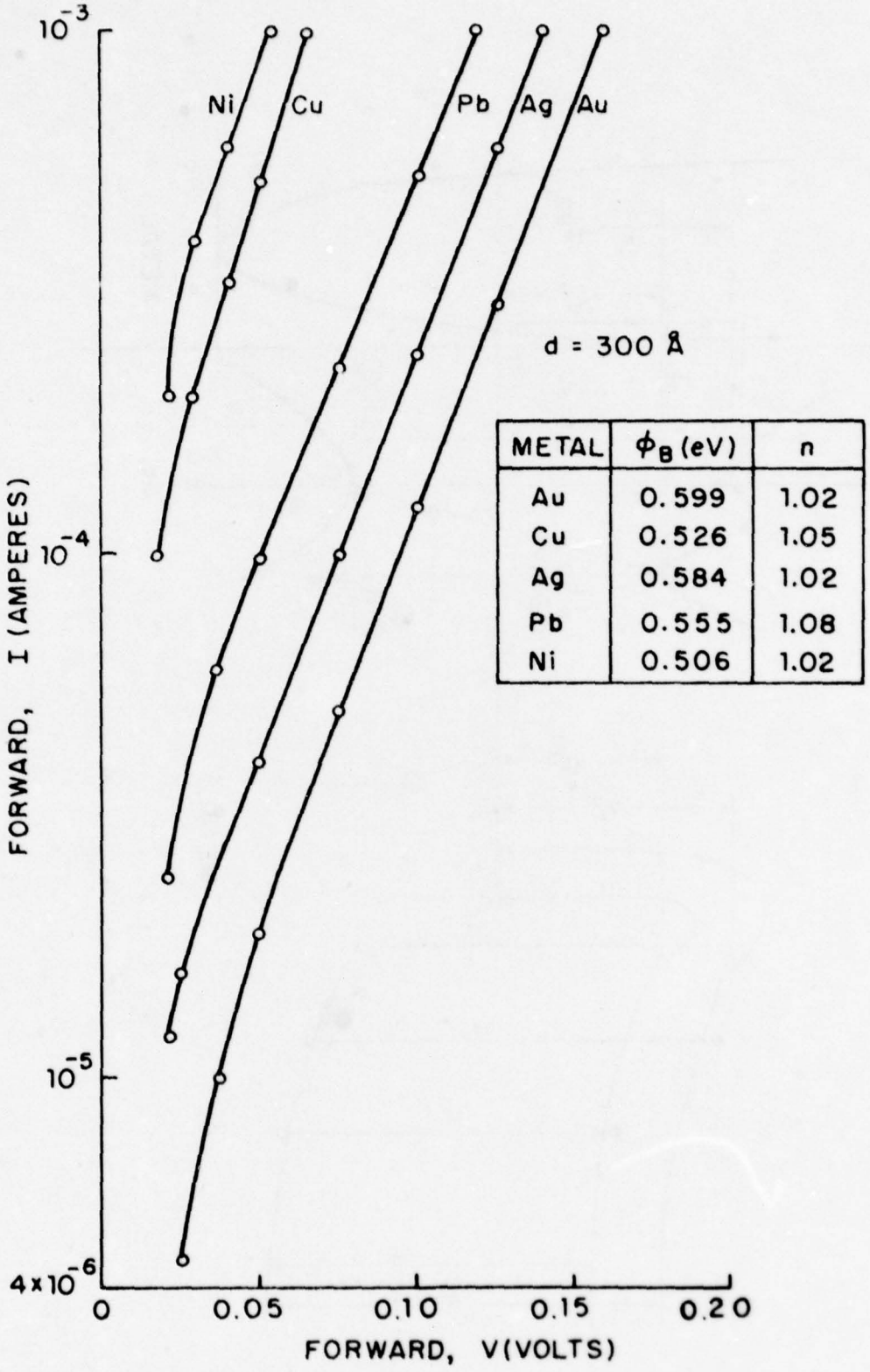

METAL	ϕ_B (eV)	n
Au	0.599	1.02
Cu	0.526	1.05
Ag	0.584	1.02
Pb	0.555	1.08
Ni	0.506	1.02

Figure 2: Semilogarithmic plot of the I-V characteristics for five different metal-Ge contacts with d = 300 Å. Table in the insert shows the corresponding n values and ϕ_B is obtained by extrapolation of the linear portion of the I-V curve to V=0 axis.

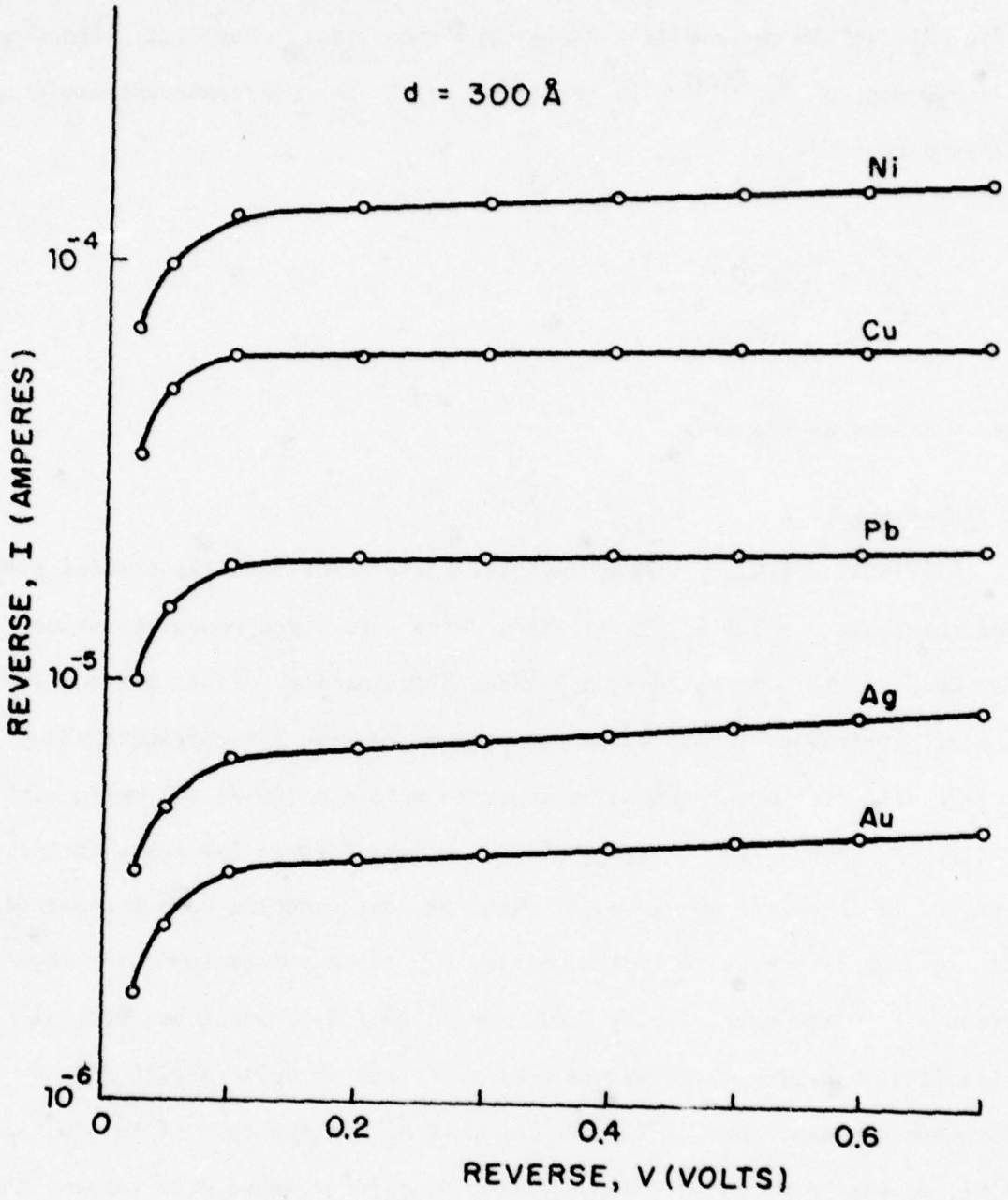

Figure 3: Reverse saturation currents (I_s) for the same five metal-Ge contacts of Fig. 4, I_s in this fig. are in close agreement with those obtained by extrapolation in Fig. 4.

where the parameter n is the ideality factor, ϕ_B is the barrier height ($=\phi_{B1}$ in Fig. 2), A** is the modified Richardson's constant. For (111) germanium, A** is 50 Amp/cm^2 ^oK.[2,3] The capacitance voltage (C-V) characteristic is described by

$$1/C^2 = \frac{2(\phi_o - V - KT/q)}{q \varepsilon a^2 N_d} \qquad (2)$$

where a is the device area.

I-V Characteristics

Fig. 3 is a typical linear I-V plot for a Au-Ge Schottky barrier with metal thickness d = 300 Å. Excellent reverse saturation characteristics were observed both in the dark and under illumination. Figs. 2 and 3 are the semilogarithmic plots for the forward and reverse I-V characteristics for five different metal-germanium contacts with d = 300 Å; all agree with Eq. (1). I_s found from the extrapolation of the forward I-V characteristics in Fig. 2 is in very good agreement with the corresponding values obtained from reverse I-V characteristics in Fig. 3. The n values found for these devices are in the range $1.03 \pm 0.01 \leq n \leq 1.08 \pm 0.01$ which are very close to ideality. The I-V measurements were performed on devices with metal thicknesses in the range of 50 Å $\leq$ d $\leq$ 2000 Å. In the case of Au, Cu, Ag and Ni, ϕ_B was found to be independent of d; ϕ_B's averaged over various thicknesses are: (Au) 0.589 eV, (Cu) 0.522, (Ag) 0.544 eV, (Ni) 0.496. In the case of Pb-Ge contacts, a pronounced decrease in ϕ_B with d is observed. Ideal devices are obtainable for all metal-Ge contacts including the lower d cases.

C-V Measurements

Fig. 4 shows $1/C^2$ vs. V_R (reverse bias) for various metal-germanium contacts at d ≈ 300 Å. These are good straight lines at high reverse bias voltages. Deviations from straight lines occur at low biasing voltages and this tendency is more pronounced for Pb and Ag. The ϕ_B's found by extrapolation of the linear portion of the $1/C^2$ vs. V from Eq. (2) are: 0.596 eV for Au-Ge contact, 0.519 eV for Cu-Ge contact, 0.506 eV for Ni-Ge contact, 0.5745 eV for Ag-Ge contact and 0.576 eV for Pb-Ge contact. These values are in good agreement with the values obtained from the I-V data. The doping density N_d determined from the slope of these straight lines are in good agreement with the specified resistivity range. ϕ_B's found from the two measurements are in close agreement within an error of ± 0.03 eV. The deviation from straight lines at low bias voltages for the $1/C^2$ vs. V plots are due to the presence of inversion layers in metal-Ge contacts. The high ϕ_B to E_g (energy gap) ratio in metal-Ge contacts requires a modification of the depletion approximation expressed in Eqs. (1) and (2).

$$\frac{1}{C^2} = \frac{2(U(V) - V)}{q\epsilon a^2 N_d} \tag{3}$$

where U is now function of voltage (V). At high reverse bias, $U(V) \rightarrow \phi_o - KT/q$ and Eq. (3) will approach the depletion approximation of Eq. (2). The more pronounced deviation in the case of Ag and Pb is attributed to the presence of deep traps as explained in reference 5. C-V measurements performed under HeNe laser illumination also indicated the existence of traps. The effect of illumination on the C-V data is negligible in the case of Au, Cu, Ni-Ge contacts, but becomes significant in the case of Ag and Pb. N_d's determined from the slope at lower biases are smaller than those obtained at high bias

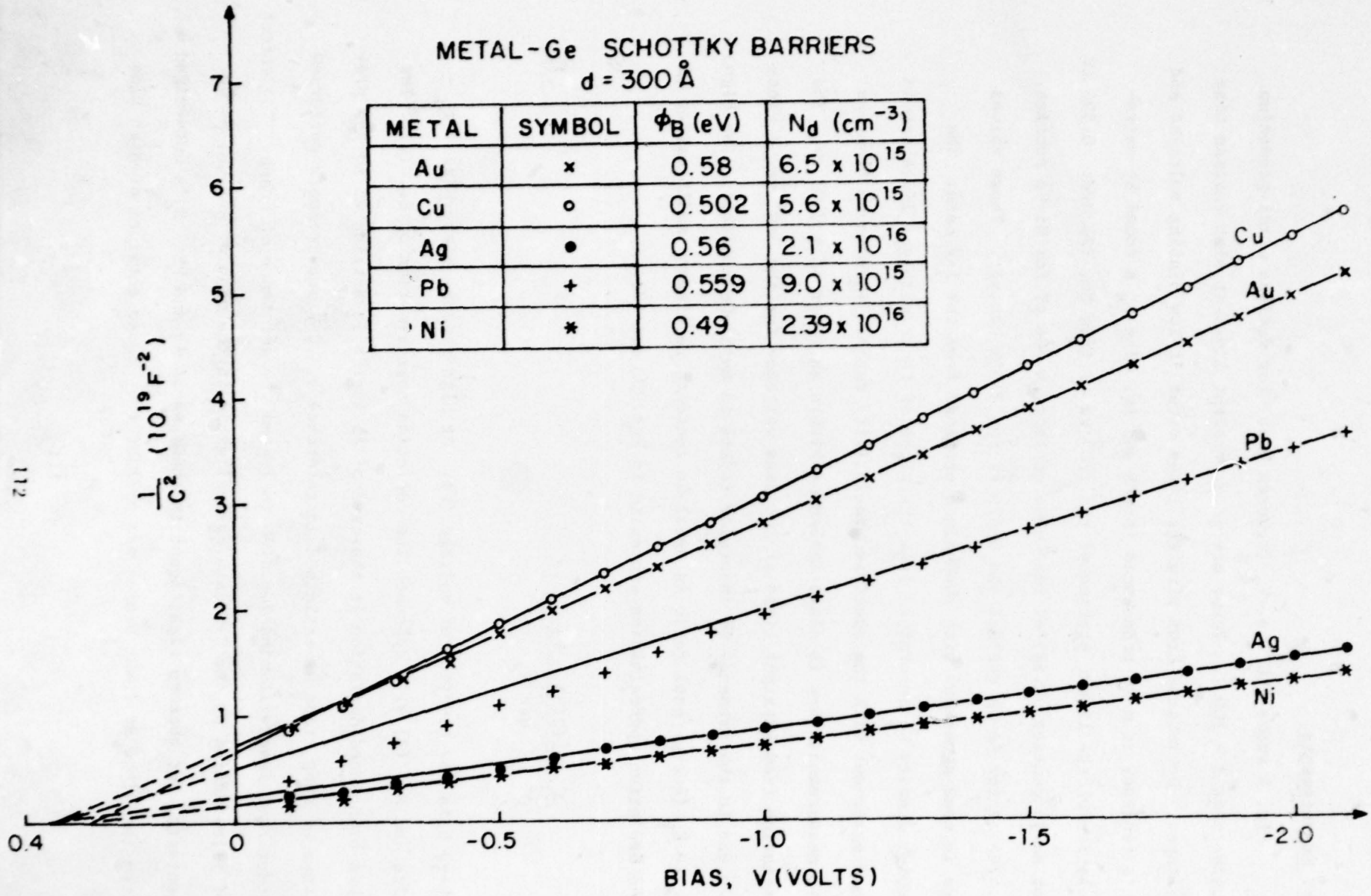

Figure 4: Capacitance-voltage (C^{-2} vs. V) plots for metal-Ge contacts with d = 300 Å.

and still smaller under laser illumination. This we feel is due to the filling of traps in the depletion layer by photoexcited electrons. C-V measurements have also revealed minority carrier injection-induced inductance at large forward bias as predicted in reference 6.

Optical Response

I-V measurements under HeNe laser illumination were performed (for ideal devices only) at various metal film thicknesses. I_{sc} and I_{ph} are photogenerated current at V = 0 and V = -1.0 respectively. The number of electrons generated/sec at V = 0 is given as $N_{pho} = I_{sc}/q$ and at V = -1.0 V as $N_{phi} = I_{ph}/q$. The quantum efficiencies (Q.E.) at V = 0 and V = -1.0V are given as $\eta_o = (N_{pho}/N) \times 100\%$ and $\eta_R = (N_{phi}/N) \times 100\%$.

Figs. 5 and 6 summarize the results of η_o and η_R for all devices. Both η_o and η_R decline with metal thickness above a critical thickness d $\simeq$ 100 Å. For d $\leq$ 100 Å, η_o for Au is approximately 52%, for Cu 45%, for Ag 43%, with considerably lower values for Pb and Ni; η_R for Au is 66%, Cu is 78%, Ag is 56% which are higher than η_o. It was found that for V < -1.0V virtually all photoelectrons were collected since J_{ph} saturated for larger reverse V. The difference observed for η_o and η_R amongst various metal-Ge contacts at the same d is due to the differences in metal reflectivity of the HeNe laser illumination.

(1) E. Y. Chan and H. C. Card, "Optoelectronic Properties of Metal-Ge Schottky Barrier Quantum Detectors", IEEE-IEDM Digest of Tech. Papers, 653-656 (1978).

(2) C. R. Crowell, "The Richardson Constant for Thermionic Emission in Schottky Barrier Diodes," Solid-State Electron. 8, 395-399.

(3) C. R. Crowell and S. M. Sze, "Current Transport in Metal-Semiconductor Barriers," Solid-State Electron. 9, 1035-1048 (1966).

(4) R. F. Schwartz and J. F. Walsh, "Part V-The Properties of Metal to Semiconductor Contacts," IRE Proc. 41 1715-1720 (1953)

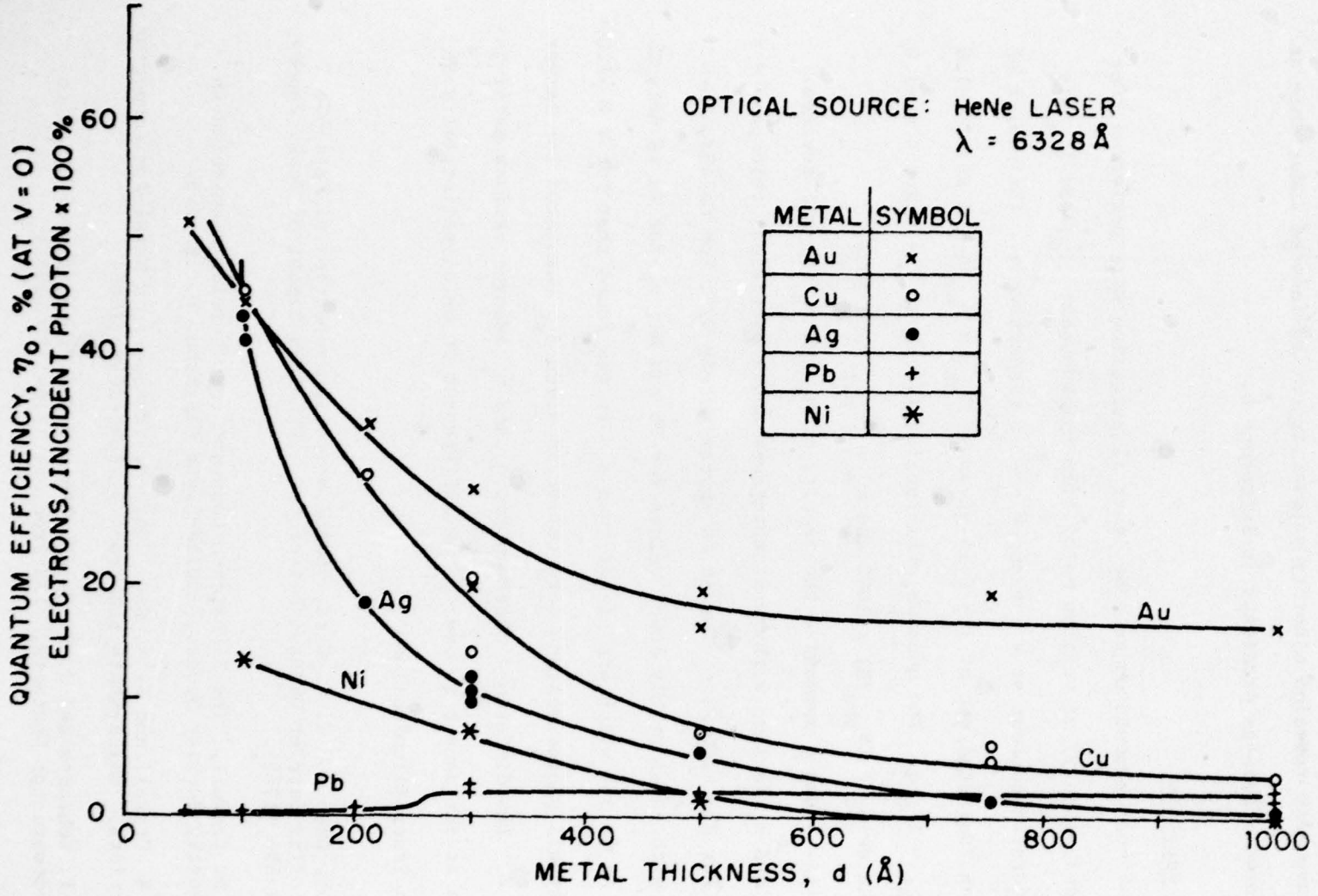

Figure 5: Quantum efficienty (Q.E.) at zero bias for metal-Ge contacts vs. metal thickness.

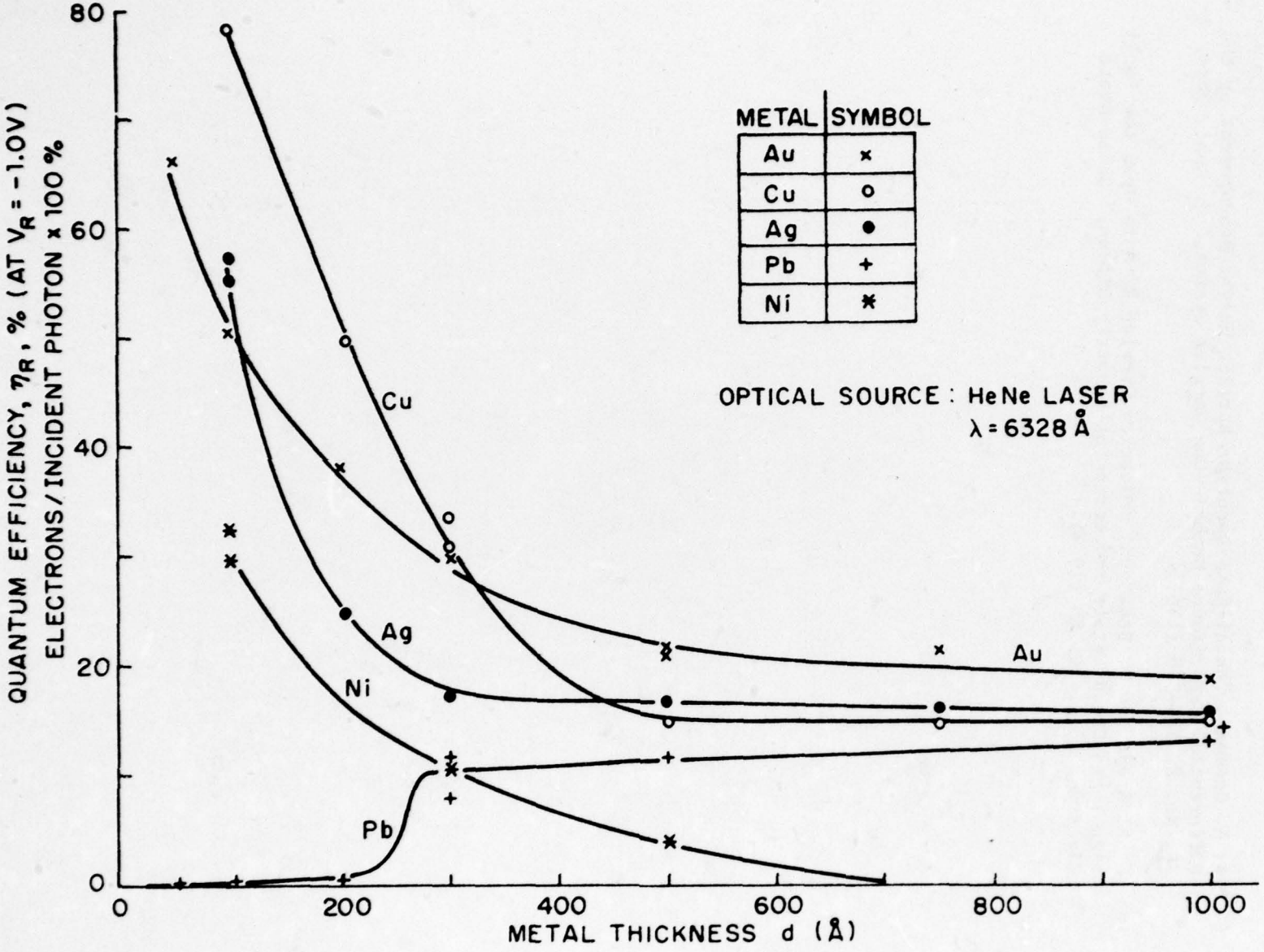

Figure 6: Quantum efficienty (Q.E.) for metal-Ge contacts vs. metal thickness at a reverse bias = -1.0 volt.

(5) A. M. Goodman, "Metal-Semiconductor Barrier Height Measurement by the Differential Capacitance Method--One Carrier System," J. Appl. Phys. 34, No. 2, 324-338 (1963).

(6) M. A. Green and J. Shewchun, "Minority Carrier Effects Upon the Small Signal and Steady-State Properties of Schottky Diodes," Solid-State Electron. 16 114101150 (1973).

PERSONNEL

Faculty

N. D. Bhaskar, Assistant Professor of Physics
H. C. Card, Associate Professor of Electrical Engineering
K. Eisenthal, Professor of Chemistry
G. W. Flynn, Professor of Chemistry, Director
W. Happer, Professor of Physics
S. R. Hartmann, Professor of Physics
J. M. Luttinger, Professor of Physics
I. I. Rabi, University Professor Emeritus
M. C. Teich, Professor of Engineering Science
P. Thaddeus, Adjunct Professor of Physics
C. S. Wu, Pupin Professor of Physics
E. Yang, Professor of Electrical Engineering

Research Associates and Physicists

Dr. Y. Chen
Dr. A. Kerr
Dr. J. Liran
Dr. T. Mossberg
Dr. P. Prucnal
Dr. Y. Taur

Graduate Research Assistants

J. Ahl
J. Camparo
E. Chan
K. Chiang
M. Hou
R. Kachru
M. Lester
K. Leung
R. Meyers
K. Ng
B. Novak
J. Pietras
T. Poon
R. Sheorey
P. Siegel
B. Suleman
G. Vannucci
A. Vasilakis
E. Whittaker
C. Wu
E. Zouboulis

Technical Research Assistants

Mr. I. Beller

Mr. E. Deery

Physics Department Electronics Engineering and Construction Shop*

Mr. J. Packer

Physics Department Machine Shop*

Mr. E. Jauch

Administration

Ms. T. Brasfield

Ms. I. Moon

Ms. P. Pohlman

*The Machine Shop and Electronics Shop facilities are available for the Columbia Radiation Laboratory.

JSEP REPORTS DISTRIBUTION LIST

DEPARTMENT OF DEFENSE

Director
National Security Agency
ATTN: Dr. T. J. Beahn
Fort George G. Meade, MD 20755

Defense Documentation Center
(12 copies)
ATTN: DDC-TCA
(Mrs. V. Caponio)
Cameron Station
Alexandria, VA 22314

Dr. George Gamota
Acting Assistant for Research
Deputy Under Secretary of Defense
for Research & Engineering
(Research & Advanced Technology)
Room 3D1079, The Pentagon
Washington, D.C. 20301

Mr. Leonard R. Weisberg
Office of the Under Secretary
of Defense for Research &
Engineering/EPS
Room 3D1079, The Pentagon
Washington, D.C. 20301

Defense Advanced Research Projects
Agency
ATTN: (Dr. R. Reynolds)
1400 Wilson Boulevard
Arlington, VA 22209

DEPARTMENT OF THE ARMY

Commandant
US Army Air Defense School
ATTN: ATSAD-T-CSM
Fort Bliss, TX 79916

Commander
US Army Armament R&D Command
ATTN: DRDAR-RD
Dover, NJ 07801

Commander
US Army Ballistics Reserach Lab.
ATTN: DRXRD-BAD
Aberdeen Proving Ground
Aberdeen, MD 21005

Commandant
US Army Command and General Staff College
ATTN: Acquisitions, Lib. Div.
Fort Leavenworth, KS 66027

Commander
US Army Communication Command
ATTN: CC-OPS-PD
Fort Huachuca, AZ 85613

Commander
US Army Materials and Mechanics Research
Center
ATTN: Chief, Materials Sciences Div.
Watertown, MA 02172

Commander
US Army Materiel Development and
Readiness Command
ATTN: Technical Library, Rm. 7S 35
5001 Eisenhower Avenue
Alexandria, VA 22333

Commander
US Army Missile R&D Command
ATTN: Chief, Document Section
Redstone Arsenal, AL 35809

Commander
US Army Satellite Communications Agency
Fort Monmouth, NJ 07703

Commander
US Army Security Agency
ATTN: IARD-T
Arlington Hall Station
Arlington, VA 22212

Project Manager
Army Tactical Data Systems
EAI Building
West Long Branch, NJ 07764

Commander
Atmospheric Sciences Lab. (ERADCOM)
ATTN: DELAS-BL-DD
White Sands Missile Range, NM 88002

Director
US Army Electronics R&D Command
Night Vision & Electro-Optics Labs
ATT: Dr. Ray Balcerak
Fort Belvoir, VA 22060

Commander
US Army Communications
R&D Command
ATTN: DRDCO-COM-C
(Dr. Herbert S. Bennett)
Fort Monmouth, NJ 07703

Commander
US Army Research Office
ATTN: DRXRO-MA (Dr. Paul Boggs)
P.O. Box 12211
Research Triangle Park, NC 27709

Commander
US Army Missile R&D Command
Physical Sciences Directorate
ATTN: DRDMI-TRD (Dr. Charles Bowden)
Redstone Arsenal, AL 35809

Director
TRI-TAC
ATTN: TT-AD (Mrs. Briller)
Fort Monmouth, NJ 07703

Commander
US Army Missile R&D Command
Advanced Sensors Directorate
ATTN: DRDMI-TER (Dr. Don Burlage)
Redstone Arsenal, AL 35809

Commander
US Army Electronics R&D Command
Night Vision & Electro-Optics Labs
ATTN: DELNV (Dr. Rudolf G. Buser)
Fort Monmouth, NJ 07703

Director
US Army Electronics R&D Command
Night Vision & Electro-Optics Labs
ATTN: John Dehne
Fort Belvoir, VA 22060

Director
US Army Electronics R&D Command
Night Vision & Electro-Optics Labs
ATTN: Dr. William Ealy
Fort Belvoir, VA 22060

Director
US Army Electronics R&D Command
ATTN: DELEW (Electronics Warfare Lab.)
White Sands Missile Range, NM 88002

Executive Secretary, TAC/JSEP
US Army Research Office
P.O. Box 12211
Research Triangle Park, NC 27709

Commander
US Army Missile R&D Command
Physical Sciences Directorate
ATTN: DRDMI-TER (Dr. Michael D. Fahey)
Redstone Arsenal, AL 35809

Commander
US Army Missile R&D Command
Physical Sciences Directorate
ATTN: DRDMI-TRO (Dr. William L. Gamble)
Redstone Arsenal, AL 35809

Commander
White Sands Missile Range
ATTN: STEWS-ID-SR (Dr. Al L. Gilbert)
White Sands Missile Range, NM 88002

Project Manager
Ballistic Missile Defense Program Office
ATTN: DACS-DMP (Mr. A. Gold)
1300 Wilson Blvd.
Arlington, VA 22209

Commander
US Army Communications R&D Command
ATTN: CENTACS (Dr. David Haratz)
Fort Monmouth, NJ 07703

Commander
Harry Diamond Laboratories
ATTN: Mr. John E. Rosenberg
2800 Powder Mill Road
Adelphi, MD 20783

HQDA (DAMA-ARZ-A)
Washington, D. C. 20310

Commander
US Army Electronics R&D Command
ATTN: DELET-E (Dr. Jack A. Kohn)
Fort Monmouth, NJ 07703

Commander
US Army Electronics Technology
and Devices Lab.
ATTN: DELET-EN (Dr. S. Kroenenberg)
Fort Monmouth, NJ 07703

Commander
US Army Communications R&D Command
ATTN: CENTACS (Mr. R. Kulinyi)
Fort Monmouth, NJ 07703

Commander
US Army Communications R&D Command
ATTN: DRDCO-TCS-BG (Dr. E. Lieblein)
Fort Monmouth, NJ 07703

Commander
US Army Electronics Technology
and Devices Lab.
ATTN: DELET-MM (Mr. N. Lipetz)
Fort Monmouth, NJ 07703

Director
US Army Electronics R&D Command
Night Vision & Electro-Optics Labs.
ATTN: Dr. Randy Longshore
Fort Belvoir, VA 22060

Commander
US Army Electronics R&D Command
ATTN: DRDEL-CT (Dr. W. S. McAfee)
2800 Powder Mill Road
Adelphi, MD 20783

Commander
US Army Research Office
ATTN: DRXRO-EL (Dr. James Mink)
P.O. Box 12211
Research Triangle Park, NC 27709

Director
US Army Electronics R&D Command
Night Vision Laboratory
ATTN: DELNV
Fort Belvoir, VA 22060

COL Robert Noce
Senior Standardization Representative
US Army Standardization Group, Canada
Canadian Force Headquarters
Ottawa, Ontario, Canada KIA)K2

Commander
Harry Diamond Laboratories
ATTN: Dr. Robert Oswald, Jr.
2800 Powder Mill Road
Adelphi, MD 20783

Commander
US Army Communications R&D Command
ATTN: CENTACS (Dr. D. C. Pearce)
Fort Monmouth, NJ 07703

Director
US Army Electronics R&D Command
Night Vision & Electro-Optics Labs.
ATTN: DELNV-ED (Dr. John Pollard)
Fort Belvoir, VA 22060

Commander
US Army Research Office
ATTN: DRXRO-EL (Dr. William A. Sander)
P.O. Box 12211
Research Triangle Park, NC 27709

Commander
US Army Communications R&D Command
ATTN: DRDCO-COM-RH-1
(Dr. Felix Schwering)
Fort Monmouth, NJ 07703

Commander
US Army Electronics Technology and Devices Lab.
ATTN: DELET-I (Dr. C. G. Thornton)
Fort Monmouth, NJ 07703

U.S. Army Research Office
(3 copies)
ATTN: Library
P.O. Box 12211
Research Triangle Park, NC 27709

Director
Division of Neuropsychiatry
Walter Reed Army Institute of Research
Washington, D.C. 20012

Commander
USA ARRADCOM
ATTN: DRDAR-SCF-CC (Dr. N. Coleman)
Dover, NJ 07801

DEPARTMENT OF THE AIR FORCE

Mr. Robert Barrett
RADC/ES
Hanscom AFB, MA 01731

Dr. Carl E. Baum
AFWL (ES)
Kirtland AFB, NM 87117

Dr. E. Champagne
AFAL/DH
Wright-Patterson AFB, OH 45433

Dr. R. P. Dolan
RADC/ESR
Hanscom AFB, MA 01731

Mr. W. Edwards
AFAL/DH
Wright-Patterson AFB, OH 45433

Professor R. E. Fontana
Head Dept. of Electrical Eng.
AFIT/ENE
Wright-Patterson AFB, OH 45433

Dr. Alan Garscadden
AFAPL/POD
Wright-Patterson AFB, OH 45433

USAF European Office of Aerospace Research
ATTN: Major J. Gorrell
Box 14, FPO, New York 09510

LTC Richard J. Gowen
Department of Electrical Engineering
USAF Academy, CO 80840

Mr. Murray Kesselman (ISCA)
Rome Air Development Center
Griffiss AFB, NY 13441

Dr. G. Knausenberger
Air Force Member, TAC
Air Force Office of Scientific Research
(AFSC) AFSOR/NE
Bolling Air Force Base, DC 20332

Col. R. V. Gomez
Air Force Member, TAC
Air Force Office of Scientific Research
(AFSC) AFSOR/NE
Bolling Air Force Base, DC 20332

Mr. R. D. Larson
AFAL/DHR
Wright-Patterson AFB, OH 45433

Dr. Edward Altshuler
RADC/EEP
Hanscom AFB, MA 01731

Mr. John Mottsmith (MCI)
HQ ESD (AFSC)
Hanscom AFB, MA 01731

Dr. Richard Picard
RADC/ETSL
Hanscom AFB, MA 01731

Dr. J. Ryles
Chief Scientist
AFAL/CA
Wright-Patterson AFB, OH 45433

Dr. Allan Schell
RADC/EE
Hanscom AFB, MA 01731

Mr. H. E. Webb, Jr. (ISCP)
Rome Air Development Center
Griffiss AFB, NY 13441

Dr. R. Kelley
Air Force Office of Scientific Research
(AFSC) AFOSR/NP
Bolling Air Force Base, DC 20332

LTC G. McKemie
Air Force Office of Scientific Research
(AFSC) AFOSR/NM
Bolling Air Force Base, DC 20332

DEPARTMENT OF THE NAVY

Office of the Naval Research
800 North Quincy Street
Arlington, VA 22217
Attn: Codes 220/221
427
432

Naval Research Laboratory
4555 Overlook Avenue, SW
Washington, DC 20375
Attn: Codes 1405 - Dr. S. Teitler
2627 - Mrs. D. Folen
5200 - A. Brodzinsky
5210 - J. E. Davey
5270 - B. D. McCombe
5403 - J. E. Shore
5464/5410 - J. R. Davis
5510 - W. L. Faust
7701 - J. D. Brown

Director
Office of Naval Research Branch Office
495 Summer Street
Boston, MA 02210

Director
Office of Naval Research
New York Area Office
715 Broadway, 5th Floor
New York, NY 10003

Director
Office of Naval Research Branch Office
536 South Clark Street
Chicago, IL 60605

Director
Office of Naval Research Branch Office
1030 East Green Street
Pasadena, CA 91101

Office of Naval Research
San Francisco Area Office
760 Market Street, Room 447
San Francisco, CA 94102

Naval Surface Weapons Center
Attn: Technical Library
Code DX-21
Dahlgren, VA 22448

Dr. J. G. Mills, Jr.
Naval Surface Weapons Center
Code DF
Dahlgren, VA 22448

Naval Air Development Center
Johnsville
Warminster, PA 18974
Attn: Codes 01 - Dr. R. Lobb
202 - T. Shopple
Technical Library

Dr. Gernot M. R. Winkler
Director, Time Service
U.S. Naval Observatory
Mass. Ave. at 34th Street, NW
Washington, DC 20390

Dr. G. Gould
Technical Director
Naval Coastal Systems Laboratory
Panama City, FL 32401

Dr. W. A. VonWinkle
Associate Technical Director
for Technology
Naval Underwater Systems Center
New London, CT 06320

Naval Underwater Systems Center
Attn: J. Merrill
Newport, RI 02840

Technical Director
Naval Underwater Systems Center
New London, CT 06320

Naval Research Laboratory
Underwater Sound Reference Division
Technical Library
P.O. Box 8337
Orlando, FL 32806

Naval Ocean Systems Center
San Diego, CA 92152
Attn: Codes 01 - H. L. Blood
015 - P. C. Fletcher
9102 - W. J. Dejka
922 - H. H. Wieder
532 - J. H. Richter

Naval Weapons Center
China Lake, CA 93555
Attn: Codes 601 - F. C. Essig
5515 - M. H. Ritchie

Donald E. Kirk
Professor & Chairman
Electronic Engineering
Sp-304
Naval Postgraduate School
Monterey, CA 93940

Mr. J. C. French
National Bureau of Standards
Electronics Technology Division
Washington, DC 20234

Harris B. Stone
Office of Research, Development, Test
& Evaluation
NOP-987
The Pentagon, Room 5D760
Washington, DC 20350

Dr. A. L. Slafkosky
Code RD-1
Headquarters Marine Corps
Washington, DC 20380

Dr. H. J. Mueller
Naval Air Systems Command
Code 310
JP #1
1411 Jefferson Davis Hwy.
Arlington, VA 20360

Mr. Larry Sumney
Naval Electronics Systems Command
Code 03R
NC #1
2511 Jefferson Davis Hwy.
Arlington, VA 20360

Naval Sea Systems Command
NC #3
2531 Jefferson Davis Hwy.
Arlington, VA 20362
Attn: Code 03C - J. H. Huth

Officer in Charge
Carderock Laboratory
Code 522.1 - Technical Library
(Cont'd. on next page)

Code 18 - G. H. Gleissner
David Taylor Naval Ship Research
& Development Center
Bethesda, MD 20084

Naval Surface Weapons Center
White Oak
Silver Spring, MD 20910
Attn: Codes WX-40 - Technical Library
WR-303 - R. S. Allgaier
WR-34 - H. R. Riedl

OTHER GOVERNMENT AGENCIES

Dr. Howard W. Etzel
Deputy Director
Division of Materials Research
National Science Foundation
1800 G Street
Washington, DC 20550

Mr. J. C. French
National Bureau of Standards
Electronics Technology Division
Washington, DC 20234

Dr. Jay Harris
Program Director
Devices and Waves Program
National Science Foundation
1800 G Street
Washington, DC 20550

Los Alamos Scientific Laboratory
ATTN: Reports Library
P.O. Box 1663
Los Alamos, NM 87544

Dr. Dean Mitchell
Program Director, Solid-State Physics
Division of Materials Research
National Science Foundation
1800 G Street
Washington, DC 20550

Mr. F. C. Schwenk, RD-T
National Aeronautics & Space
Administration
Washington, DC 20546

M. Zane Thornton
Deputy Director Institute for
Computer Sciences and Technology
National Bureau of Standards
Washington, DC 20234

Head, Electrical Sciences & Analysis
Section
National Science Foundation
1800 G Street, NW
Washington, DC 20550

NON-GOVERNMENT AGENCIES

Director
Columbia Radiation Laboratory
Columbia University
538 West 120th Street
New York, NY 10027

Director
Coordinated Science Laboratory
University of Illinois
Urbana, IL 61801

Director
Division of Engineering and
Applied Physics
Harvard University
Pierce Hall
Cambridge, MA 02138

Director
Electronics Research Center
The University of Texas
P.O. Box 7728
Austin, TX 78712

Director
Electronics Research Laboratory
University of California
Berkeley, CA 94720

Director
Electronics Sciences Laboratory
University of Southern California
Los Angeles, CA 90007

Director
Microwave Research Institute
Polytechnic Institute of New York
333 Jay Street
Brooklyn, NY 11201

Director
Research Laboratory of Electronics
Massachusetts Institute of Technology
Cambridge, MA 02139

Director
Stanford Electronics Laboratory
Standord University
Stanford, CA 94305

Director
Stanford Ginzton Laboratory
Stanford University
Stanford, CA 94305

Dr. Lester Eastman
School of Electrical Engineering
Cornell University
Ithaca, NY 14850

Chairman
Department of Electrical Engineering
Georgia Institute of Technology
Atlanta, GA 30332

Dr. Carlton Walter
ElectroScience Laboratory
The Ohio State University
Columbus, OH 43212

Dr. Richard Saeks
Department of Electrical Engineering
Texas Tech University
Lubbock, TX 79409

Dr. Roy Gould
Executive Officer for Applied Physics
California Institute of Technology
Pasadena, CA 91125